4-2013

Integrating Depositional Facies and Sequence Stratigraphy in Characterizing Unconventional Reservoirs: Eagle Ford Shale, South Texas

Seth Jordan Workman
Western Michigan University

INTEGRATING DEPOSITIONAL FACIES AND SEQUENCE STRATIGRAPHY IN CHARACTERIZING UNCONVENTIONAL RESERVOIRS: EAGLE FORD SHALE, SOUTH TEXAS

by

Seth Jordan Workman

A thesis submitted to the Graduate College
In partial fulfillment of the requirements
For the degree of Master of Science
Department of Geosciences,
Western Michigan University
April 2013

Thesis Committee:

G. Michael Grammer, Ph.D., Chair
Robert Gillespie, Ph.D.
William B. Harrison III, Ph.D.
Robert K. Garrison, M.S.

INTEGRATING DEPOSITIONAL FACIES AND SEQUENCE STRATIGRAPHY IN CHARACTERIZING UNCONVENTIONAL RESERVOIRS: EAGLE FORD SHALE, SOUTH TEXAS

Seth Jordan Workman, M.S.

Western Michigan University, 2013

The Mid-to-Late Cretaceous Eagle Ford Shale of South Texas is a mixed siliciclastic/carbonate, unconventional resource play with considerable oil and natural gas. Characterization of Eagle Ford reservoir quality and potential is made difficult by complex, small-scale heterogeneities.

The limited availability of subsurface data constrains previous subsurface Eagle Ford investigations. As a result, the internal variability of depositional facies and reservoir attributes remain poorly understood for these Eagle Ford rocks.

This investigation incorporates a representative group of four Eagle Ford cores, and core data, from within the current play area in order to: 1) determine facies successions, 2) establish a hierarchal classification of vertical stacking patterns constrained within a sequence stratigraphic framework, and 3) relate intervals of reservoir-quality porosity-/permeability with specific facies-/units.

Results of this investigation demonstrate how techniques of identifying, and linking depositional facies to reservoir quality, and then tying these to wire-line log data assist in the evaluation of unconventional reservoirs and, ultimately, enhance the predictability of reservoir potential away from core observations.

ACKNOWLEDGMENTS

Above all, I would like to acknowledge and express my appreciation for the continued guidance, and support of my thesis advisor, Dr. G. Michael Grammer throughout the completion of this manuscript. I would also like to thank my committee members, Dr. Robb Gillespie, Dr. William B. Harrison III and Robert K. Garrison for their continued help and support throughout this study.

I would like to thank EOG Resources, Inc. for making this project possible through the data and financial support provided. The staff and faculty at the Michigan Geological Repository for Research and Education (MGRRE) and the Department of Geosciences at Western Michigan University also deserve recognition for their involvement and assistance with my graduate education.

I would also like to thank my friends and colleagues for their continued support and insight.

I am deeply grateful for my family who has instilled in me a set of values and desire to learn that have made me who I am today. I extend my deepest thanks and sincere appreciation to my parents, Richard and Rhonda Workman, for their unwavering love and support and active involvement in my education. Lastly, I would like to thank and express my deep appreciation to my loving and devoted wife, Kaitlin, for her support and understanding throughout the completion of my graduate education.

Seth Jordan Workman

TABLE OF CONTENTS

Table of Contents—continued

CHAPTER

Table of Contents—continued

LIST OF TABLES

LIST OF FIGURES

List of Figures—continued

CHAPTER I: INTRODUCTION

Summary of the Problem

The Mid-to-Late Cretaceous (Cenomanian-Turonian) Eagle Ford Shale of South Texas is a mixed siliciclastic/carbonate unconventional resource play and is representative of similar resource plays including the Marcellus, Barnett, Bakken and Woodford Shales. Resource plays are continuous and spatially extensive reservoirs where traditional traps, seals and distinct gas-water contacts are absent and are characterized by low matrix permeabilities, generally less than 0.1 millidarcy (mD), which inhibit buoyancy-driven hydrocarbon migration (Roelofsen, 2011; Roundtree *et al.,* 2010; Bartberger *et al.,* 2002). Though fundamentally different, reported variations in well producibility indicate that these reservoirs, like conventional reservoirs, are characterized by considerable small-scale geologic heterogeneities that significantly influence reservoir quality and potential. The Eagle Ford is commonly referred to as the Eagle Ford Formation, Shale, or Group but will be referred to as the Eagle Ford for this discussion.

Industry attention was initially drawn to the Eagle Ford by its high calcite content, and the effect this has on the ability to artificially propagate natural fractures to enhance production from these rocks (Cherry, 2011). Interest in understanding the geologic and well performance variability in the Eagle Ford decreased soon after its discovery was publicized in 2008. This drove the industry to competitively explore and acquire all available acreage (Treadgold *et al.,*

2011a). Well performance is governed by the spatial distribution of key reservoir properties that are primarily controlled by mineralogy, organic content and diagenetic processes (Prince *et al.*, 2011; Slatt and Abousleiman, 2011; Flügel, 2010; Eseme *et al.*, 2007; Mazzullo, 2004). Increased industry activity (illustrated in Figures 1, 2 and 3), and concerns of confidentiality has limited the availability and analysis of subsurface data (i.e. cores and well logs) and created an industry-wide demand for tools capable of high-grading production potential and reducing drilling risks (Treadgold *et al.*, 2011b).

Industry investigations were primarily rock property studies that utilized 3-D seismic datasets and employed seismic inversion techniques to extract geologic rock property information from geophysical attributes; including porosity, density, fracture networks and mechanical strength (Treadgold *et al.*, 2011a). These were important because they linked well performance to geophysical attributes and ultimately: 1) enhanced the predictability of reservoir quality away from well control, 2) enabled the optimization of development plans, and 3) aided efforts to maximize recovery (Stephens *et al.*, 2011, personal communication; Treadgold *et al.*, 2011; Treadgold *et al.*, 2011b; Bratovich and Sommer, 2009). These studies demonstrate how geophysical attributes can serve as useful proxies for, but do not provide direct understandings of geologic heterogeneities responsible for variable reservoir quality.

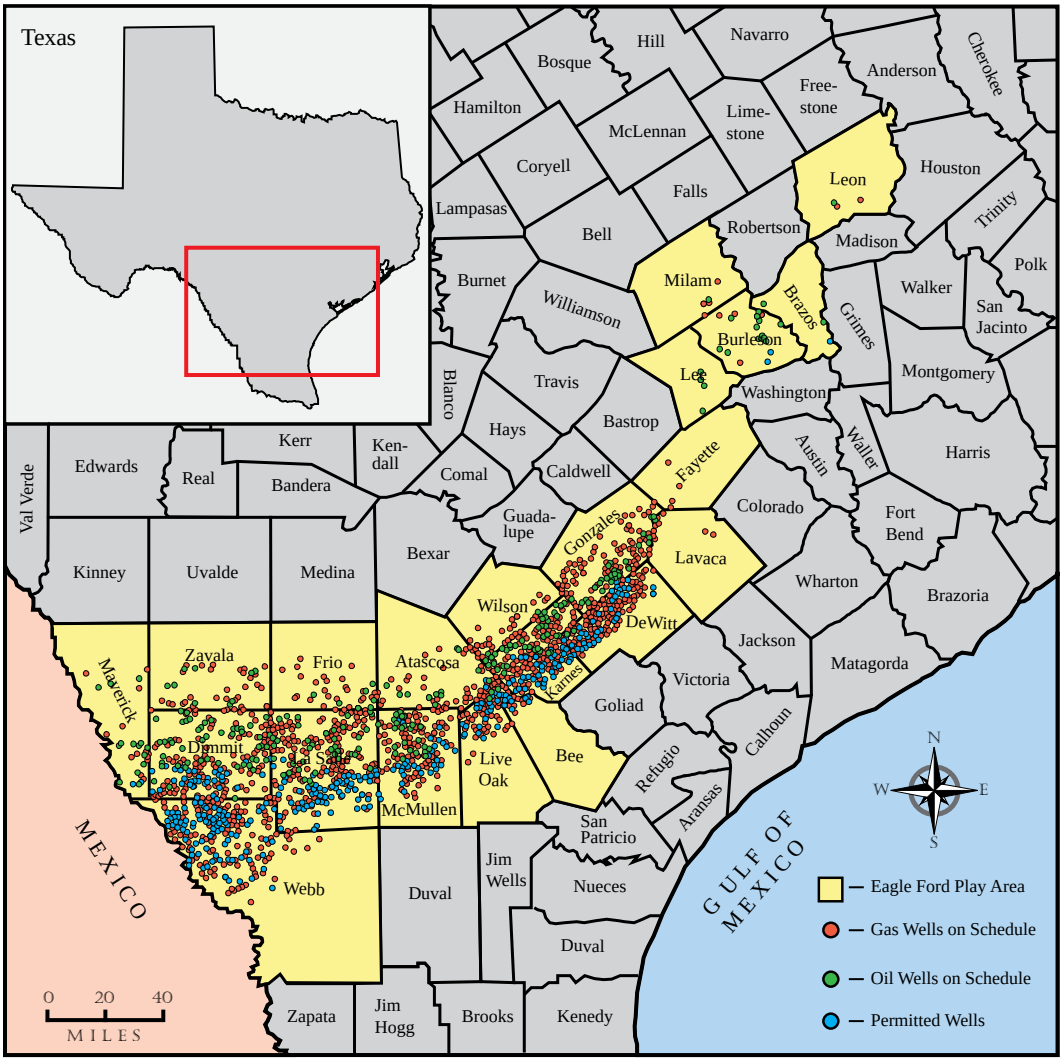

Figure 1: Map of Texas that shows the geographic extent of the current Eagle Ford play area and drilling activity. Modified from the Railroad Commission of Texas, 2012.

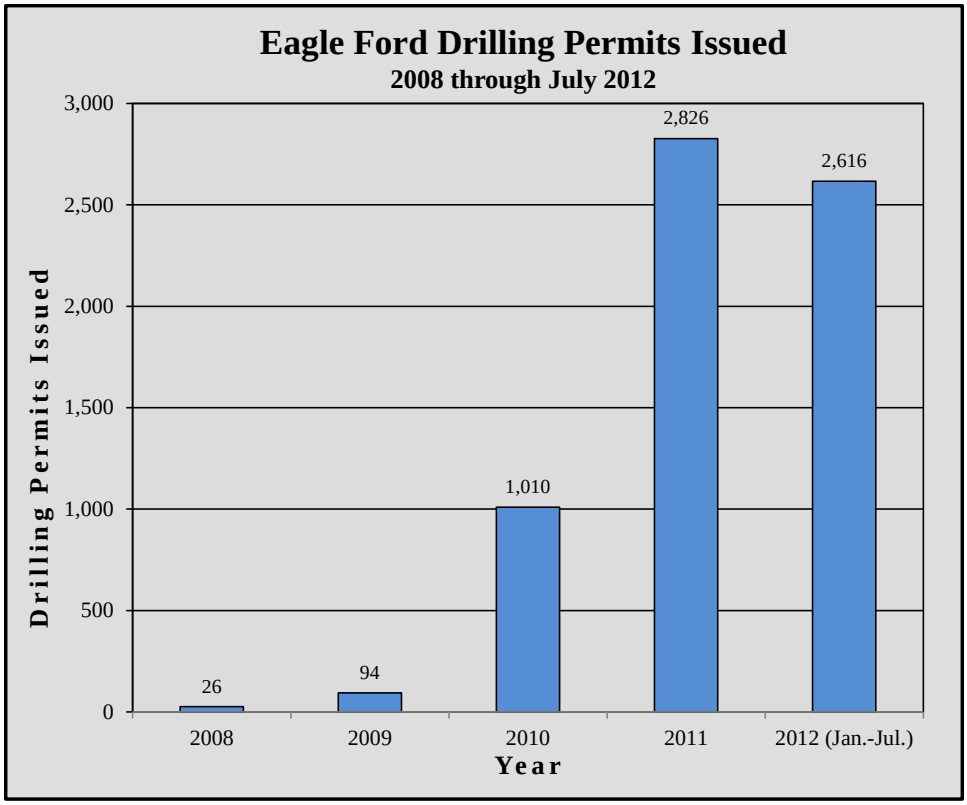

Figure 2: Chart of the annual Eagle Ford drilling permits issued. The number of permits issued has continued to rise since 2008. Data from the Railroad Commission of Texas, 2012.

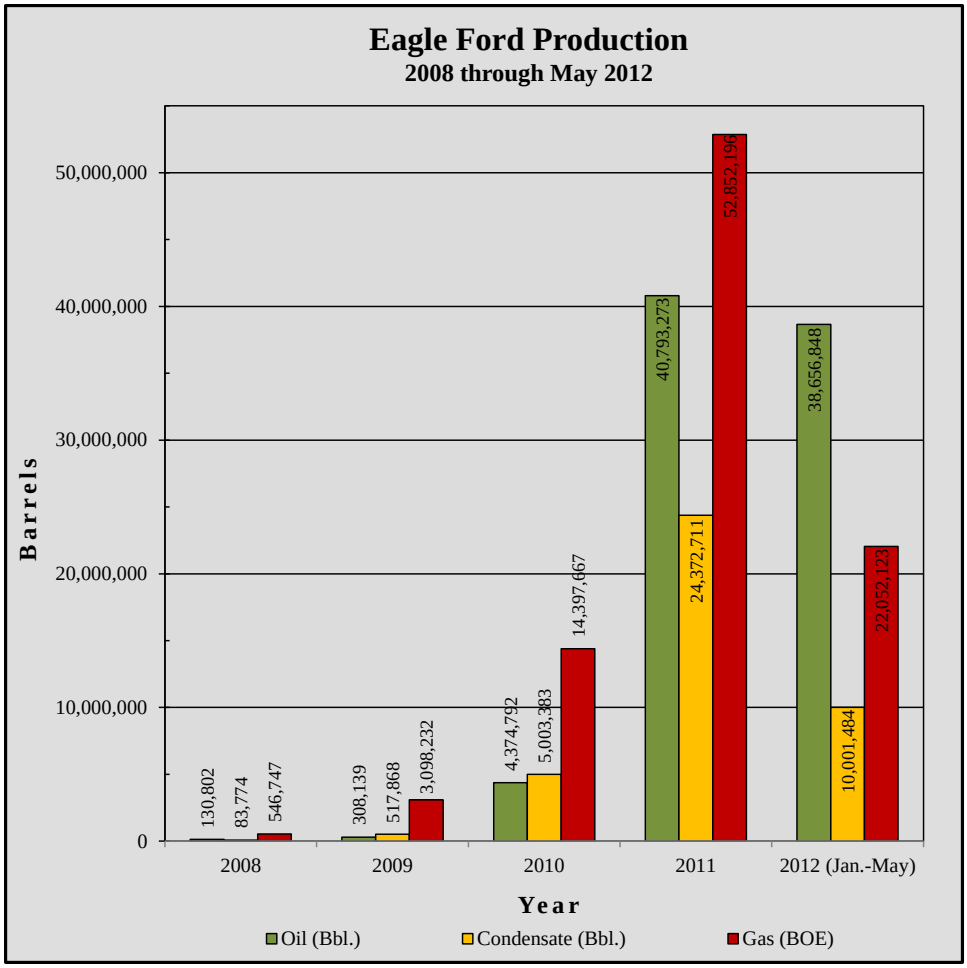

Figure 3: Chart that shows the steady rise in the annual production of oil, condensate, and dry gas from the Eagle Ford since 2008. Data from the Railroad Commission of Texas, 2012.

Previous academic studies mapped and correlated the regional lithostratigraphy of the Eagle Ford and its lateral equivalents using wire-line log datasets (Hentz and Ruppel, 2010). Outcrop investigations utilized roadcuts along U.S. Highway 90 in Val Verde and Terrell counties (Figure 4 and 5; Peschier, 2011; Donovan and Staerker, 2010; Lock *et al.*, 2010; Lock and Peschier, 2006;

Lock *et al.*, 2001) and core-based studies investigated subsurface facies characteristics (Harbor, 2011). These investigations focused on the evaluation of macro-scaled lithofacies, source-rock characteristics and biostratigraphic variability to improve the geologic understanding for variable reservoir quality and performance. These studies are not only constrained by the extent of outcrop exposure, but also by the limited availability of subsurface data and warrant additional rock-based study.

This study is unique in that it is an integrated approach combining subsurface data (core, core petrophysical data, and wire-line log data) with detailed data from modern analogs, evaluated within a well-constrained sequence stratigraphic framework to enhance the overall understanding of the Eagle Ford, and to provide insight into the probable lateral and vertical distributions of reservoir units in the subsurface. Furthermore, consideration is given, but not focused on the influence of micro- to nano-scaled heterogeneities as it is these, particularly in pore networks, that most significantly govern reservoir quality in these unconventional reservoirs (Dawson and Almon, 2010; Loucks *et al.*, 2010; Aplin *et al.*, 1999).

Objectives and Goals

A representative group of four Eagle Ford cores was selected from within the current play area for analysis of depositional facies and interpretation of

depositional environment (Table 1). Facies successions were determined, and a hierarchal classification of vertical stacking patterns was established and constrained within a sequence stratigraphic framework. Core, core analyses, and conventional wire-line log data were used to relate intervals of reservoir-quality porosity and permeability values with specific facies and/or intervals in order to better predict the subsurface distribution and character of facies where rock data is limited or unavailable.

This reservoir characterization approach is predicated on the hypothesis that the reservoir potential for these Eagle Ford rocks is fundamentally dependent on the distribution of primary rock fabric and the influence of depositional setting. Furthermore, that the integration of core data, in conjunction with wire-line logs, will improve the understanding of complex heterogeneities within the Eagle Ford, and may improve hydrocarbon exploration and development for these rocks.

The overarching questions addressed in this research include:

1. What is the environmental setting/paleogeography during deposition of Eagle Ford sediments?
2. Do depositional facies and vertical successions relate to sea level fluctuations, and if so, do they record multiple orders of cyclicity in relative sea level?
3. Is reservoir quality strictly controlled by depositional facies and/or are structural elements influential?

4. Does facies cyclicity observed in core correlate to conventional wire-line log signatures? And can conventional wire-line log data be used to differentiate and predict the lateral and vertical distribution of depositional facies and reservoir potential?

API No.	Lease Name	Well No.	Operator	County	Field Name	Core Interval (Ft.)			Available Core Data				
						Btm	Top	Total	Thin Sections (#)	XRD	GSCA	TOC	Core GR
17732183	Hill	1	EOG Resources, Inc.	Gonzales	Eagleville	10,916	10,670	246	67	Y	Y	Y	Y
17732077	T.R. Marshall	1	EOG Resources, Inc.	Gonzales	Eagleville	11,430	10,980	450	175	Y	Y	Y	Y
25531740	Nixon	6	EOG Resources, Inc.	Karnes	Eagleville	8,623	8,415	208	66	Y	NA	NA	NA
31134159	Hundley	1	EOG Resources, Inc.	McMullen	Eagleville	10,029	9,820	209	32	Y	Y	Y	Y

Table 1: List of wells integrated into this investigation including well header information, available data and the cored interval. Refer to figure 4 for the geographic location of these wells. Well information collected from the Railroad Commission of Texas (2012).

CHAPTER II: EAGLE FORD PLAY HISTORY

Developments and advancements in horizontal drilling and completion techniques have augmented traditional exploration views regarding organic-rich shales as being simple source-rocks. Such shales are now also considered to be increasingly important and commercially viable self-contained petroleum systems both within the United States and internationally (Hildred *et al.,* 2011). Well-known unconventional resource plays within the United States include: the Mississippian Bakken Shale (Williston Basin), Mississippian Barnett Shale (Fort Worth Basin), Late Devonian Woodford Shale (Arkoma Basin), Middle Devonian Marcellus Shale (Appalachian Basin), and the Upper Cretaceous Eagle Ford (Maverick Basin) (Peschier, 2011). The most recent of these is the Eagle Ford, which has become one of the "hottest" shale plays in the United States (Howard Weil Incorporated, 2011).

Eagle Ford exploration began in earnest in the Fall of 2008 after Petrohawk Energy Corporation publically announced their wildcat, the STS-241 #1H, in LaSalle County and were credited with the discovery of the Hawkville Field (Figures 1 and 4; Stephens *et al.,* 2011, personal communication). Test results for the STS-241 #1H were 7.6 MMcfgd (million cubic feet of gas per day) and 250 barrels of condensate per day (Durham, 2010). Condensate, or 'wet gas', is a natural gas liquid that condenses from natural gas vapor during production when reservoir pressures drop below the dew point of natural gas (Schlumberger).

The Dora Martin #1H was drilled 22.5 km (14 mi) to the southeast of the STS-241 #1H discovery well and tested 8.3 MMcfgd (Cusack *et al.,* 2010). The Hawkville Field encompasses 4,144 square kilometers (1,600 square miles). It extends for 193 km (120 miles) from west to east through Webb, LaSalle, McMullen and Live Oak Counties County and between 8 km to 48 km (5 mi to 30 mi) north to south (Figures 1 and 4; Cusack *et al.,* 2010).

Major operators such as Anadarko, Apache, EOG Resources, BP, Pioneer and SM Energy expanded early exploration efforts away from the Hawkville Field. Initial exploration and acreage acquisitions were focused primarily upon the southern, down-dip region of the Maverick Basin where thermal maturity was highest. These early wells produced dry gas with lesser amounts of condensate (Railroad Commission of Texas, 2012).

EOG Resources concentrated exploration and acreage acquisition activities on the northern, up-dip regions of the play where troughs accumulated thickened Eagle Ford sections that are less mature and oil prone. EOG acquired 535,000 net acres within the oil window (EOG Resources Investor Presentation, 2011). This is the largest acreage position of any operator within the oil window. Early in 2009, EOG Resources announced oil production from their own discovery well, the Milton #1H. Mark Papa, Chairman of the Board and Chief Executive Officer of EOG Resources, described this as “one of the most significant oil discoveries in the lower 48 during the last 40 years” (EOG Resources First Quarter Results, 2011). Throughout the play area, wells within the

oil window have achieved peak oil rates as high as 2,000 barrels per day with gas to oil ratios between 1,000 to 4,000 (Cherry, 2011).

Eagle Ford play boundaries have continued to expand since the discovery in 2008. The current play area averages 80.5 km (50 mi) in width and extends northward for nearly 644 km (400 mi) from the Texas/Mexican border in Maverick and Webb counties (Figure 1; Railroad Commission of Texas, 2012). The play consists of 20 active fields. Reported well production across the play established the Eagle Ford as a well-defined down-dip gas play that transitions rapidly into well-defined up-dip condensate and oil fairways (Treadgold *et al.*, 2011b).

Well-defined fairways (Figure 4) with proven oil production escalated industry activity and focused exploration efforts to areas within the oil fairway. This is reflected by the dramatic increase in the number of drilling permits issued from 26 in 2008, 94 in 2009, 1,010 in 2010, 2,826 in 2011, and as of July, a total of 2,616 permits have been issued in 2012 (Figure 2; Railroad Commission of Texas, 2012). Annual production statistics for the play show a dramatic rise in oil, condensate and gas production (Figure 3). These are expected to continue to rise as the industry begins to concentrate on development and recovery optimization.

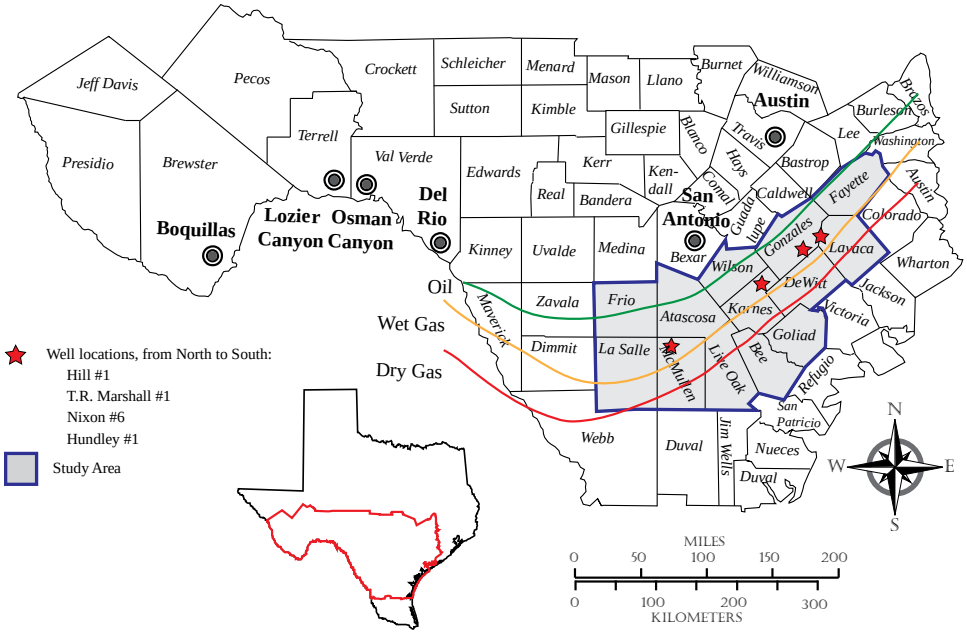

Figure 4: Map of Central Texas that shows the location of the study area and wells included in the study. The Boquillas Formation outcrops in the Big Bend and Trans Pecos regions (Brewster and Pecos counties) in addition to Lozier Canyon and Osman Canyon. These outcrops and roadcrops along U.S. Highway 90 to Del Rio were utilized in Boquillas investigations. Modified from EOG Resources Investor Presentation (2011), Lock *et al.* (2010), and Lock and Peschier (2006).

CHAPTER III: GEOLOGIC BACKGROUND

Geologic Setting

Extensional rifting and sea floor spreading during the Early Mesozoic (Late Triassic-Middle Jurassic) characterize the initial opening of the Gulf of Mexico (Montgomery *et al.*, 2002). Rift-related tectonism had largely ceased by the Late Jurassic, and was followed by a period of basement cooling and thermal subsidence which continued through the Early Cretaceous (Lehmann *et al.*, 1999; Winker and Buffler, 1988). During this time, regional subsidence increased accommodation and promoted carbonate deposition. As a result, a shallow-marine carbonate shelf complex developed a 4,800 km long (2,983 mi) arcuate trend that rimmed the proto- Gulf of Mexico (Almon and Cohen, 2008; Mancini *et al.*, 2008; Wilson and Jordan, 1983).

A series of carbonate platforms developed during the Cretaceous Period. In the northern Gulf Coast region, these were amalgamated into a single platform called the Comanche Shelf (Figure 5). The Comanche Shelf is characterized by a series of stacked, prograding carbonate platforms separated by back-stepping, transgressive, organic-rich facies (Figure 6; Montgomery *et al.*, 2002). Two primary episodes of platform development characterize the Comanche Shelf (Figure 6). Each exhibit two principle depositional profiles, consisting of: 1) regressive, flat-topped reef-rimmed platforms, and 2) transgressive to high-stand, storm-dominated ramp profiles (Harbor, 2011). Rudists, a group of massive-shelled bivalves, were the primary reef constituents during the Cretaceous Period,

particularly the caprinids, requiniids and radiolitids (Scott and Weaver, 2010; Kerans, 2002; Young, 1972).

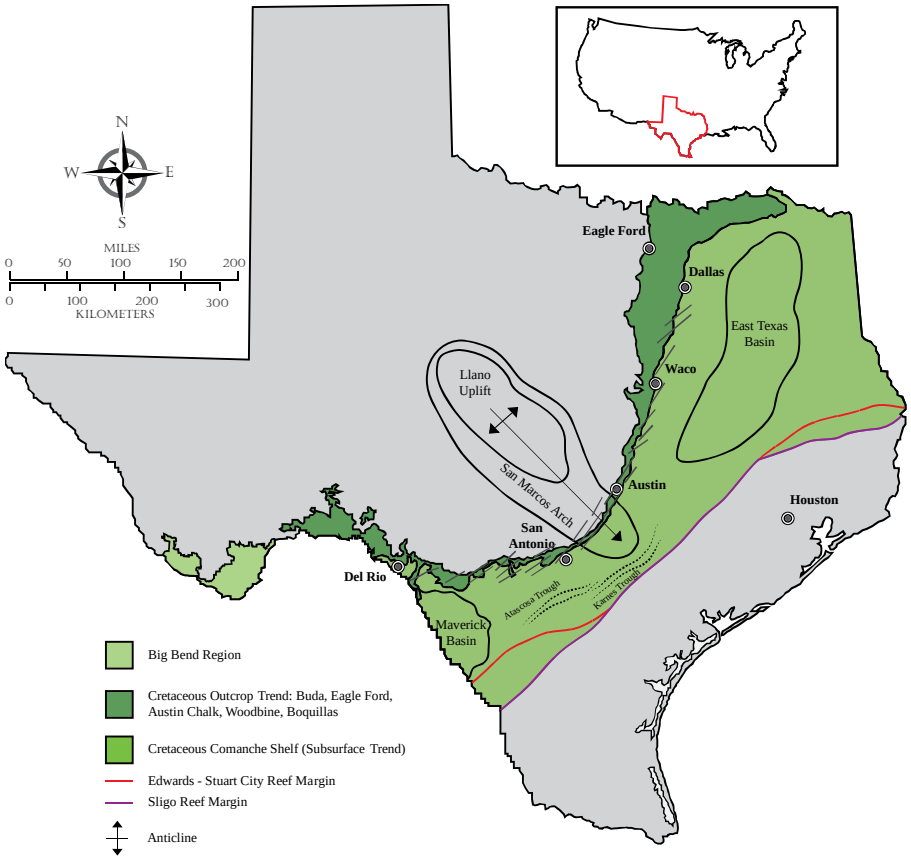

Figure 5: Map of Texas that shows the distribution of the Eagle Ford and equivalent formations in both outcrop trends and subsurface. Key cities and prominent structural features are indicated. These structural features controlled the spatial distribution and rock character during and following initial deposition. Modified after the Geology of Texas Map (1992), Phelps *et al.* (2010), Winker and Buffler (1988) and Young (1972).

Deposition of the Sligo Limestone occurred in the northern Gulf Coast during the Early Cretaceous Barremian stage. This represents the initial development of carbonate platforms in this area (Figure 6). The Sligo formed as a shallow, rimmed carbonate platform characterized by, a: 1) broad, restricted interior platform, 2) narrow, high-energy, well-circulated outer platform, 3) well-defined platform margin, and 4) a gently dipping foreslope (Phelps *et al.*, 2010; Yurewicz, 1993). Throughout the Cretaceous, geometries of the Comanche Shelf margin were predominantly progradational in nature, but periodically, the geometry shifted toward a late-stage aggradational form (Scott, 1993; Winker and Buffler, 1988). The Edwards-Stuart City developed during the Albian stage (107 Ma) and maintained the near continuous rimmed platform architecture of the Comanche Shelf through the Late Albian to Early Cenomanian (Figure 6; Phelps, 2010; Trevino, 1988; Winker and Buffler, 1988).

Back-stepping of the Comanche shelf margin coincided with rapid marine transgressions and thick, organic-rich deposits on the platform. These organic-rich, argillaceous lime mudstone and shale deposits include the Pearsall, Del Rio and Eagle Ford (Figure 6). Each of these represent periods of platform inundation and drowning during the Late Aptian (~115 Ma) and Late Albian-Cenomanian (~96 Ma) (Fritz *et al.*, 2000; Scott, 1993). The thickest transgressive deposit was the Eagle Ford (Figure 6). Primary deposition occurred within troughs and along the margin of the Maverick Basin and the East Texas Basin (Figure 7; Wilson and Jordan, 1983; Lehmann *et al.*, 2000).

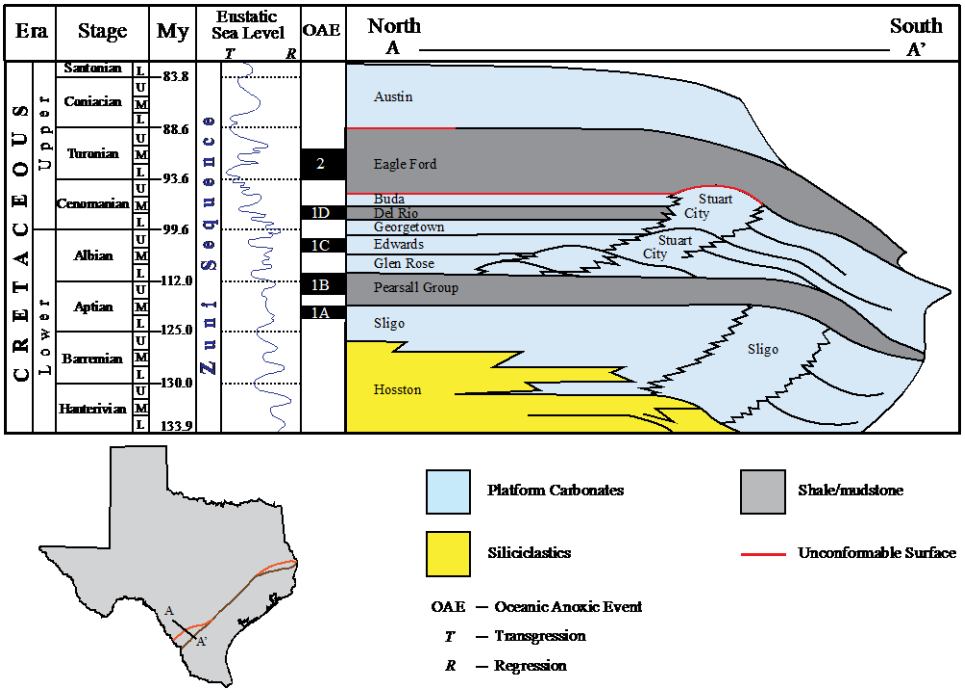

Figure 6: Diagrammatic representation of the evolution and architecture of Cretaceous carbonate platforms in the Northern Gulf Coast. Cretaceous transgression-regression cycles of the Zuni Sea are summarized. The Comanche Shelf consists of alternating platform carbonates and organic-rich carbonate muds. Organic-rich mudstones coincide with global Oceanic Anoxic Events (OAEs) and represent episodes of platform inundation and drowning. These episodes define periods of open shelf and rimmed shelf architectures. Modified after Harbor (2011), Cooper *et al.* (2010), Donovan and Staerker (2010), Cronin (2010), Lehmann *et al.* (2000), and Winker and Buffler (1988).

Tectonic History

Mesozoic tectonism led to the development of predominant structural and geologic features in the study area and surrounding regions (Figure 7). These

features influenced the deposition and spatial distribution of the carbonate facies in the Eagle Ford, as supported by regional thickness trends which thin toward and over arches and thicken into the bordering embayments.

The San Marcos Arch is the southern, subsurface extension of granitic and metamorphic rocks of the Llano Uplift, and is characterized as a low amplitude, south-to-southeast plunging anticline (Figures 5 and 7; Phelps, 2011; Dravis, 1980; Beebe, 1968). The arch formed a topographic high in central Texas that experienced lesser subsidence than the nearby East Texas and Maverick Basins (Laubach and Jackson, 1990). Decreased subsidence established shallow-marine platform environments over the arch characterized by marked internal unconformities. Deeper shelfal and basinal environments flanked these carbonate platforms to the north and south (Ewing, 2009).

The Maverick Basin is an intra-shelf depocenter that developed on the southeast flank of the Edwards Platform (Figures 5 and 7). Increased sedimentation within the Maverick Basin resulted from prolonged subsidence and development of accommodation. This was primarily controlled by sediment loading and thermal subsidence, and is associated with underlying basement structures and half-grabens that formed during the failed Rio Grande rifting event (Hull, 2011; Phelps, 2011; Donovan and Staerker, 2010; Scott, 2004; Goldhammer and Johnson, 2001; Galloway, 1989). Movement of the underlying Jurassic Louann Salt began soon after it was deposited, and is believed to have

continued through the Paleogene, compounding the effects of thermal subsidence in the Maverick Basin (Ewing, 2010; Pearson, 2010).

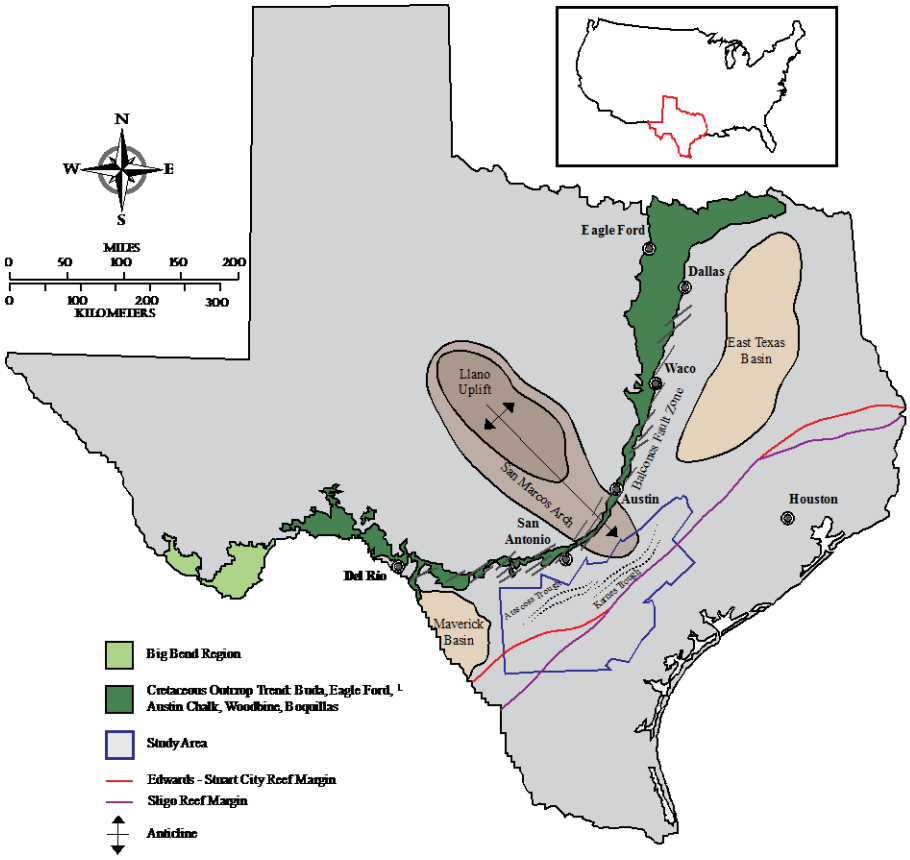

Figure 7: Map of Texas that shows prominent structural and geologic features. Tectonic structures controlled bathymetry and geologic processes that governed the deposition and spatial distribution of carbonate facies. Modified after the Geology of Texas Map (1992), Phelps *et al.* (2010), Winker and Buffler (1988) and Young (1972).

Regional and local fault zones in the Maverick Basin developed that influenced the development of accommodation and affected patterns of

sedimentation. Faulting initiated during the Late Albian continued into the Eocene and likely resulted from salt withdrawal and sediment loading (Ewing, 2010; Dyer and Bartolini, 2004). This contributed to increased subsidence associated with the Karnes and Atascosa Troughs (Figures 5 and 7; Ewing, 2010; Dyer and Bartolini, 2004). These fault-controlled graben systems experienced contemporaneous growth with Cretaceous sedimentation and accumulated thickened Eagle Ford sections (Corbett, 2010; Tucker, 1968; Keahey, 1962). The formation of the Balcones Fault system is related to post-Cretaceous deformation and the Oligocene through Miocene uplifting of Central Texas (Fullmer and Lucia, 2005; Galloway, 2000). The Balcones system is characterized by a discontinuous series of tensional, *en echelon* normal faults that form an arcuate trend concave to the Llano uplift, and parallel to the Ouachita orogenic front (Figures 5 and 7; Pearson, 2010; Abbott, 1974). Fault blocks are downthrown to the southeast and vertical displacement along the fault reaches a maximum of 610 m (2,000 ft.) in northeast Texas and decreases to the southeast toward the Maverick Basin (Fullmer and Lucia, 2005).

Paleogeography and Climate

Early Mesozoic tectonism initiated the fragmentation of Pangea and the opening of the proto-Gulf of Mexico. At this time the northern Gulf Coast was situated within the Caribbean province of the Tethyn seaway and paralleled the pantropic equatorial belt (Figure 8; Scott, 1993). The North American plate

drifted northward as sea-floor spreading continued to open the Gulf of Mexico. During the Cretaceous Period (±145.5—65.5 Ma), the Gulf Coast region was located near the junction of the southern end of the Western Interior Seaway and the westernmost part of the Tethys Ocean near 30° North Latitude (Figure 8; Winker and Buffler, 1988; Sohl, 1987).

The Cretaceous was a non-glacial period characterized by long-term greenhouse climatic conditions with four times the present-day atmospheric carbon dioxide (CO_2) concentrations (1,380 ppm) (White *et al.*, 2001). Terrestrial surface temperatures were as much as 6°C to 10°C (43° F to 50° F) above present temperatures (Bice *et al.*, 2002; Schlanger and Jenkyns, 1976). Ocean temperatures were also elevated and Late Cretaceous (Cenomanian-Turonian) equatorial ocean temperatures may have reached 43°C (109° F) (Lehmann *et al.*, 1999). Cretaceous ocean temperatures had a low pole-to-equator gradient of ~10°C (50° F) which slowed oceanic circulation (Linnert *et al.*, 2011).

The Cretaceous Period was also characterized by marine transgressive and regressive cycles (Figure 6). The most significant transgressive events occurred during the Albian (Early Cretaceous), Cenomanian-Turonian (Late Cretaceous), and the Early Coniacian-Late Santonian (Late Cretaceous). These correspond to worldwide phases of bottom-water anoxia (Oceanic Anoxic Events or OAEs). Two OAEs were first recognized, the Aptian-Albanian and the Cenomanian-Turonian (Schlanger and Jenkyns, 1976). More recent work has identified additional OAEs associated with positive and negative $\delta^{13}C$ excursions (Linnert *et*

al., 2011). Excursions in $\delta^{13}C$ are controlled by interrelated factors, including fluctuations in: 1) sea level, 2) volcanism, 3) marine carbonate production, 4) terrestrial organic material, 5) basinal upwelling of nitrogen and phosphate enhanced water, and 6) the stalled oceanic circulation by glacial melt (Linnert, 2011; Turgeon and Creaser, 2008; White *et al.,* 2001; Scott, 1995; Schlanger and Jenkyns, 1976).

Global OAEs correspond to worldwide deposits of thick organic-rich black shales (Figure 6). In the Texas Gulf Coast region, Cretaceous OAEs include the Late Aptian OAE 1A (Pine Island), Aptian/Albian OAE 1B (upper Bexar/lower Glen Rose), Albian/Cenomanian OAE 1D (Upper Georgetown/Del Rio), and the Cenomanian/Turonian OAE 2 (Eagle Ford) (Harbor, 2011; Hull, 2011; Phelps, 2011). The OAE 2 is marked by an abrupt positive $\delta^{13}C$ excursion attributed to large-scale pulses of magmatic activity during the Late Cretaceous (Turgeon and Creaser, 2008).

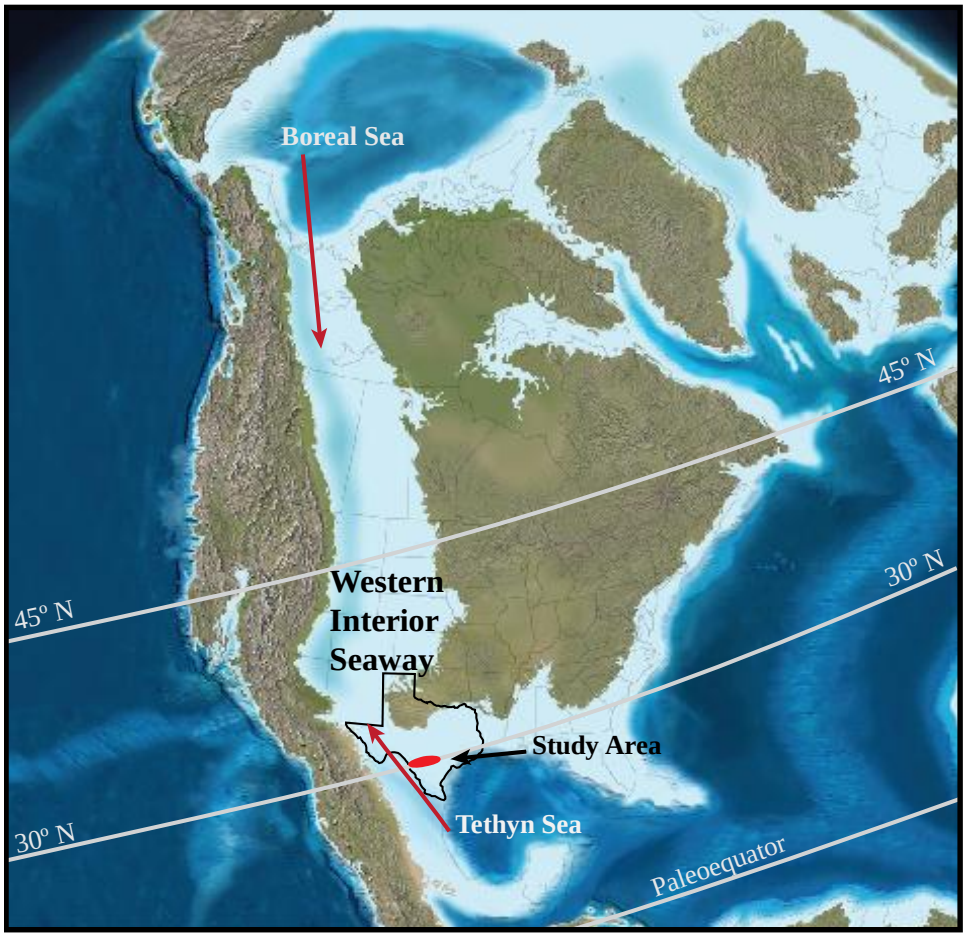

Figure 8: Late Cretaceous (85 Ma) paleogeographic map of North America. Approximate paleolatitude is indicated on the map showing the northern Gulf Coast was situated at approximately 30° North latitude. Arrows indicate the direction of water circulation and the confluence of the Boreal and Tethyan waters in the Western Interior Seaway. Modified from Blakey (1994) and Slingerland *et al.* (1996).

Regional Stratigraphy

The Upper Cretaceous Eagle Ford and its lateral equivalents are widely distributed across Texas (Figure 4). In West Texas, a lateral equivalent outcrops in the Del Rio and Trans Pecos region. In East Texas, the Eagle Ford and lateral equivalents are exposed in outcrops along the western margin of the East Texas Basin. Historically, these outcrops have served as type localities for establishing nomenclature and stratigraphic relationships. Initial workers independently described and developed stratigraphic divisions in outcrop (Pessagno, 1969; Powell, 1965; Winter, 1961; Freeman, 1961; Moreman *in* Sellards *et al., 1932;* Hill, 1901, 1887a, 1887b; Marcou, 1862; Shumard, 1860a, 1860b). This complicated correlations as variable boundaries and names were established for similar groups, formations and members. More recent work refined some of the initial nomenclature to develop more uniform names and descriptions of stratigraphic relationships between type localities (Peschier, 2011; Dawson and Almon, 2010; Donovan and Staerker, 2010; Hentz and Ruppel, 2010; Lock *et al.*, 2010: Lock and Peschier, 2006; Lock *et al.*, 2001; Dawson, 2000, 1997). These facilitated the regional correlation of nomenclature and lithologic trends in outcrop and enabled them to be extended into the subsurface of South Texas.

West Texas

In West Texas the Boquillas Formation is equivalent to the Eagle Ford. Some of the initial outcrop work and descriptions of the Boquillas was done by Freeman (1961) and Powell (1965) in the Big Bend and Trans Pecos regions (Figures 4, 5, 7 and 9). More recent work has utilized deep road cuts along U.S. Highway 90 in Val Verde County where the Boquillas is nearly 61 m thick (200 ft.) and divided it into a lower, middle and upper member (Figures 4, 5, 7 and 9; Peschier, 2011; Lock *et al.,* 2010; Lock and Peschier, 2006; Lock *et al.,* 2001).

The lower member (Figure 9) averages 9 m thick (30 ft.) and consists of interbedded limestone, ash layers and calcareous shales. Freeman (1961) initially described this member as the "1st (pinch and swell) unit". Lock and Peschier (2006) interpreted the lower member as a lowstand system tract (LST) consisting of mass flow and unstable slope deposits. This contradicts previous interpretations of tidal-flat to shallow-shelf sediments. Sedimentary features include slump folds, debris flows, turbidite deposits, tepee structures and shallow channels (Lock and Peschier, 2006; Lock *et al.,* 2001). Diagenetic differentiation, the repartitioning of carbonate from the shales to the limestones, is evident throughout the lower member (Peschier, 2011). Faunal assemblages consist of planktonic foraminifers, calcispheres, ammonites, and *Inoceramus* sp. (Lock and Peschier, 2006). The absence of bioturbation and fossils indicates deep water and anoxic bottom conditions. Lock and Peschier (2006) suggest that the lower member represents the beginning of sea level rise with sediment deposition in moderately deep water

on the upper margin of the basin's slope. This is evidenced by the observed lithofacies and faunal assemblages.

The middle member (Figure 9) is approximately 18 m thick (60 ft.). It has the greatest reservoir potential based on outcrop measurements of 80% calcite content, total organic carbon (TOC) values up to 5.7% and matrix porosities between 6-8% (Lock *et al.,* 2010). The base of the middle member is marked by an abrupt end of the unstable slope features which are characteristic of the lower member. This member corresponds to Freeman's (1961) "2d (Flagstone) unit" and consists of recrystallized, intermixed marlstones, argillaceous lime mudstones and more resistant limestones (Lock and Peschier, 2006). Carbonate content and limestone layers decrease upward from the base of the member before increasing toward the top of the member. This represents a transition from a transgressive systems tract (TST), or retrogradational parasequence set to a highstand systems tract (HST), or progradational parasequence set and lacks a precise boundary (Lock *et al.,* 2010). The faunal assemblage consists of planktonic foraminifera, *Inoceramids* sp., and calcispheres with rare fish scales and teeth (Lock and Peschier, 2006). This member is interpreted to be deposited in anaerobic to dysaerobic bottom conditions in deeper water than the lower member (Lock *et al.,* 2010).

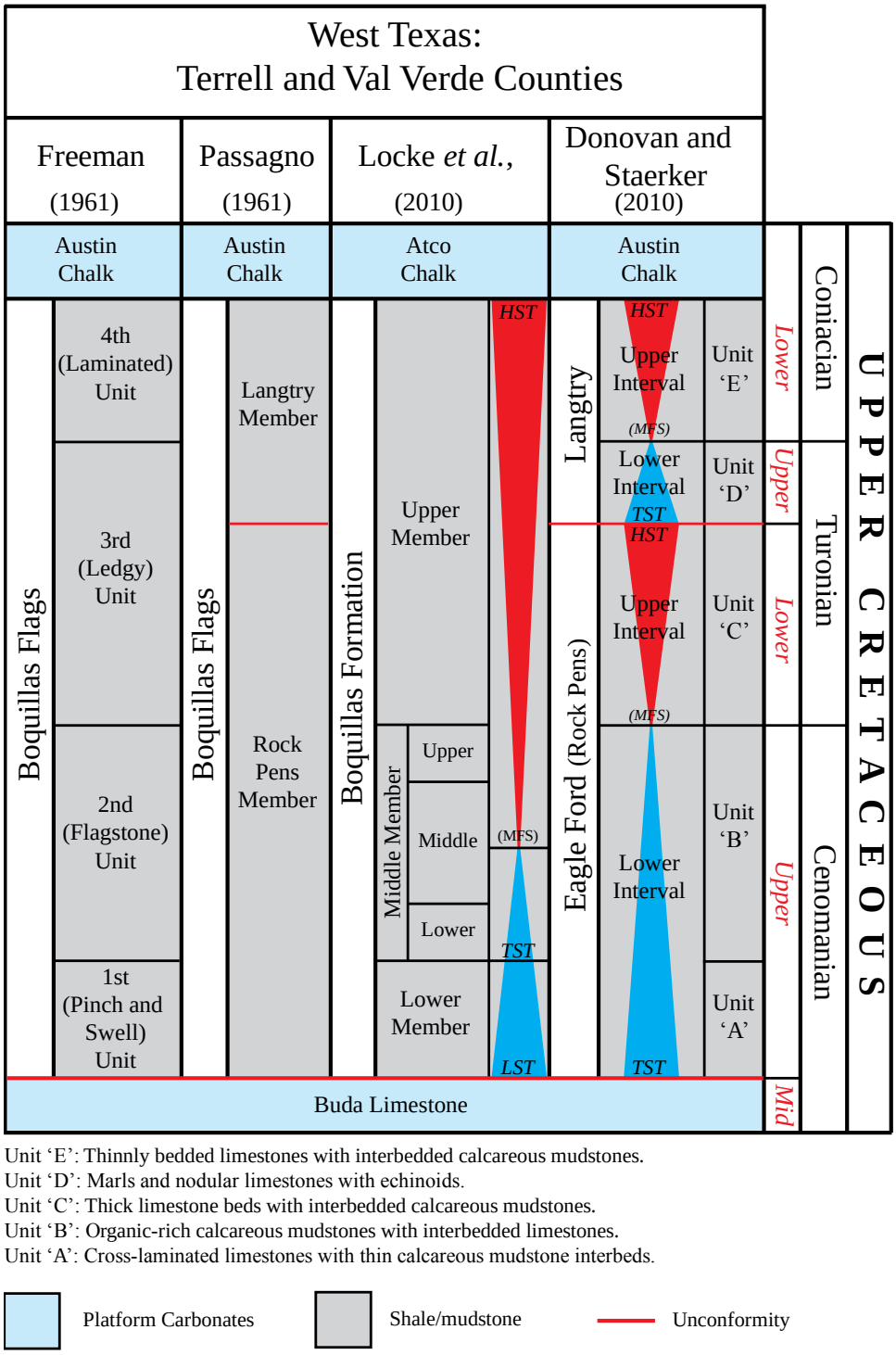

Figure 9: Summary and comparison of previous interpretations and nomenclature of the Eagle Ford in West Texas. Work by Lock

> *et al.* (2010) and Donovan and Staerker (2010) were the first to include sequence stratigraphic interpretations. Ages were documented by Donovan and Staerker (2010) using biostratigraphy.

The upper member (Figure 9) has a low organic content and represents a progressive return to shallower and better oxygenated conditions. The upper member corresponds to Freeman's (1961) "3d (Ledgy) unit" and "4th (Laminated) unit" (Lock and Peschier, 2006). Near the base of the member, limestone beds consist of *Chondrites* burrows which correspond to a low oxygen environment. Toward the top of the member, limestone beds and echinoids increase in abundance, indicating the return of normal oxygen conditions. Lock and Peschier (2006) report a sharp contact between the upper member and the overlying Atco (Austin Chalk) member which was contradicted later by Donovan and Staerker (2010).

Following the work and nomenclature developed by Pessagno (1969), Donovan and Staerker (2010) studied the Boquillas Formation in outcrop at Lozier Canyon and Osman Canyon (Figure 4). Here, Donovan and Staerker (2010) identified two transgressive-regressive sedimentary cycles corresponding to their divisions of the Boquillas, a: 1) Lower, Eagle Ford (Rock Pens) member and 2) an upper, Langtry member. Five facies (A, B, C, D, and E) were identified and described (Figure 9). Facies A, B, and C correspond to Freeman's (1961) "1st

(pinch and swell) unit", "2d (Flagstone) unit", and "3d (Ledgy) unit" (Figure 9). Freeman's (1961) "4th (Laminated) unit" corresponds to facies D and E.

The Eagle Ford (Rock Pens) member is 46 m thick (150 ft.) and consists of medium-to-thick beds of grey, calcareous siltstones, mudstones, and limestones (Pessagno, 1969). Donovan and Starker (2010) identified facies A, B, and C within this member. The Langtry member averages 12 m thick (40 ft.) and includes facies D and E. Within this member, Donovan and Staerker describe thin beds of tan colored calcareous mudstones, marls, and chalky limestones (Figure 9).

South Texas: Maverick Basin to San Marcos Arch

With the exception of minor outcrops in the San Antonio area (Ewing, 2011), Eagle Ford outcrops and core data are limited in South Texas. As a result, much of the descriptions, stratigraphic divisions and correlations have been done using wire-line log data. More recent and comprehensive work by Hentz and Ruppel (2010, 2011) correlated and described lithologic variability in both the Maverick Basin and along the southwest flank of the San Marcos Arch (Figures 5 and 7). Hentz and Ruppel (2010, 2011) adopted divisions established by Grabowski (1995) and incorporated gamma ray and resistivity logs to better understand regional variability of lithology and thickness (Figures 10, 11 and 12).

The Upper Eagle Ford was deposited during a marine transgression and is generally restricted to areas southwest of the San Marcos Arch (Figures 5, 6 and 7; Dawson, 2000). It reaches a maximum thickness of 146 m (480 ft.) in the Maverick Basin. A thinning trend extends southeast toward the Edwards and Sligo shelf margins and to the northeast toward the San Marcos arch (Figures 11 and 12). The Upper Eagle Ford consists predominantly of light-gray calcareous mudrocks with low organic content and low gamma ray values ranging from 45 API to 60 API units (American Petroleum Institute) (Hentz and Ruppel, 2010). Thin beds of organic, dark-gray noncalcareous mudrocks with gamma ray values as high as 120 API units were also locally identified in the upper interval.

The lower interval was deposited during a second-order transgressive systems tract and attains a maximum thickness of 63 m (207 ft.) within the Maverick Basin. The lower interval also thins to the southeast toward the Cretaceous shelf margins, and northeastward toward the San Marcos arch (Figures 11 and 12). The lower interval consists predominantly of dark-gray mudrocks with TOC values between 1.0% to 8.3%, averaging 2.3%, and high gamma ray values typically between 90 API to 135 API units (Hentz and Ruppel, 2010, 2011). Light-gray calcareous mudrocks, marls, and limestones with low gamma ray values also occur locally.

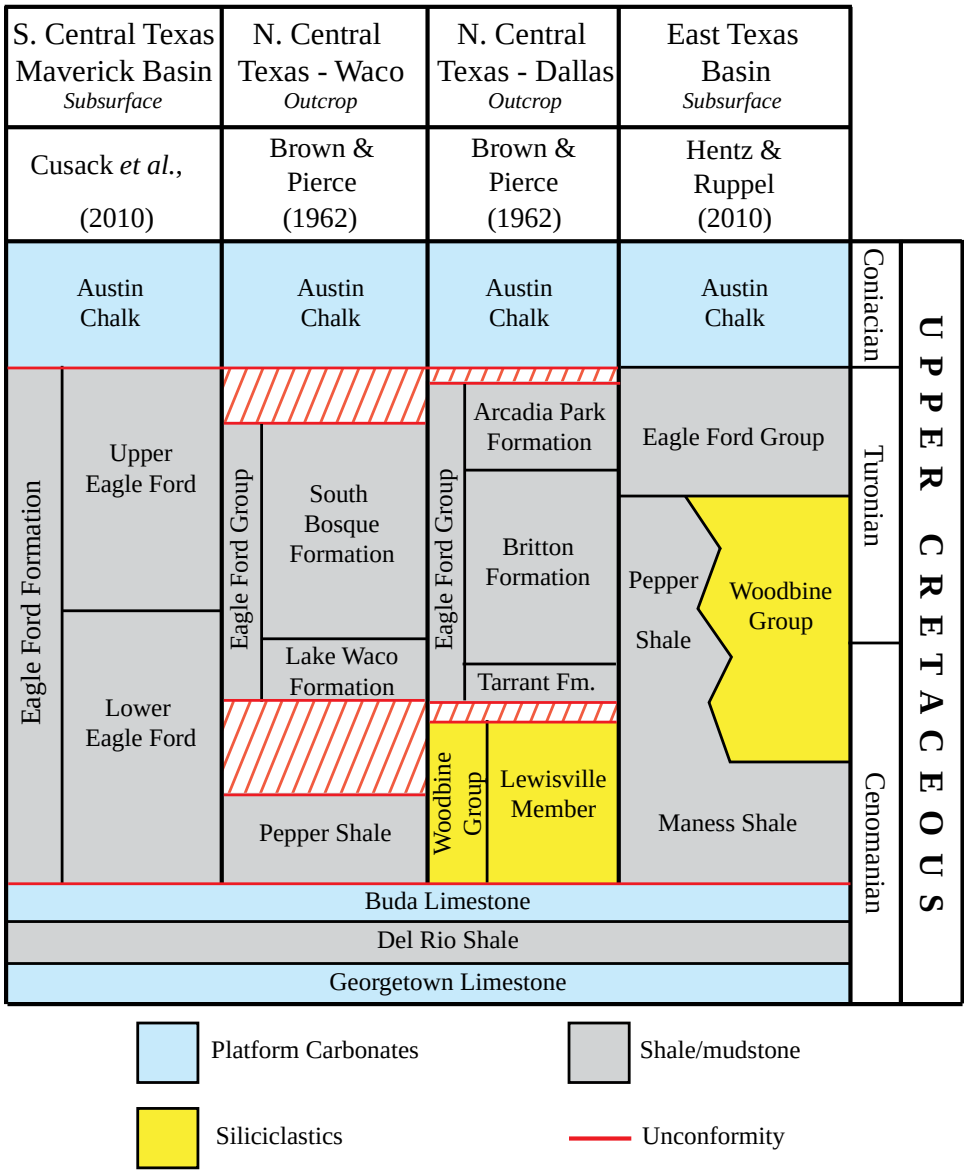

Figure 10: Summary and comparison of nomenclature for the Eagle Ford and equivalent units in South Texas and East Texas. In the Maverick Basin, the Eagle Ford consists of organic-rich mudrocks situated between two subtidal platform deposits: the Buda and Austin. The thickness and lithology of the Eagle Ford change considerably extending toward the northeast from the Maverick Basin. Locations are depicted in Figures 4 and 5.

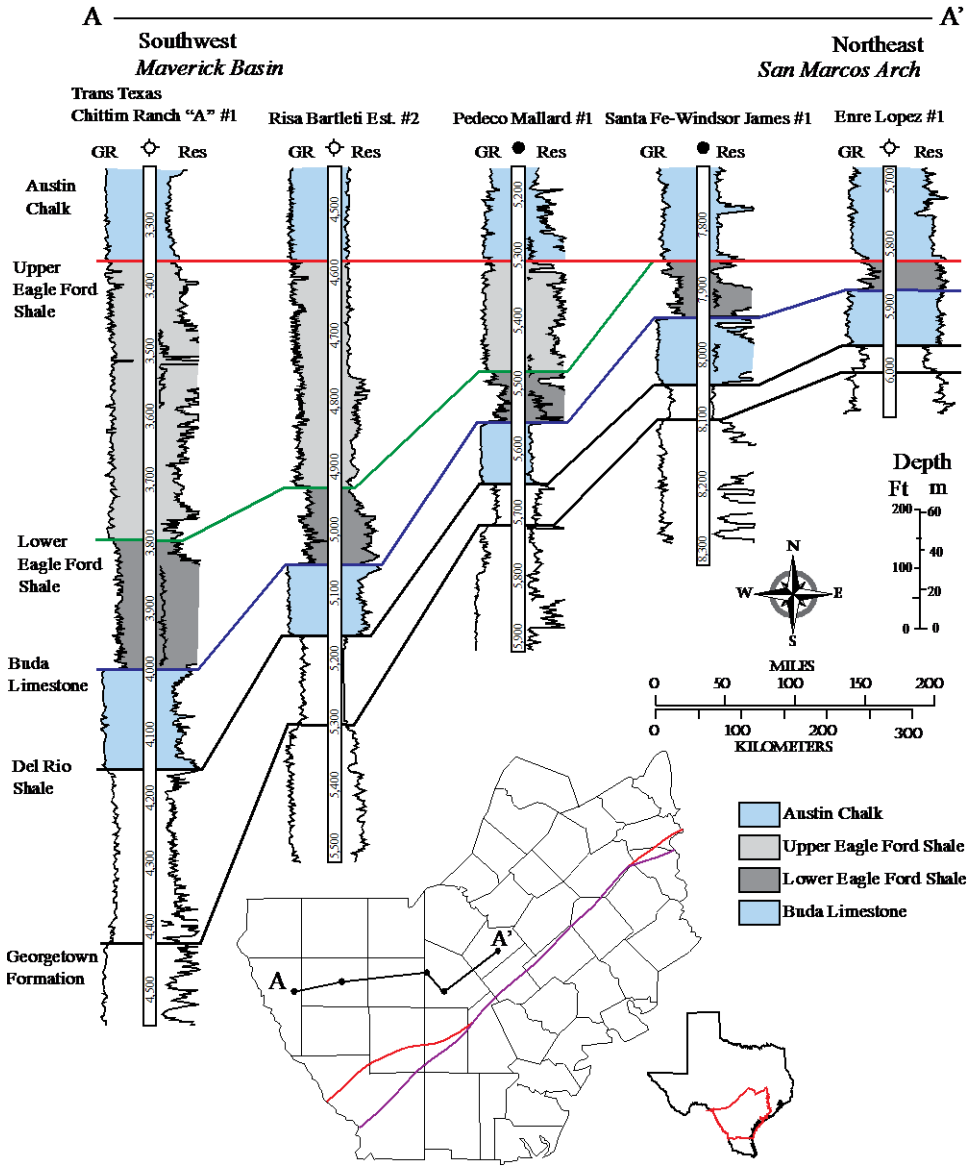

Figure 11: Strike oriented cross section (A—A') illustrating thickness and stratigraphic trends of the Eagle Ford and related sections from the Maverick Basin to the San Marcos Arch area. Refer to Figures 4 and 7 for its proximity to the study area and structural features. Modified from Hentz and Ruppel (2010).

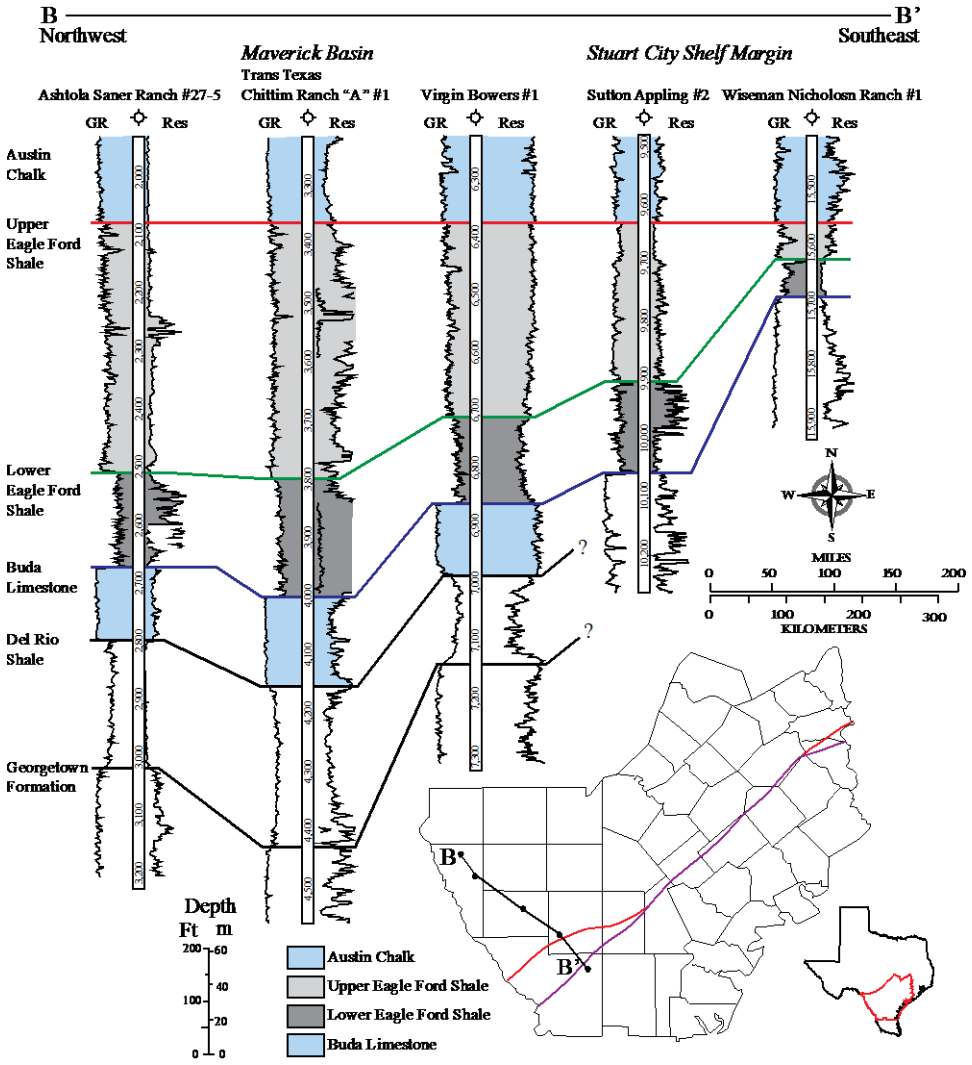

Figure 12: Dip oriented cross section (B—B') showing thickness and stratigraphic trends of the Eagle Ford and related sections from the Maverick Basin to the Sligo shelf margin. Refer to Figures 4 and 7 to see its proximity to the study location and structural features. Modified from Hentz and Ruppel (2011).

East Texas: East Texas Basin to San Marcos Arch

In East Texas, some of the earliest divisions of the Eagle Ford were identified in outcrop by Moreman (*in* Sellards *et al.,* 1932). In ascending stratigraphic order, the Eagle Ford is divided into the Tarrant, Britton, and Arcadia Park Formations (Figure 10). The type locality for the Tarrant Formation is in Tarrant County, Texas and ranges from 4.5 m to 6.0 m thick (15 to 20 ft.). The Tarrant constitutes the basal unit of the Eagle Ford and consists of interbedded calcareous, brownish-to light-gray sandy clays, siltstones, and shales (Brown and Pierce, 1962). The Britton overlies the Tarrant and ranges from 76 m to 91 m thick (250 ft. to 300 ft.) near its type locality in Ellis County, Texas (Brown and Pierce, 1962). The lower Britton lithology consists of dark-brown to olive-gray silty to chalky shales interbedded with bentonite seams, very fine-grained sandstones and thin laminae of calcarenites that grade upward into bluish-gray chalky shales (Christopher, 1982). The upper part of the Britton consists of dark-gray clay-shale with minor quartz silt and abundant small, flattened, reddish-brown clay-ironstone nodules and light-gray limestone concretions (Christopher, 1982). The Arcadia Park ranges from 30.5 m to 36.5 m thick (100 ft. to 120 ft.) and constitutes the uppermost Eagle Ford (Jiang, 1989). The type locality for the Arcadia Park section is in Dallas County, Texas where it consists of 6 m (20 ft.) of basal blue clay, 0.3 m to 1.0 m (1 ft. to 3 ft.) of thinly bedded limestone flags, and 23 m (75 ft.) of blue shale containing various sizes of calcareous concretions (Jiang, 1989).

The Eagle Ford Group thins southwestward toward the San Marcos Arch where changes in nomenclature and lithology of the Tarrant, Britton, and Arcadia Park Formations also occur. Near Waco and Austin, Texas (Figure 5) the Eagle Ford is subdivided into the South Bosque and Lake Waco Formations (Figure 10). The South Bosque Formation ranges from 36.5 m to 49 m thick (120 ft. to 160 ft.) and can be divided into two parts. The lower part consists of laminated calcareous shale, interbedded with silty limestone flags. The upper part consists of a dark-gray to black, fossiliferous shale or mudstone (Jiang, 1989). The Lake Waco Formation varies from 18 m to 24 m thick (60 ft. to 80 ft.) and consists of a grayish-white to brownish-gray flaggy limestone and a dark to bluish gray, silty, calcareous shale with bentonite (Jiang, 1989).

Further to the southeast along the northeast flank of the San Marcos Arch (Figures 5 and 7), the lithology of the Buda to Austin Chalk interval changes dramatically with the addition of the Woodbine Group, Pepper Shale, and the Maness Formation (Figure 10; Hentz and Ruppel, 2010). The Woodbine Group is unconformably overlain by the Eagle Ford. It includes a lower, shaly sandstone unit and an upper, sandy shale unit with thin fossiliferous sandstone interbeds (Lee, 1997). The Woodbine Group pinches out toward the southeast into the Pepper Shale along the northwestern flanks of the San Marcos Arch (Figures 5 and 7). The Pepper Shale is 15 m thick (49 ft.) at its type locality in Bell County, Texas (Figure 1) and is a fossiliferous, black, lustrous shale that is purplish when dry (Loeblich, 1946). Underlying the Woodbine Group and Pepper Shale is the

Maness Formation, which conformably overlies the Buda Formation (Figure 10; Loeblich and Tappan, 1961). The Maness extends from the East Texas Basin to the southwest edge of the San Marcos Arch. It is characterized by an overall higher gamma ray signature than the overlying mudrocks (Ambrose *et al.*, 2009).

CHAPTER IV: DATA AND METHODS

Core and Thin Section Analyses

Four representative cores drilled through part or all of the Eagle Ford were selected from a number of conventional cores collected by EOG Resources, Inc. within the current play area (Table 1, Figure 4). These cores were selected based upon the following criteria: 1) completeness of cored interval, 2) availability of conventional wire-line log suites (i.e. gamma ray, bulk density), 3) availability of core analyses, 4) well location, and, 5) regional dissimilarities in lithology and reported production.

Each of the four cores was used to: 1) analyze facies (and microfacies) for interpretation of depositional environments, 2) determine facies successions and establish a hierarchal classification of vertical stacking patterns, 3) identify sequence-/cyclostratigraphically significant surfaces and horizons, 4) delineate recognized associations of intervals with reservoir-quality porosity and permeability values and specific facies and/or boundaries.

The core interval described was stratigraphically constrained to the upper and lower boundaries of the Eagle Ford section. Three of the cores include portions of formations directly overlying and underlying the Eagle Ford. The T.R. Marshall #1 is the only incomplete core. Based on gamma ray logs, approximately 15 m (50 ft.) of basal Eagle Ford is missing.

The core was described on a centimeter-scale using Swanson's (1981) Sample Examination Manual as a rudimentary guide. Descriptions include details of lithology, grain types, Dunham (1962) textural classification (Figure 13), Choquette and Pray (1970) classification of pore types (Figure 14), dry color (Munsell Color Chart), sedimentary structures, diagenetic features, and biotic content.

Thin sections and thin section photomicrographs were obtained throughout the entire described interval of each core and were utilized to augment initial hand sample-scale core observations (Table 1). Photomicrographs were taken with a Leica M420 microscope equipped with a Leica DC 480 camera at the Michigan Geological Repository for Research and Education (MGRRE) facilities at Western Michigan University. Additional photomicrographs were taken during the preparation of standard (1" x 1 7/8") and over-size (2" x 3") thin sections by Weatherford Laboratories. These were cut ultra-thin (20 µm) and impregnated with blue epoxy to recognize and evaluate the distribution of porosity. Thin sections were commonly stained on one half of each slide with alizarin-red and potassium ferricyanide to provide mineralogical, and some qualitative elemental, data of carbonate minerals. Staining with alizarin-red helps distinguish calcite from dolomite, and potassium ferricyanide facilitates differentiation of ferroan and non-ferroan carbonate minerals (Adams and MacKenzie, 1998, Scholle and Ulmer-Scholle, 2003). A list of carbonate minerals and their diagnostic stains are outlined in Table 2.

Preexisting thin sections from the T.R. Marshall #1 (175) and Hundley #1 (32) cores provided adequate coverage and did not require additional sampling. The Hill #1 (67) and Nixon #6 (66) cores were selectively sampled to collect representative and detailed data of lithofacies. Thin sections were utilized to help evaluate vertical and lateral heterogeneities from within higher frequency cycles determined from core description, while also enabling more detailed observation of diagenetic features and alterations (i.e. cementation, recrystallization, and dissolution).

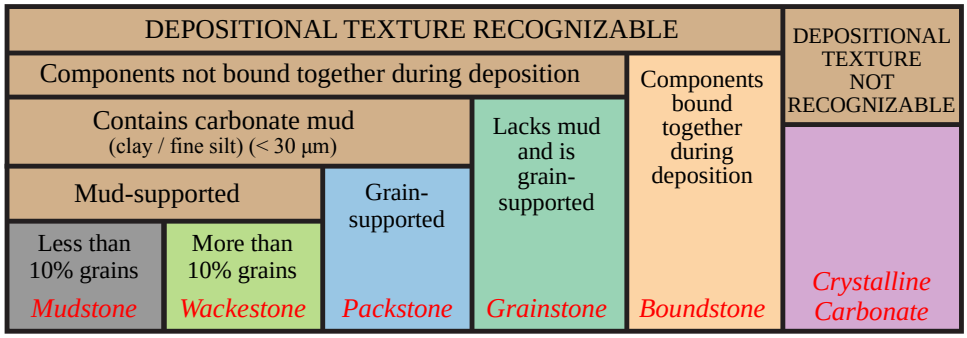

Figure 13: Diagrammatic representation of the Dunham (1962) classification of carbonate rocks according to depositional textures and whether a rock is matrix (mud) or framework (grain) supported. Modified after Scholle and Ulmer-Scholle (2003).

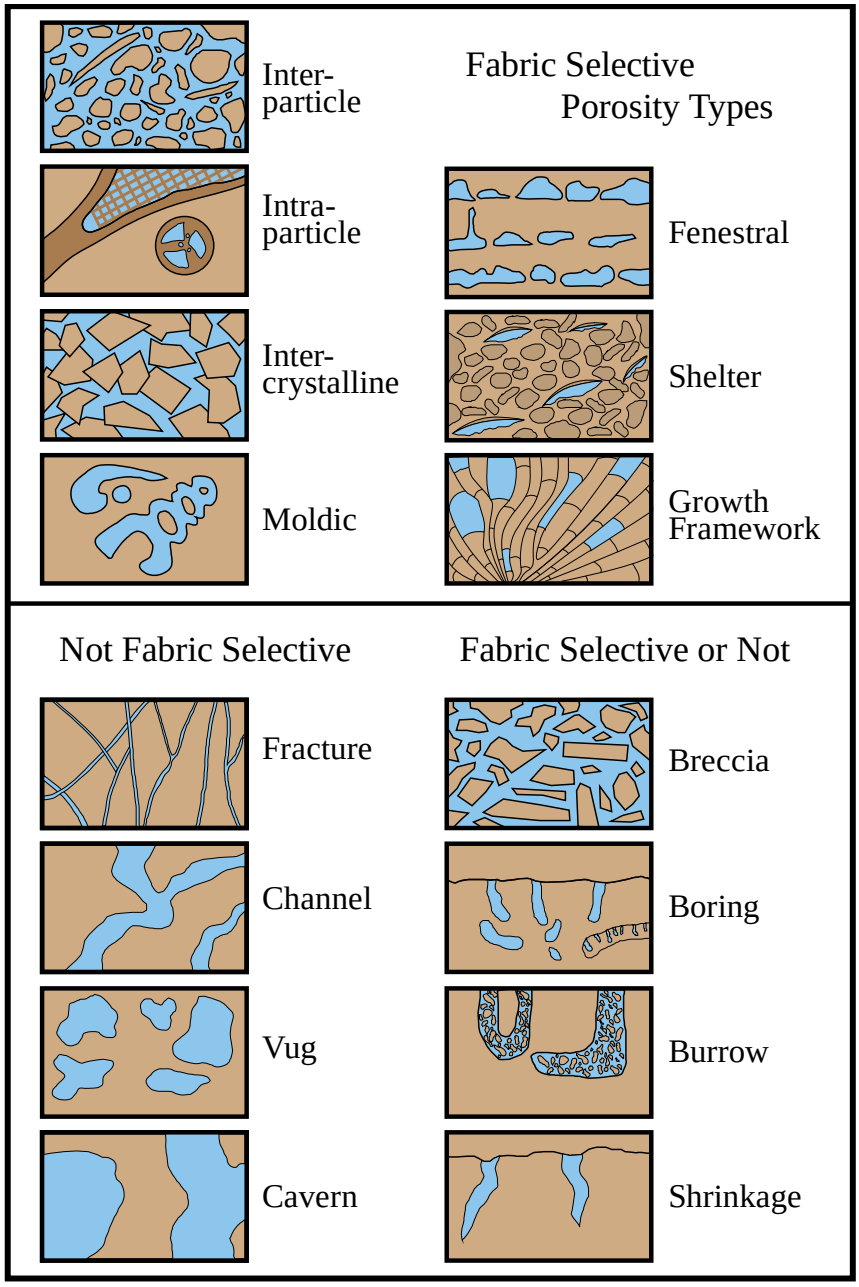

Figure 14: Diagrammatic representation of the Choquette and Pray (1970) classification of pore types in carbonate rocks. Diagram portrays the basic fabric-selective and non-fabric selective types of porosity. Modified from Scholle and Ulmer-Scholle (2003).

	Mineral	Typical Color from Staining		Effects of Etching on Relief	Combined Result
		Alizarin Red S	Potassium Ferricyanide		
Calcite	Low-Mg	Colorless			
	High-Mg	Purple			
	Non-Ferroan	Pink to red-brown	None	Considerable (reduced)	Pink to red-brown
	Ferroan (Fe^{2+})	Pink to red-brown	Pale to deep blue	Considerable (reduced)	Mauve to blue
Dolomite	Non-Ferroan	None	None	Negligible (maintained)	Unstained
	Ferroan (Fe^{2+})	None	Very pale blue	Negligible (maintained)	Very pale blue (may appear turquoise or greenish in thin section)

Table 2: Summarization of the common results from etching and staining carbonate minerals with alizarin-red and potassium ferricyanide based on Scholle and Ulmer-Scholle (2003) and Adams and MacKenzie (1998). Similar optical properties shared by calcite and dolomite make visual estimates of mineralogy difficult. Staining techniques provide a reliable method utilized to assist in mineral determination, and provide some qualitative elemental data on carbonate phases.

Gas Shale Core Analysis

Petrophysical data from full-diameter gas shale core analyses were available from three wells included in this study (Table 1). Data were commercially measured and obtained from Core Laboratories, Inc. These data include sample depth, matrix permeability, percent porosity, gas-filled porosity, gas saturation, gamma ray, and bulk density measurements. Techniques and methods employed by gas shale core analyses are optimized for shale formations where reservoir properties are laterally and vertically heterogeneous, and may not

be accurately represented in conventional whole core or plug measurements (Honarpour *et al.*, 2003; Perez *et al.*, 2010). This study accepted gas shale core analysis data as the fundamental measure of reservoir quality and used these data to delineate associations of intervals with enhanced/marginal porosity and permeability values and particular facies and/or boundaries.

X-ray Diffraction (XRD) Analysis

Samples collected for thin section preparation were also commonly analyzed using X-ray Diffraction (XRD) to provide a qualitative or semiquantitative determination of whole rock and clay mineralogy. X-ray diffraction analysis and interpretation were performed by Core Laboratories, Inc. and Weatherford Laboratories in accordance with the general methods described by Hardy and Tucker (1988). These data were used to estimate mineralogy, and to help substantiate interpretations of lithologic variability, depositional cyclicity, and depositional setting.

Wire-line Log Analysis

Wire-line log responses record petrophysical attributes of a rock formation's character. Interpretation of geological information from petrophysical data is a major task in reservoir characterization and modeling (Grammer *et al.*, 2004). Using core, depositional facies were identified and categorized into a

hierarchal stacking pattern. Depositional facies were integrated into Petra®, a geological data management and display software, to ground-truth conventional wire-line log data with core interpretations (i.e. gamma ray, bulk density, and porosity). Once calibrated to core, wire-line logs were used to make regional correlations of depositional facies and sequences.

Data Limitations

The characterization of the Eagle Ford reservoir in this study is fundamentally limited by the number and spatial distribution of available core and core data (Table 1; Figure 4). This group of wells is believed to represent the regional character of the Eagle Ford within study area; however, the regional distribution of these wells may not accurately represent local variations in lithology or reservoir character (Tables 1; Figures 1 and 7). Future studies might expand the current investigation by incorporating additional cores and subsurface data to overcome these limitations.

Gas shale core analyses data were limited to three of the cores. These samples and thin sections are limited and unevenly distributed between cores and depositional facies. As a result, core and-/or facies may be misrepresented. Future studies might overcome this by consistently sampling both cores and facies.

CHAPTER V: DEPOSITIONAL SYSTEM EVALUATION

Facies Associations

Eight lithofacies were identified through the analyses of four cores (339 total linear meters; 1,113.0 ft.) (Table 1). They were defined based upon texture, grain types, sedimentary structures, diagenetic features, biotic content and color (Munsell Color Chart). Core observations were augmented by the review of 289 ultra-thin sections (20 μm). Thin sections were stained with alizarin-red and potassium ferricyanide to provide mineralogical, and some qualitative elemental data about the carbonate minerals that were present. XRD analyses were integrated to aid in the identification and determination of mineralogical abundance within each lithofacies identified. Table 3 provides a detailed summary of each facies and their characteristics. Facies are described in a shallowing upward sequence (Figure 15):

1. Laminated Argillaceous Mudstone
2. Weakly Laminated Calcareous Foraminiferal Mudstone
3. Laminated Foraminiferal Wackestone
4. Bioturbated Skeletal Lime Wackestone
5. Laminated Inoceramid and Foraminiferal Wackestone to Packstone
6. Skeletal Packstone to Wackestone
7. Foraminiferal Packstone to Grainstone
8. Massive to Bioturbated Claystone (Volcanic Ash)

	Facies	Color	Dominant Mineralogy (Avg. %)			Sedimentological Character	Primary Grain Constituents	TOC	Matrix Permeability	Gas-Filled Porosity	Gas Saturation	No. of Samples
			Clays	Quartz	Calcite			(Avg. %)	(nD)	(%)	(%)	
1	Laminated Argillaceous Mudstone	Dark Greenish Black to Black	42.71 (n=14)	20.54 (n=14)	25.21 (n=14)	Fissile, Planar Laminated (mm), Localized Burrowing	Planktonic Foraminifera	3.29 (n=8)	1.94	2.61	26.11	*10*
2	Weakly Laminated Calcareous Foraminiferal Mudstone	Brownish Black to Olive Black	20.32 (n=51)	13.25 (n=51)	57.60 (n=51)	Planar, and truncated and wavey Ripple Laminae (mm), Erosive Bases, Localized Burrowing	Globigerinid Foraminifera, Fragmented Inoceramid Bivalves	3.71 (n=38)	2.35	3.28	32.02	*25*
3	Laminated Foraminiferal Wackestone	Light-to-Medium Grey	11.80 (n=27)	9.19 (n=27)	71.47 (n=27)	Planar and Ripple Laminae, Localized Burrowing	Globigerinid Foraminifera	2.46 (n=12)	1.70	2.67	49.49	*15*
4	Bioturbated Skeletal Lime Wackestone	Light Bluish Grey to Medium Dark Grey	5.37 (n=17)	4.59 (n=17)	86.04 (n=17)	Bioturbated, Mineralized Fractures	Bivalve Fragments and Undifferentiated Skeletal Material	0.82 (n=16)	5.85	4.46	54.11	*2*
5	Laminated Inoceramid and Foraminiferal Wackestone to Packstone	Black to Medium Bluish Grey	16.50 (n=2)	12.50 (n=2)	64.00 (n=2)	Imbricated- and Cross-Bedded Skeletal Debris (mm-cm), Planar Laminae (mm)	Fragmented Inoceramid bivalves, Globigerinid Foraminifera, Peloids, Phosphatic Grains	1.89 (n=1)	1.11	2.77	47.73	*2*
6	Skeletal Packstone to Wackestone	Medium-to-Light Grey	11.73 (n=11)	4.73 (n=11)	78.15 (n=11)	Cross Laminated and Imbricated bedding, Scour Surfaces, Fining Upward Sequences (cm)	Globigerinid Foraminifera, Fragmented Inoceramid Bivalves, Ostracods, Phosphatic Grains	0.98 (n=13)	0.24	2.19	46.74	*4*
7	Foraminiferal Packstone to Grainstone	Light Grey	4.63 (n=15)	7.56 (n=15)	84.19 (n=15)	Planar and Ripple Laminae (mm), Recrystallized, Mineralized Fractures	Planktonic Foraminifera	0.57 (n=2)	1.18	2.10	32.68	*7*
8	Massive to Bioturbated Claystone (Volcanic Ash)	Greenish Grey to Pale Olive	43.83 (n=4)	6.38 (n=4)	30.98 (n=4)	Massive Bedded, Localized Bioturbation	NA	NA	NA	NA	NA	*0*

Table 3: Outline of the facies identified in Eagle Ford cores including the primary sedimentological characteristics, grain constituents and average total organic carbon (TOC) associated with each facies. Measurements of key reservoir properties (porosity and permeability) are averaged from each well with the total number of measurements included.

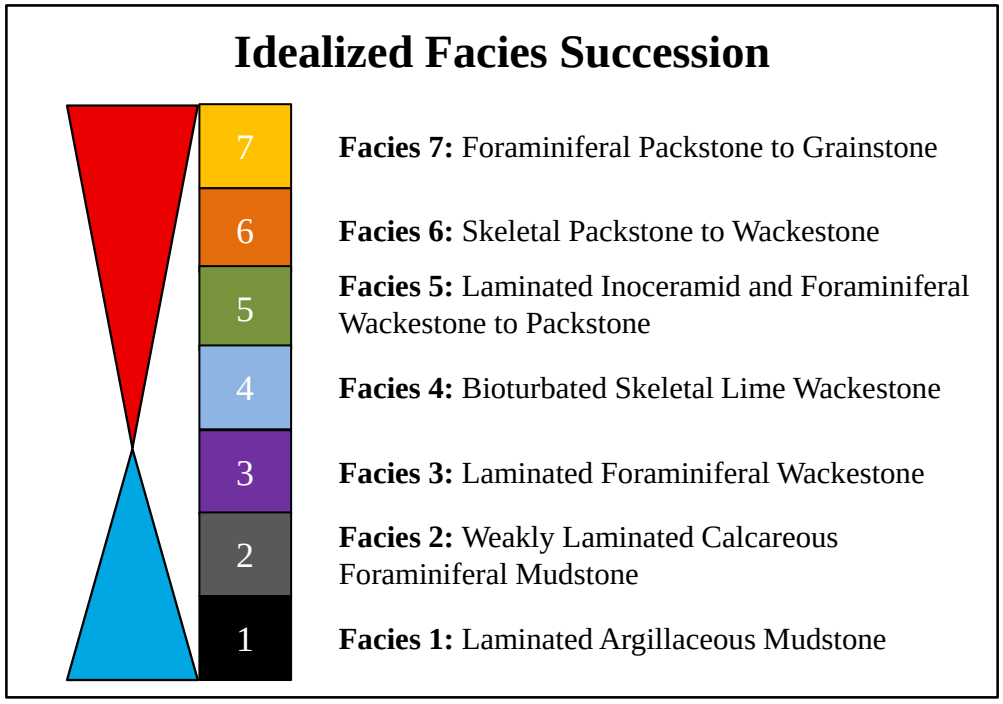

Figure 15: Idealized shallowing-upward facies succession observed in the Eagle Ford section. Shown are the anticipated facies stacking patterns given uniform sedimentation/subsidence, change in relative sea level, and not accounting for autogenic sedimentation influences.

The massive to bioturbated claystone facies represent volcanic ash deposits and are not a depositional facies used for interpretations of depositional environments. Volcanic ash beds are well recognized within the Eagle Ford with suggested source areas in Arkansas, West Texas, and the Western Interior (Driskill *et al.*, 2010; Harbor, 2011; Donovan and Staerker, 2010; Lock *et al.*, 2010; Dean and Arthur, 1998; Kauffman, 1984).

Organically-enriched dark shales are typically viewed as having lithological, geochemical, and biological characteristics that collectively indicate long-term stagnant, anaerobic to dysaerobic conditions at the sediment-water interface (e.g. modern Black Sea- as described by Kauffman and Sageman, 1990). The identification of macro- and micro-fossil assemblages in dark shales, and recognized variations in their distribution, are helpful in paleoenvironmental interpretations and depositional modeling. Though important environmental indicators, discretion must be applied as the distribution of faunal assemblages exhibit small scale variations in response to cyclic environmental and/or preservational changes incurred through diagenetic alteration (Arthur *et al.*, 1990).

The dominant fauna identified in these cores consist of inoceramids, planktonic and benthonic foraminifera, and calcispheres. Planktonic foraminifera are the primary constituent near the base of the Eagle Ford and decrease in abundance up-section. Benthonic foraminifera are absent lower in the section and become increasingly abundant up-section. Calcispheres are commonly observed throughout the core, whereas inoceramids are most abundant lower in the cores. Trends in the occurrence and relative abundance of these fauna indicate initial, deeper-water, lower-energy, and oxygen-deficient environments that transition upward into shallower, higher-energy and better-oxygenated environments. Identification of, and interpretations based on these fauna are consistent with previous work conducted on similar, and age-related rocks (Harbor, 2011; Hentz

and Ruppel, 2011; Hull, 2011; Peschier, 2011; Phelps, 2011; Donovan and Staerker, 2010; Grosskopf, 2010; Hentz and Ruppel, 2010; Lock *et al.,* 2010; Lock and Peschier, 2006; Lock *et al.,* 2001; Kauffman and Sageman, 1990; Weimer, 1990, Jiang, 1989; Travino, 1988; Kauffman, 1984; Loeblich and Tappan, 1961; Loeblich, 1946).

Inoceramid bivalves are well known organisms from Cretaceous sediments throughout the Western Interior and Gulf Coast regions (e.g. Greenhorn and Niobrara, Boquillas, and Eagle Ford formations; Refer to Grosskopf, 2010; Lock *et al.,* 2010; Phelps, 2010; Lock and Peschier, 2006; Kauffman and Sageman, 1990; Weimer, 1990, Travino, 1988; Kauffman, 1984). Inoceramid shells are characterized by two distinctive layers, an outer layer composed of calcite and an inner layer composed of aragonite (Grosskopf, 2010). Inoceramids are believed to have adapted to, and been able to inhabit low-oxygen environments unsuitable for other benthic organisms (Kauffman and Sageman, 1990).

Planktonic and benthonic foraminifera are chambered, unicellular, heterotrophic protists that range from 0.1 mm to 1.0 mm in size and are generally restricted to shallow-marine, nutrient-rich waters within the photic zone (Flügel, 2010; Scholle and Ulmer-Scholle, 2003; Haq and Boersma, 1978). Benthonic foraminifera primarily construct high or low Mg-calcite tests and dwell on or in sediments on the sea floor (Flügel, 2010; Scholle and Ulmer-Scholle, 2003; Haq and Boersma, 1978). Planktonic foraminifera construct low Mg-calcite tests and

inhabit water depths between 50 m to 100 m (164 ft. to 328 ft.) (Flügel, 2010; Scholle and Ulmer-Scholle, 2003; Haq and Boersma, 1978). Planktonic and benthonic foraminifera are important index fossils used to determine biostratigraphic zonations and serve as proxies for paleoceanographic, paleoclimatologic and paleobathymetric reconstructions particularly in Cretaceous age sediments (Flügel, 2010).

Calcispheres are spherical, single-or-double walled, calcitic microfossils found with-or-without openings or pores and range from 10 µm to 100 µm in size (commonly about 40 µm) (Flügel, 2010; Scholle and Ulmer-Scholle, 2003; Adams and MacKenzie, 1998). The origin of these microfossils is not definitive, but they are commonly interpreted as algal cysts, often associated with pelagic foraminifera, calpionellids and radiolarians found in upper slope and basinal carbonates, as well as outer shelf carbonates of low- and mid-latitude settings (Flügel, 2010; Tucker, 2001).

Lithofacies

Laminated Argillaceous Mudstone

Laminated argillaceous mudstones are variable in thickness and are characteristically fissile and dark greenish-black to black in color. Observed thicknesses of this facies range from less than 1.5 m (5 ft.) to greater than 11 m (35 ft.). These deposits exhibit massive-to-planar laminated internal fabrics within

a clay- to silt-sized matrix (0.06µm to 62.5µm). In hand sample, individual laminae are horizontally layered and typically less than 0.5 cm thick (0.2 in). Thin sections show evidence of sub-millimeter scale traction laminae, consisting of climbing and undulatory ripples with organic-rich mud drapes (Figure 16 B). Pyrite and phosphate grains are common in thin section and core (Figure 16 A). The calcareous skeletal component consists primarily of planktonic foraminifera (globigerinid) and inconsistent distributions of bivalve fragments (inoceramid) that are commonly oriented parallel to bedding (Figure 16 C and D). Local zones show evidence of bioturbation where sediments are mottled.

Mineralogy was determined through comparison of thin sections and XRD analyses (14 samples) from each core. These data show that this facies consists predominantly of clay minerals (avg. 43%, range 18-71%), calcite (25%, range 1.5-57%), quartz (avg. 21%, range 2-32%), and plagioclase and K-feldspar (avg. 3%, range 0.5-8%). Thin sections stained with alizarin-red and potassium ferricyanide indicate calcite is non-ferroan. The clay mineral fraction consists of nearly equal amounts of illite (avg. 17%), mixed illite/smectite (avg. 15%) and kaolinite (avg. 11%). This facies is organic rich with an average TOC of 3.3% and a range from 2.3-5.3% (8 samples). Visible porosity within this facies in thin section and core is 0.0% (Figure 16).

Laminated argillaceous mudstones are interpreted as transgressive deposits and represent deposition by pelagic and hemipelagic suspension settling near storm-wave base. Thin sections reveal sub-millimeter scale traction laminae

that indicate episodic reworking by winnowing currents (Figure 16 B). Elevated organic content, dark color, general absence of bioturbation and the paucity of benthic organisms are evidence of oxygen deficient water conditions during deposition (Flügel, 2010).

Laminated argillaceous mudstones are most common at the base of the Eagle Ford, directly above the Buda Limestone. This transition is characterized by a sharp, erosive surface with rip-up clasts and grain beds and interpreted as a type 3 sequence boundary. Type 3 sequence boundaries correspond to platform drowning events and are produced when sea level rises faster than the system can aggrade so that a transgressive systems tract directly overlies the preceding highstand systems tract and are often accompanied by significant marine hiatuses and erosion surfaces (Schlager, 2005). Laminated argillaceous mudstones transition gradually into weakly laminated calcareous foraminiferal mudstones. The boundary between these facies is indistinct and determined based on visual observations of rock character (e.g. loss of shale partings and fissile nature) and changes in composition from XRD data (e.g. quartz and clay minerals decrease while calcite increases).

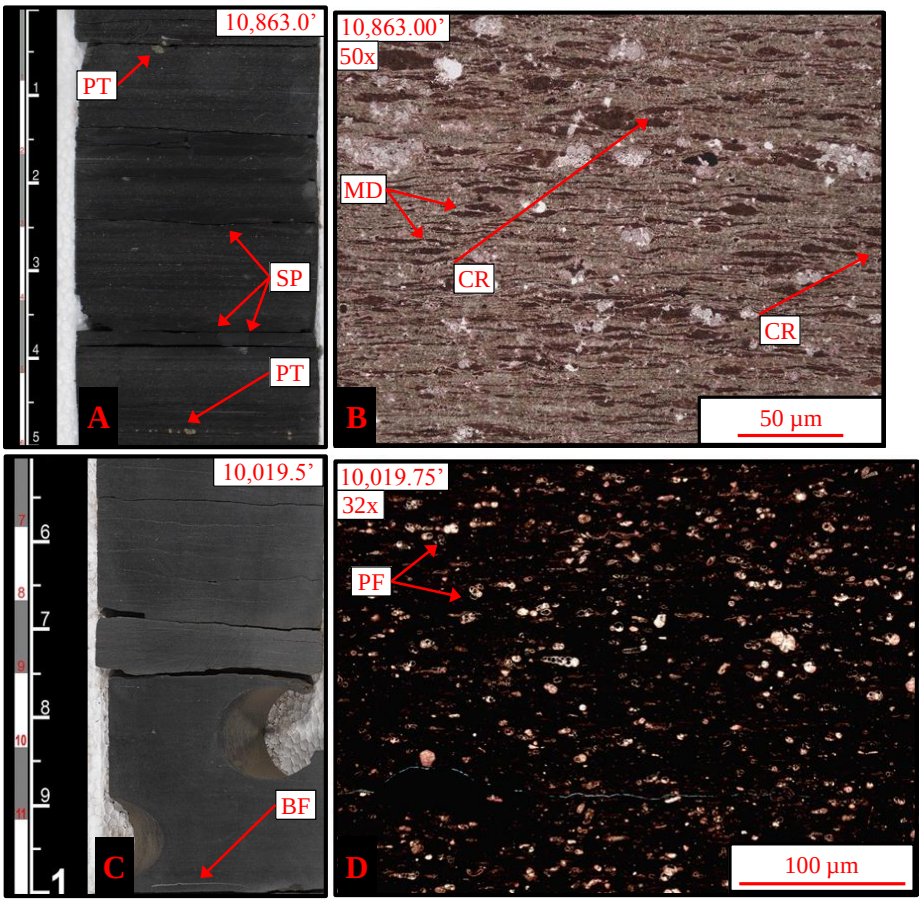

Figure 16: Facies 1 core and thin section photomicrographs. (A) Core photograph illustrating the characteristic dark greenish black to black, fissile nature of laminated argillaceous mudstones with visible shale partings (SP) along laminae, Hill #1, 3,311.0 m to 3,311.2 m (10,863.0 ft. to 10,863.5 ft.); (B) Thin section from core photo (A) showing evidence of sub-millimeter scale climbing ripples (CR) with organic-rich mud drapes (MD), Hill #1; 3,311.0 m (10,863.0 ft.); (C) Core photo showing massive fabric and a rare occurrence of bedding- parallel bivalve fragments (BF), Hundley #1, 3,054.0 m to 3,054.1 m (10,019.5 ft. to 10,020.0 ft.); (D) Stained thin section from core in photo (B) showing calcareous tests of planktonic foraminifera (PF)

within an organic-rich matrix, Hundley #1, 3,054.0 m (10,019.75 ft.).

At the base of the Eagle Ford, the thickness of this facies changes considerably (10 m to 1.5 m; 35 ft. to 5 ft.) and shows a progressive thinning trend that extends from the northeast to the southwest. XRD and thin section data show similar trends in the abundance of detrital quartz which decreases southwestward and planktonic foraminifera which increases to the southwest. These trends indicate that areas to the northeast, nearer the San Marcos Arch, were located closer to and therefore more strongly influenced by terrigenous clastic sources. This interpretation is consistent with previous work that suggests the San Marcos Arch served as a buffer and protected areas to the southwest from terrigenous clastics derived from the East Texas Woodbine Delta (Driskill et al., 2012).

The laminated argillaceous mudstone facies is regionally consistent where it is most prevalent at the base of the Eagle Ford. Additional intervals occur locally within the Eagle Ford section that range from 0.3 m to 2.0 m thick (1 ft. to 7 ft.) and show consistent sedimentologic character and composition. Multiple occurrences of this facies were observed in two of the four cores indicating these intervals lack the regional continuity typical of the argillaceous mudrocks at the base of the Eagle Ford. The reoccurrence of this facies may reflect periodic rejuvenation of sediment source areas in Oklahoma and Arkansas (Harbor, 2011).

Weakly Laminated Calcareous Foraminiferal Mudstone

The weakly laminated calcareous foraminiferal mudstone facies is organic-rich and brownish-black to olive-black in color (Figure 17). Millimeter-scale planar, and truncated and wavy ripple laminae consist primarily of well-sorted planktonic foraminifera within a clay- and silt-size matrix (0.06 μm to 62.5 μm) (Figure 17 A and C). The abundance of traction laminae increases upsection toward the top of the Eagle Ford. Fragmented inoceramids are common accessory grains and exhibit both random and bedding parallel orientations (Figure 17 A). Less common components include pyrite and phosphate grains. Mottled intervals are locally present and are generally less than 10 cm (4 in.) thick.

Combined XRD analyses (51 samples) show this facies consists predominantly of calcite (avg. 58%, range 28-85%), clay minerals (avg. 20%, range 3-45%), quartz (avg. 13%, range 4-24%), and plagioclase and K-feldspar (avg. 3.5%, range 1-7%). Thin sections stained with alizarin-red and potassium ferricyanide indicate calcite is non-ferroan. With respect to the laminated argillaceous mudstones, clay mineral compositions are less equally divided between mixed illite/smectite (avg. 10%), illite (avg. 8%) and kaolinite (avg. 2%). Overall, this facies shows elevated TOC values averaging 3.7% with a range of 0.2%-6.1% (38 samples). TOC values greater than 2.0% are prevalent and occur 71% of the time (27 samples) with an average TOC of 4.9%. In core and thin section, visible porosity within this facies is 0.0% (Figure 17).

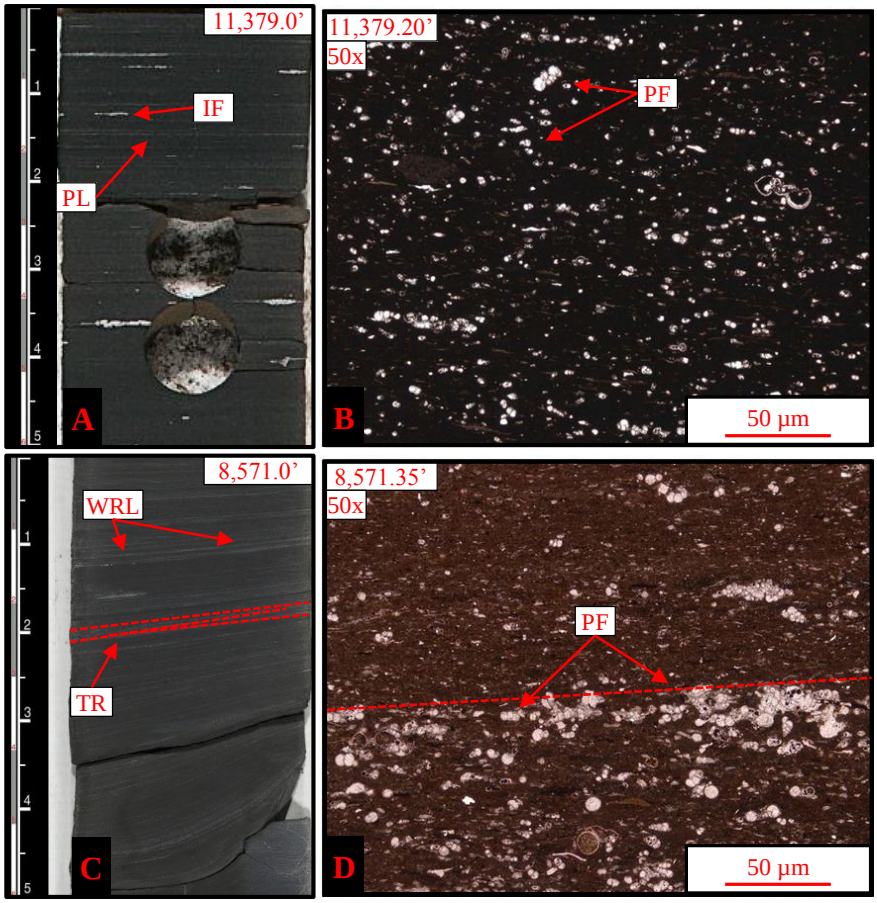

Figure 17: Facies 2 core and thin section photomicrographs. (A) Core photograph showing weak millimeter-scale planar laminae (PL) and oriented inoceramid fragments (IF), T.R. Marshall #1, 3,468.3 m to 3,468.5 m (11,379.0 ft. to 11,379.5 ft.); (B) Thin section photomicrograph from core in photo (A) showing planktonic foraminifera tests (PF) within a black, organic-rich matrix, T.R. Marshall #1, 3,468.4 m (11,379.2 ft.) (C) Core and thin section photo (D) portraying concentrations of planktonic foraminifera tests (PF) along weak planar and millimeter-scale truncated (TR) and wavy ripple laminae (WRL) indicative of

intermittent reworking by low-energy winnowing currents, Nixon #6, 2,612.4 m to 2,612.6 m (8,571.0 ft. to 8,571.5 ft.); (D) Photomicrograph from core in photo (C) of Nixon #6, 2,612.5 m (8,571.35 ft.).

Based on observations from core and thin-section analysis, weakly laminated calcareous foraminiferal mudstones are interpreted as transgressive- to early highstand- deposits that were deposited in an oxygen-deficient, low-energy environment below storm wave base. Evidence supporting oxygen-deficient bottom water conditions include: 1) dark color, 2) high organic content, 3) abundance of planktonic foraminifera and inoceramids, 4) the absence or rareness of benthic organisms, and 5) fine planar laminations (Flügel, 2010). The prevalence of planar laminations in contrast to truncated and wavy ripple laminae indicate primary sedimentation by pelagic and hemipelagic suspension settling with intermittent reworking by low-energy currents (Tucker, 2001). Isolated intervals have mottled textures. These intervals are believed to represent short lived periods of increased oxygenation on the sea floor and are well documented in similar organic-rich pelagic sediments (Tucker and Wright, 1990; Longman *et al.*, 1998; Stefani and Burchell; 1990; Fischer *et al.*, 1990). Though scarce, individual burrows were identified in previous work as *Chondrites* traces which are commonly associated with low oxygen conditions (Harbor, 2011; Lock *et al.*, 2010; Lock and Peschier, 2006).

Laminated Foraminiferal Wackestone

Laminated foraminiferal wackestones are characterized by light- to medium-grey; millimeter-scale planar and traction laminations of calcareous skeletal debris within a black, organic-rich, clay- to silt-size matrix (0.06 µm to 62.5 µm). Traction laminae include millimeter-scale truncated and wavy starved ripples (Figure 18). Concentrations of well-sorted planktonic foraminifera and poorly-sorted inoceramid bivalve fragments constitute the dominant skeletal component (Figure 18). Though uncommon, additional grains include pyrite and phosphate. Local intervals have mottled textures. Microfractures are locally present and predominantly mineralized with calcite. Mineralized microfractures have also been reported by Dawson and Almon (2010).

Combined XRD analyses (27 samples) show calcite (avg. 72%, range 47-90%), clays (avg. 12%, range 2-34%), quartz (avg. 9%, range 2-19%), and plagioclase and K-feldspar (avg. 3%, range 1-6%) are the primary mineral constituents of the rock matrix. Thin sections stained with alizarin-red and potassium ferricyanide indicate calcite is non-ferroan. The clay mineral fraction consists of mixed illite/smectite (avg. 7.5%), illite (avg. 2.5%) and lesser amounts of kaolinite (avg. 1.8%). Based on 12 samples, TOC values average 2.5% and range from 0.5%-5.2%. There is no visible porosity within this facies in either core or thin section (Figure 18).

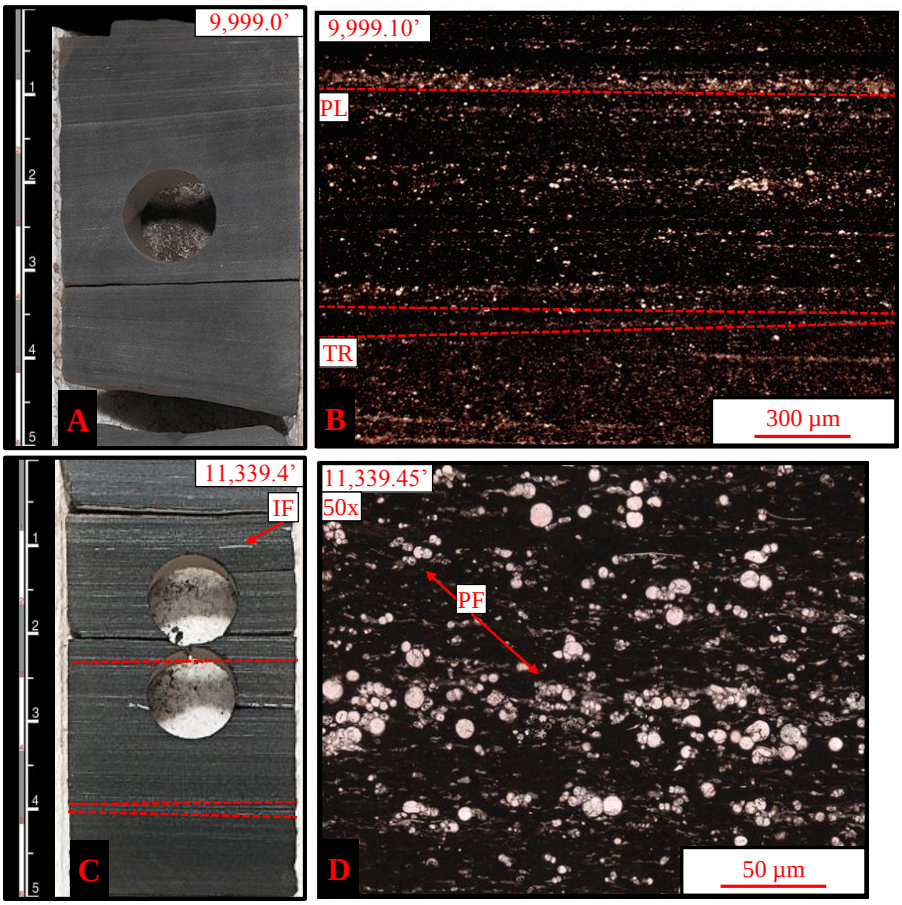

Figure 18: Facies 3 core and thin section photomicrographs. (A) core photograph illustrating the characteristic light- to medium-grey color of laminated foraminiferal wackestone facies, Hundley #1, 3,047.7 m to 3,047.8 m (9,999.0 ft. to 9,999.5 ft.); (B) Stained thin section from core in photo (A) showing millimeter-scale planar (PL) and truncated (TR) laminae within an organic-rich matrix, Hundley #1; 3,047.7 m (9,999.1 ft.); (C) Core photograph illustrating coarsening-upward trend with well-developed laminae of planktonic foraminifera tests (PF) and bedding parallel inoceramid fragments (IF), T.R. Marshall #1, 3,456.2 m to 3,456.4 m (11,339.4 ft. to 11,339.9 ft.); (D) Thin section photo from core in photo (C) showing abundant

planktonic foraminifera tests (PF) within a black, organic-rich matrix, T.R. Marshall #1, 3,456.3 m (11,339.45 ft.).

Laminated foraminiferal wackestone deposits are common throughout the Eagle Ford section and found interstratified cyclically with weakly laminated calcareous foraminiferal mudstone deposits. These facies are interpreted as late transgressive- to early-highstand deposits that accumulated primarily out of suspension settling in an oxygen-deficient environment near storm wave base where weak contour currents developed concentrations of foraminifera tests with well-defined erosive bases (Figure 18). Concentrations of skeletal material forming laminations with well-defined erosive bases suggest reworking by contour currents (Shanmugam, 1997; Tucker and Wright, 1990). The dark, organic-rich rock matrix and lack of benthic fauna support the interpretation of an oxygen-deficient environment.

Bioturbated Skeletal Lime Wackestone

The bioturbated skeletal lime wackestone facies is characteristically light-bluish-grey to medium-dark-grey (Figure 19). Pervasive bioturbation and homogenization is reflected by the absence of any hydrodynamic sorting preserved in thin section. This is illustrated by the ‘free floating’ nature of skeletal debris within a calcareous, micritic matrix (less than 4μm). Previous work identified *Zoophycos*, *Thallassinoides, Planolites,* and *Chondrites* traces (Harbor,

2011). Color changes relate to subtle variations in clay and organic matter content, both of which are minimal. Along with benthonic and planktonic foraminifera, undifferentiated bivalve fragments and ostracods are the dominant grain types (Figure 19). Additional grains associated with this facies include calcispheres and echinoid fragments. Microfractures mineralized with calcite are common and are rarely partially open (Figure 19).

XRD analyses (17 samples) show that the mineralogy of this facies is dominated by calcite (avg. 86%, range 75-92%) with lesser amounts of clays (5.4%), quartz (avg. 4.6%), and plagioclase and K-feldspar (1.8%). TOC values from bioturbated skeletal lime wackestone deposits average 0.82% (16 samples). In core and thin section, partially open microfractures are rare and represent the only visible porosity associated with this facies.

Bioturbated skeletal lime wackestone facies are common at the top of the Eagle Ford section and represent deposition during sea level highstands in an oxygenated, shallower-subtidal environment relative to facies 1, 2 and 3. This is indicated by the low organic content, light rock color, presence of benthic organisms and trace fossils (Flügel, 2010). Sedimentary structures are rare to absent due to pervasive bioturbation (Figure 19).

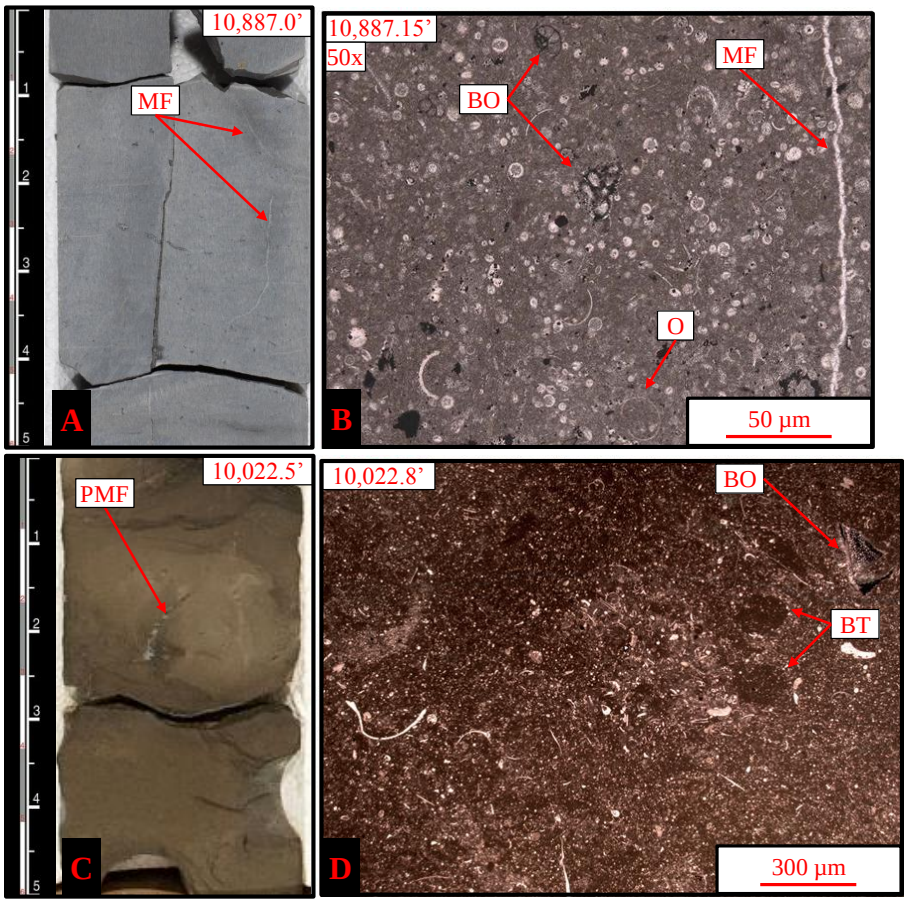

Figure 19: Facies 4 core and thin section photomicrographs. (A) Core photograph of light-bluish-grey bioturbated skeletal lime wackestone with microfractures (MF), Hill #1, 3,318.4 m to 3,318.5 m (10,887.0 ft. to 10,887.5 ft.). (B) Photomicrograph from core in photo (A) with abundant benthic organisms (BO), ostracods (O) and mineralized microfractures (MF), Hill #1; 3,318.4 m (10,887.15 ft.); (C) Core photograph of medium-dark-grey bioturbated skeletal lime wackestone facies with partially open microfracture (PMF), Hundley #1, 3,054.9 m to 3,055.0 m (10,022.5 ft. to 10,023.0 ft.); (D) Stained thin section from core in photo (C) illustrating the 'free floating' nature of undifferentiated skeletal debris and benthonic organisms (BO)

within a micritic matrix with visible burrow traces (BT), Hundley #1, 3,054.9 m (10,022.8 ft.).

Laminated Inoceramid and Foraminiferal Wackestone to Packstone

Laminated inoceramid and foraminiferal wackestone to packstone facies are characteristically black to medium-bluish-grey in color (Figure 20). This facies is characterized by an organic-rich, clay- to silt-size matrix (0.06 μm to 62.5 μm) with abundant whole and fragmented skeletal material. Centimeter-scale cross laminated beds have abraded bases and consist of poorly sorted skeletal debris that exhibit random and bedding parallel orientations. Disaggregated inoceramid valves and planktonic foraminifera constitute the dominant skeletal assemblage (Figure 20) with additional peloids, pyrite, phosphate, trace amounts of dolomite, and an assortment of undifferentiated skeletal debris.

The mineralogy of this facies is based on the XRD analyses of two samples. Mineral composition shown by these data include calcite (avg. 64%, range 64-64%), clays (avg.17%, range 14-19%), quartz (avg. 13%, range 11-14%), and plagioclase and K-feldspar (avg. 2%, range 1-3%). The clay mineral fraction is made of up illite (avg. 8.5%, range 3-14%), mixed illite/smectite (avg. 5%, range 2-8%) and minor amounts of kaolinite (avg. 2%, range 1-3%). The organic nature of this facies is based solely upon 1 sample that has a TOC value of 1.9%. Stained thin sections indicate calcite and dolomite are non-ferroan

(Figure 20 D). This facies has no visible porosity in either core or thin section (Figure 20).

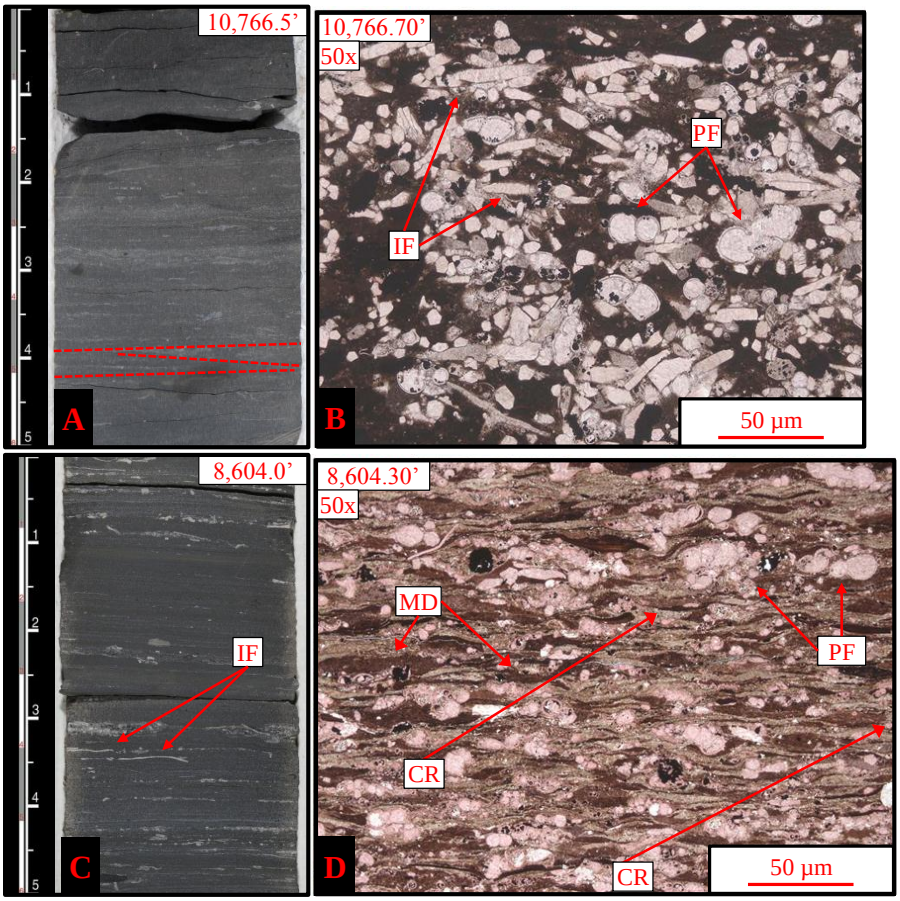

Figure 20: Facies 5 core and thin section photomicrographs. (A) Core photograph showing centimeter-scale cross laminated beds of skeletal debris, Hill #1, 3,281.6 m to 3,281.8 m (10,766.5 ft. to 10,767.0 ft.); (B) Photomicrograph from core photo (A) that shows disoriented and poorly sorted disaggregated inoceramids (IF) with planktonic foraminifera (PF), Hill #1; 3,281.7 m (10,766.7 ft.); (C) Core photograph with abundant inoceramid fragments (IF) oriented parallel to bedding, Nixon #6, 2,622.5 m to 2,622.7 m (8,604.0 ft. to 8,604.5 ft.); (D) stained thin section

from core photo (C) showing abundant planktonic foraminifera tests (PF) and evidence of sub-millimeter scale climbing ripples (CR) with organic-rich mud drapes (MD), Nixon #6, 2,622.6 m (8,604.3 ft.).

The thickest deposits of the laminated inoceramid and foraminiferal wackestone to packstone facies were observed near the top of the Eagle Ford section, whereas thinner intervals were common near the base of the Eagle Ford, overlying laminated argillaceous mudstone facies. These facies are interpreted as mid-highstand deposits that were deposited in an oxygen-deficient subtidal environment where higher-energy conditions periodically interrupted periods of lower-energy suspension sedimentation (Figure 20). Concentrations of skeletal material with well-defined erosive bases and centimeter-scale cross-laminations may indicate reworking by contour currents (Shanmugam, 1997; Tucker and Wright, 1990).

Skeletal Packstone to Wackestone

Skeletal packstone to wackestone deposits occur as fining-upward beds that are commonly made up of individual, centimeter-scaled, medium- to light-grey colored couplets (Figure 21). Sharply-defined bases and gradational upper boundaries are characteristic of these beds as well as the intercalated couplets. Beds are variable in thickness but often range from 5 cm to 20+ cm (2 in. to 8+

in.). Fining-upward sequences consist of moderate- to poorly-sorted, whole and fragmented skeletal material oriented both randomly and parallel to bedding. Planktonic foraminifera, fragmented bivalves and ostracods are the primary grain constituents. Phosphatic grains, peloids and undifferentiated skeletal debris are less abundant. Evidence of bioturbation is locally present where bed boundaries are homogenized and poorly defined.

XRD analyses (11 samples) show calcite (avg. 78%, range 58-90%), clay minerals (avg. 12%, range 1-28%), quartz (avg. 5%, range 3-7%), and plagioclase and K-feldspar (avg. 2%, range 1-3%) are the primary mineral constituents of the rock matrix. The clay fraction consists of mixed illite/smectite (avg. 10%, range 1-21%) and lesser amounts of illite (avg. 2%, range 1-4%), and kaolinite (avg. 1%, range 1-3.5%). The total organic carbon is generally low in skeletal packstone to wackestone deposits and average 0.98% (13 samples). Thin sections stained with alizarin-red and potassium ferricyanide indicate the carbonate content is primarily non-ferroan calcite with trace amounts of non-ferroan dolomite (Figure 21 C). There is no visible porosity in this facies in either core or thin section (Figure 21).

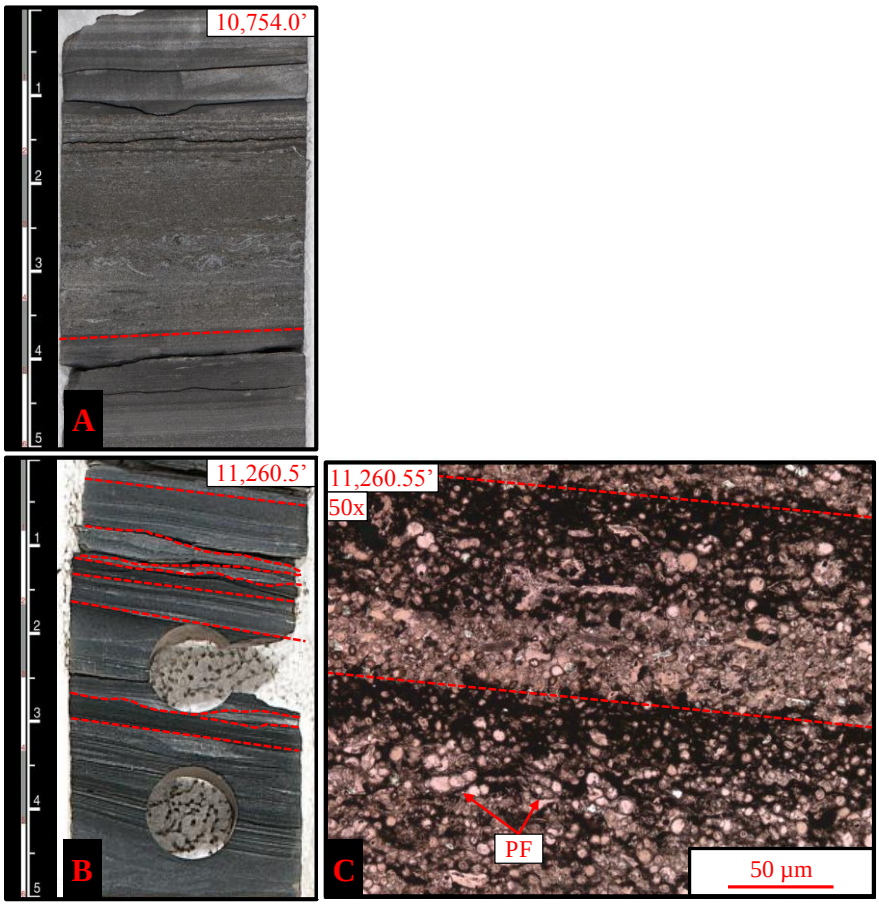

Figure 21: Facies 6 core and thin section photomicrographs. (A) Core photograph of a sharp based skeletal packstone to wackestone facies consisting of poorly sorted skeletal debris, Hill #1, 3,277.8 m to 3,278.0 m (10,754.0 ft. to 10,754.5 ft.); (B) Core photograph and thin section (C) showing thin, cyclically stacked units with sharp basal contacts, ripple cross-laminations, normal grading and planar laminations that are interpreted as turbidite deposits, (B) T.R. Marshall #1, 3,432.2 m to 3,432.4 m (11,260.5 ft. to 11,261.0 ft.); (C) T.R. Marshall #1, 3,432.2 m (11,260.55 ft.).

These are interpreted as mid- to late-highstand deposits. Sharply defined bases and normal grading are characteristic of these skeletal packstone to wackestone facies and indicate event sedimentation (Flügel, 2010). Turbidity current deposits (turbidites) are recognized as relatively thin (less than 0.3 m to 0.6 m thick; 1.0 ft. to 2.0 ft.), isolated units that often exhibit cyclical stacking patterns where multiple deposits collectively form 0.3 m to 3.0 m thick (1.0 ft. to 10.0 ft.) intervals (Asmus, 2012). Some intervals of this facies are interpreted to represent turbidite deposits based on normal grading, ripple cross-laminations, sharp basal contacts with load structures, gradational upper contacts with fluid escape structures, and planar laminations (Asmus, 2012; Mulder and Alexander, 2001; Cook and Mullins, 1983).

Foraminiferal Packstone to Grainstone

Foraminiferal packstone to grainstone deposits are characteristically light grey intervals that occur cyclically at the meter scale (Figure 22). Though variable in thickness, these deposits commonly range from 3 cm to 10s of cm thick (1 in. to 4+ in.) and show a progressive thinning trend up-section. These intervals exhibit both gradational and well-defined upper and lower boundaries (Figure 22). In core, microfractures are common and are frequently oriented oblique to faintly visible bedding planes. Microfractures are predominantly mineralized with calcite and rarely remain partially open (Figure 22 C). Accessory grains are very rare.

Original sedimentary structures are rarely visible, but faint laminations and burrow traces were observed (Figure 22 A and C).

XRD data show calcite (avg. 84%, range 73-91%) is the dominant mineral constituent with lesser amounts of quartz (avg. 7.5%, range 4-19%), plagioclase and K-feldspar (avg. 2%, range 0.8-3%), and clay minerals (avg. 4.5%, range 1-9%). TOC values for this facies average 0.57% (2 samples). Thin sections stained with alizarin-red and potassium ferricyanide indicate calcite is non-ferroan (Figure 22 B and D). Partially open microfractures were rarely observed in core and thin section, less than 1.0%, and represent the only visible porosity associated with this facies.

Foraminiferal packstone to grainstone facies are highly cyclic (meter scale) with calcareous foraminiferal mudstones and laminated foraminiferal wackestones and are interpreted as mid- to upper-slope, late-highstand to early-lowstand deposits that were subject to thorough syndepositional lithification. Core-based interpretations were made difficult by the near absence of original sedimentary structures. Because of this, interpretations were based on work along the margin of the Great Bahama Bank (ODP Leg 166; Sites 1006, 1007 and 1003) where calcareous periplatform sediments show similar, distinct cyclic variations (meter scale) in the mineralogy, grain size and faunal content of alternating well-cemented, light-grey and uncemented, dark-grey intervals (e.g. Betzler *et al*., 2000; Reuning *et al.*, 2002; Betzler *et al.*, 1999; Frank and Bernet, 2000; Kroon *et al.*, 2000; Karpoff *et al.*, 2002; Isern and Anselmetti, 2001).

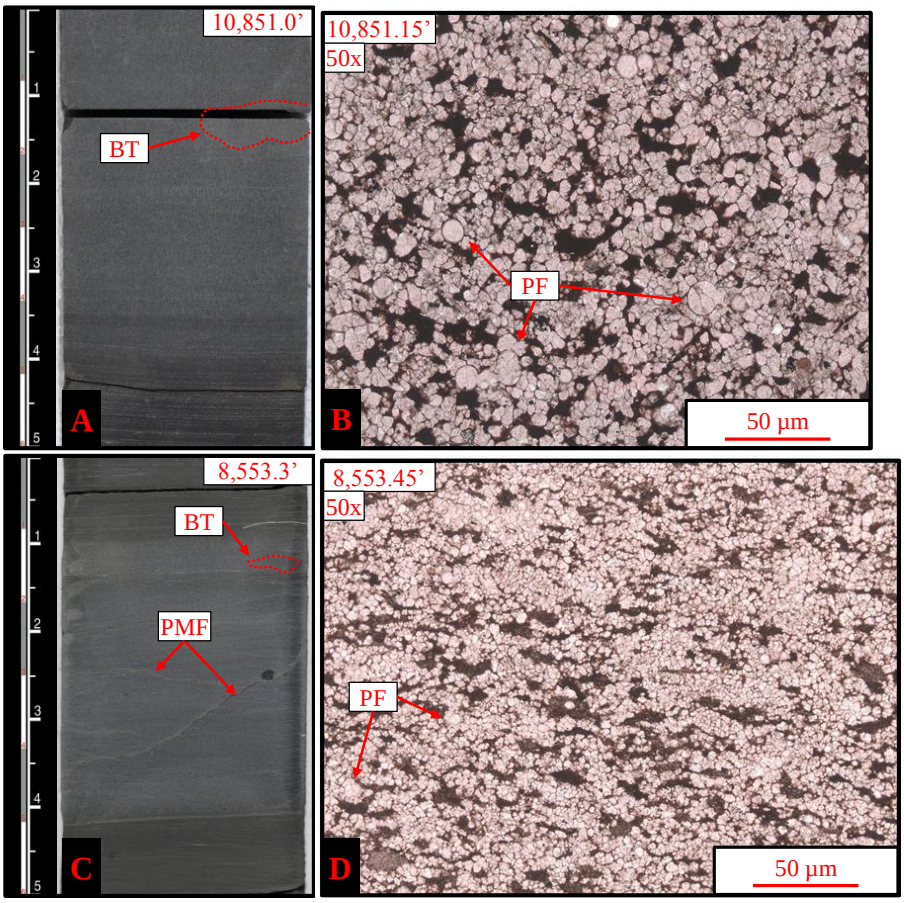

Figure 22: Facies 7 core and thin section photomicrographs. (A) Core photograph of foraminiferal packstone to grainstone facies with a gradational lower boundary, characteristic light grey color and a faint burrow trace (BT), Hill #1, 3,307.4 m to 3,307.5 m (10,851.0 ft. to 10,851.5 ft.); (B) Thin section from core in photo (A) showing planktonic foraminifera tests (PF), Hill #1; 3,307.4 m (10,851.15 ft.); (C) Core photograph with partially open microfractures (PMF), Nixon #6, 2,607.0 m to 2,607.2 m (8,553.3 ft. to 8,553.8 ft.); (D) Thin section from core in photo (C) showing the thorough lithification of calcareous planktonic foraminifera tests (PF), Nixon #6, 2,607.1 m (8,553.45 ft.).

Carbonate sediments are susceptible to marine cementation that can result in physical stabilization and lithification, as well as reduction in primary porosity and permeability which may affect later fluid migration (Grammer *et al.*, 1999). Traditionally, marine cementation was thought to occur over a period of tens to thousands of years (James and Choquette, 1983) and largely confined to shallow-subtidal to intertidal environments (Lyell, 1875; Shinn, 1969; Ginsburg *et al.*, 1971; Friedman *et al.*, 1974). However, recent work has shown, that: 1) cementation may occur "geologically instantaneous" within a matter of months, 2) this syndepositional cementation may occur in deeper platform and platform margin environments at depths of at least 60 m (197 ft.), and not just in shallower-water marine environments, and 3) that syndepositional cementation may be linked to high-frequency oscillations in sea level (Grammer *et al.*, 1993; Grammer *et al.*, 1999).

Massive to Bioturbated Claystone (Volcanic Ash)

This facies represents volcanic ash beds that are well recognized within the Eagle Ford formation, both in outcrops and in cores (Driskill *et al.*, 2010; Harbor, 2011; Donovan and Staerker, 2010; Lock *et al.*, 2010). Suggested source areas for these deposits include volcanic arcs in Arkansas, West Texas, and the Western Interior (Harbor, 2011; Dean and Arthur, 1998; Kauffman, 1984). Ash beds are chronostratigraphically significant in that they record a geologically instantaneous, regional, depositional event that is independent of spatial-

depositional relationships and blanket all depositional facies. Preservation of ash beds is variable, however, and dependent on active processes taking place at the surface of deposition at the time volcaniclastic sediments are introduced to the system (e.g. winnowing of fine grains in high-energy environments, homogenization with sediment through bioturbation, ponding of ash in low energy depressions) (Robinson, 2012).

Volcanic ash beds are most abundant in the upper half of the Eagle Ford section. Ash beds range from greenish-grey to light-pale-olive in color (Figure 23). Based on 4 samples, XRD analyses show inconsistent mineralogies where clays (avg. 43.8%, range 30-56%) and calcite (avg. 31%, range 21-48%) are dominant with lesser amounts of pyrite (avg. 14%, range 9-24%), quartz (avg. 6%, range 2-12%), and plagioclase and K-feldspar (avg. 5%, range 1-5%). The total clay mineral fraction is made up of variable distributions of mixed illite/smectite (avg. 27%, range 13-43%), illite (avg. 12%, range 0-37%) and kaolinite (avg. 4%, range 0.5-12%). There is no apparent relationship between clay mineral compositions of ash beds and depositional facies. Though inconsistent mineralogically, two types of ash beds can be distinguish based on physical appearance.

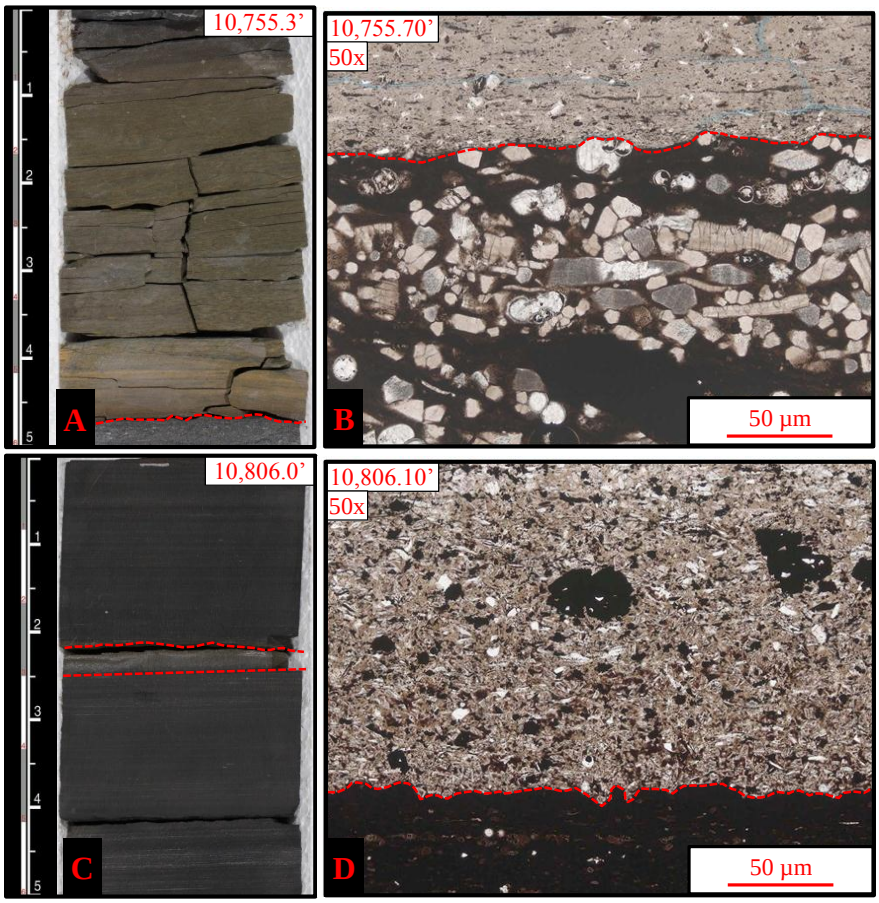

Figure 23: Facies 8 core and thin section photomicrographs. (A) Core photo showing homogenized and bioturbated ash with a sharp base and gradational upper boundary, Hill #1, 3,278.2 m to 3,278.4 m (10,755.3 ft. to 10,755.8 ft.); (B) Thin section that shows the sharp lower boundary of the ash in (A), and lack of skeletal debris and organic matter, Hill #1; 3,278.3 m (10,755.7 ft.); (C) Photo of ash with sharp upper and lower contacts with weakly laminated calcareous foraminiferal mudrock facies, Hill #1, 3,293.7 m to 3,293.8 m (10,806.0 ft. to 10,806.5 ft.); (D) Thin section showing the sharp base of the ash in core photo (C) and the absence of organic matter and calcareous skeletal

material and Photomicrograph Hill #1, 3,293.7 m (10,806.1 ft.).

Bioturbated beds were observed near the top of the Eagle Ford section are characterized by sharply defined bases and gradational-to-homogenized upper contacts (Figure 23 A and B). The observed thickness of these bioturbated beds range from ±12 cm (±5 in.) to 25+ cm (10+ in.). Sediments overlying and commonly underlying these beds lack evidence of bioturbation. This likely indicates that the environment changed suddenly, becoming better oxygenated and habitable before returning to oxygen deficient conditions unsuitable for burrowing organisms, possibly as a result of oxygen-rich waters brought downslope by turbidites or other mechanisms.

The second expression of this facies is much thinner and is characterized by a massive fabric with sharp upper and lower contacts (Figure 23 C and D). These range from ≤ 1 cm (≤ 0.4 in.) to 4 cm (1.5 in.) in thickness and occur interstratified with organic-rich calcareous mudstones. The absence of bioturbation and sedimentary structures indicate ash was deposited in a low-energy, oxygen deficient setting.

Sequence Stratigraphy and Facies Stacking Patterns

Sequence stratigraphy is a method that subdivides sedimentary strata into time-equivalent (chronostratigraphic), genetically-related units associated with

changes in global sea level (Miall, 2010; Ritter, 2008; Lucia *et al.*, 2003; Kerans and Tinker, 1997; Read *et al.*, 1995). This differs from lithostratigraphy where boundaries are often time-transgressive and sedimentary strata is divided based on physical characteristics and depositional environments without identifying relative geologic time intervals. Interpretations using the lithostratigraphic approach may yield erroneous correlations as the presumed vertical and lateral continuity of similar rock types are in fact chronostratigraphically discontinuous. Unlike lithostratigraphy, sequence stratigraphy recognizes the temporal and spatial coexistence of different facies within a depositional environment per Walther's Law. As a result, sequence stratigraphy is able to dynamically analyze depositional systems and, therefore, the distribution and architecture of facies belts through time (Grammer *et al.*, 2004). The major strength of sequence stratigraphy is the enhanced predictability of sedimentary packages, including sediment type, probable reservoir or source potential, geometry, and lateral and vertical continuity of strata across a sedimentary basin (Eberli and Grammer, 2004).

High-resolution sequence stratigraphy (cyclostratigraphy) recognizes that larger-scale (seismic scale) sequences are made up of vertically stacked, higher-frequency (4^{th}, 5^{th} order), shallowing-upward sequences (Kerans and Tinker, 1997). High-resolution sequence stratigraphy is applied through the determination of genetically-related stratigraphic units, as well as facies distribution within genetic units and facies partitioning, within a hierarchical development of vertical

stacking patterns and lower frequency sequences (Eberli and Grammer, 2004). This is important in that it enables lateral facies shifts to be better assessed from vertical data sets (Eberli and Grammer, 2004). The major strengths of high-frequency sequence stratigraphy are the enhanced ability to evaluate the direction of facies shifts (landward/seaward), and the spatial (later/vertical) variability and continuity of facies belts (Eberli and Grammer, 2004).

Application of sequence stratigraphy and high-resolution sequence stratigraphy have become increasingly important to reservoir geology, characterization, and modeling (Grammer *et al.*, 2004; Handford and Loucks, 1993). Ideally, an integrated reservoir characterization will combine outcrop and subsurface data (i.e. core, logs, petrophysical and seismic) with data from modern and ancient analogs (Grammer *et al.*, 2004; Eberli and Grammer, 2004; Kerans and Tinker, 1997). Incorporating these three data sets into a sequence stratigraphic framework not only enhances the ability to predict the: 1) subsurface spatial distribution of depositional facies and environments, 2) potential reservoir quality, and 3) petrophysical character (Eberli and Grammer, 2004; Handford and Loucks, 1993).

This study integrates a sequence stratigraphic approach that deviates from the ideal approach outlined above in that the integrated rock data is limited to core and lacks data from outcrop or seismic. Furthermore, one core captured an incomplete Eagle Ford section and impedes the ability and confidence in regional correlations of sequences. All scales of sequences were determined using the

idealized facies succession (Figure 15) established through the analysis of the vertical stacking patterns of facies in core. However, it should be noted that few sequences and cycles include the complete facies succession.

Sequence and Cycle Hierarchy

Carbonate productivity, as well as platform growth and the resultant facies distribution of marine carbonate systems are sensitive to changes in water depth, and fundamentally dependent on fluctuations in sea level (Miall, 2010; Christie-Blick, 1990; Goldhammer *et al.,* 1990; Sarg, 1988). Relative sea level changes are controlled by the sum of allogenic tectonic and eustatic (global) movements, autogenic sedimentation rates and changes in the processes and dynamics of a sedimentary system among various other factors (e.g. subsidence related to compaction/differential compaction of sediment, restriction of isolated basin waters from the global ocean) (Robinson, 2012; Schlager, 2005; Strasser *et al.,* 2000; Myers and Milton, 1996; Goldhammer *et al.,* 1989). Eustatic fluctuations in sea level generally result from changes in global basin dimensions affecting the volume of water contained or displaced, or ocean water volume influenced by variations in global ice volumes (McCloskey, 2012; Myers and Milton, 1996; Read *et al.,* 1995). These changes in global sea level result in cyclical packages of marine sedimentary facies that are referred to as ‘cycles’ or ‘sequences’ and are ordered according to time (duration, amplitude, and probable causal mechanisms (Table 4).

Sequence Stratigraphic Terminology	Eustatic Cycle (Order)		Duration (Ma)	Dominant Cause		Amplitude (m)
	1st		100 - 300	Supercontinent breakup and opening/closing of ocean basins		≤ 500
Supersequence	2nd		10 - 100	Plate tectonics		50 - 100
Sequence	3rd		0.5 - 10	Changes in global ice volume		50 - 100
Sequence, cycle	Milankovitch Cycles'	4th	0.1 - 0.4	Glacio-eustasy	Eccentricity	100 - 130
Parasequence, cycle	Milankovitch Cycles'	5th	0.04 - 0.05	Glacio-eustasy	Obliquity (tilt)	30 - 100
Parasequence, cycle	Milankovitch Cycles'	5th	0.019 - 0.023	Glacio-eustasy	Precession (wobble)	≤ 50

Table 4: Table outlining orders of stratigraphic and eustatic cyclicity. Carbonate systems are fundamentally dependent on sea level fluctuations as eustatic and relative sea level changes control carbonate productivity and the resultant facies distribution. From an applied perspective, understanding composite stratigraphic sequences and their response to sea level fluctuations enhances the ability to predict probable reservoir facies, as well as their spatial geometry and continuity. Summarized from Miall (2010), Schlager (2005), Gale *et al.* (2002), Mathews and Frohlich (2002), Carter (1998), Sarg (1998), Myers and Milton (1996), Read *et al.* (1995), and Goldhammer *et al.* (1989).

In general, a rise in relative sea level leads to an increase in accommodation that is characterized by a deepening phase or transgression that results in a vertical facies change towards deeper-marine conditions (blue upward-pointing arrow in Figure 15). A fall in relative sea level leads to a decrease in accommodation and results in a shallowing-upward, regressive phase represented by a facies shift toward increasingly shallower-marine conditions (red downward-

pointing arrow in Figure 15) (Grammer *et al.*, 1996, 2000). The symmetry of transgressive-regressive sequences is primarily a function of the duration and amplitude of changes in relative sea level, but is also influenced by the interaction of changes in the depositional system, basin geometry, subsidence, climate, and paleoceanographic conditions (Sarg *et al.*, 1999).

Three types of bounding surfaces separate transgressive-regressive depositional sequences. Type 1 sequence boundaries form when relative sea level falls below the shelf break of the preceding sequence and are characterized by a distinct lithologic signature (terrestrial overprint of marine sediments) and karst morphology (Schlager, 2005; Myers and Milton, 1996). Type 2 boundaries develop when relative sea level falls to a position between the old shoreline and shelf break, and only the inner shelf is subject to subaerial alteration (Schlager, 2005; Myers and Milton, 1996). Type 3 sequence boundaries form when relative sea level rises faster than the system can aggrade and are generally associated with platform drowning events (Schlager, 2005). These drowning unconformities are marked by a significant marine erosional surface and typically an abrupt change in sediment composition from a highstand tract to a transgressive tract with no exposure surface in between (Schlager, 2005).

Stacking patterns of carbonates like the Eagle Ford are frequently overlooked because they show no evidence of subaerial exposure. However, the facies cyclicity that is characteristic of periplatform carbonates record sea level

fluctuations that affect carbonate production in the platform interior (Betzler *et al.*, 2000).

Large Scale Sequences

Second Order Sequences

The Eagle Ford—Austin Chalk interval records a 2nd order sequence (Phelps, 2011). Second order sequences (around 10 Ma to 100 Ma) are tectonically driven and commonly form regional depositional sequences hundreds of meters thick (Miall, 2010; Read *et al.*, 1995). Core interpretations from the Eagle Ford and Austin Chalk show an overall regressive, shallowing-upward sequence (Phelps, 2011; Dawson and Almon, 2010) with higher-frequency cycles included within the larger package. This overall regressive, shallowing-upward sequence is indicated by an upward: 1) change in lithology from deeper- to shallower-water facies, 2) transition from pelagic- to traction-modes of deposition, 3) increase in coarser grains and skeletal debris, 4) increase in bioturbation, and, 5) an upward decrease in (TOC).

Third Order Sequences

Each core included in this investigation can be divided into three relatively symmetrical and regionally correlative 3rd order sequences (S1, S2, and S3). Third order sequences (around 0.5 to 5 Ma) are superimposed upon 2nd order sequences

and generally correspond to sea level changes with amplitudes of approximately 50 m (164 ft.) (Carter, 1998; Read *et al.*, 1995). These sequences are problematic in that it is unclear in exactly what the driving mechanism is. The bases of the 3rd order sequences identified in core are represented by thicker intervals of deeper-water facies that become thinner as they transition upsection into shallower-water facies (Figure 15 and 25).

Sequence Boundary 1 (SB 1) marks the base of S1 and corresponds to the Buda—Eagle Ford contact (Figure 24). Sequence Boundary 2 (SB 2) and 3 (SB 3) mark the bases of sequences 2 (S2) and 3 (S3). SB 1 is the only pronounced sequence boundary present in each of the complete cores (Figure 24). It is interpreted as a Type 3 sequence boundary that is characterized by a sharp, erosive surface with rip-up clasts, grain beds (Schlager, 2005) and an abrupt change in facies from shallower platform deposits to deeper, laminated carbonate muds. Type 3 sequence boundaries correspond to platform drowning events and are produced when sea level rises faster than the system can aggrade, resulting in a transgressive systems tract that directly overlies the preceding highstand tract. Type 3 sequence boundaries are often accompanied by a significant marine hiatus and erosion (Schlager, 2005; Saller *et al.*, 1993).

The Hill #1 core is located northeast of the other cores and lies near the northernmost boundary of the Karnes Trough nearest the San Marcos Arch (Figures 4, 5 and 7). The T.R. Marshall #1 is located approximately 16 km (10 mi) southwest of the Hill #1 and situated in the center of the Karnes Trough

(Figures 4, 5 and 7). The Karnes Trough experienced syndepositional faulting that served to increase accommodation and focus the delivery of Eagle Ford sediments into the well-developed topographic low (See discussion in Section 2.2). This influenced the thickness of individual sequences in both the Hill #1 and T.R. Marshall #1 cores. In the Hill #1 core, S1 is about 18 m thick (60 ft.), S2 is about 16 m thick (55 ft.) and S3 is approximately 9 m thick (30 ft.). In the T.R. Marshall #1 core, S1 is exceeds 31 m thick (100+ ft.), S2 is about 15 m thick (50 ft.) and S3 is nearly 29 m thick (95 ft.).

The Nixon #6 is about 48 km (30 mi) southwest of the T.R. Marshall #1 and the Hundley #1 is nearly an additional 97 km (60 mi) southeast of the Nixon #6 core (Figure 4, 5 and 7). The Nixon #6 and Hundley #1 cores are not located within topographic lows (Karnes and Atascosa Troughs) and did not accumulate thickened Eagle Ford intervals. In the Nixon #6, S1 is about 14 m thick (45 ft.), S2 is about 9 m thick (30 ft.) and S3 is approximately 18 m thick (60 ft.). In the Hundley #1, S1 is approximately 17 m thick (55 ft.), S2 is about 14 m thick (45 ft.) and S3 is nearly 15 m thick (50 ft.).

In this study, sequences were determined based on rock type and a landward shift in facies following the idealized stacking pattern of facies illustrated in Figure 15. Three relatively symmetrical 3rd order sequences were identified in each of the four cores. Sequences S2 and S3 are completely recorded in all cores whereas S1 is incomplete, and markedly asymmetrical in the T.R. Marshall #1. Because of this, it is difficult to define these sequences as being

developed solely in response to eustatic sea level fluctuations and the sequences may be related to autocyclic processes acting syndepositionally to influence accommodation development and sedimentation.

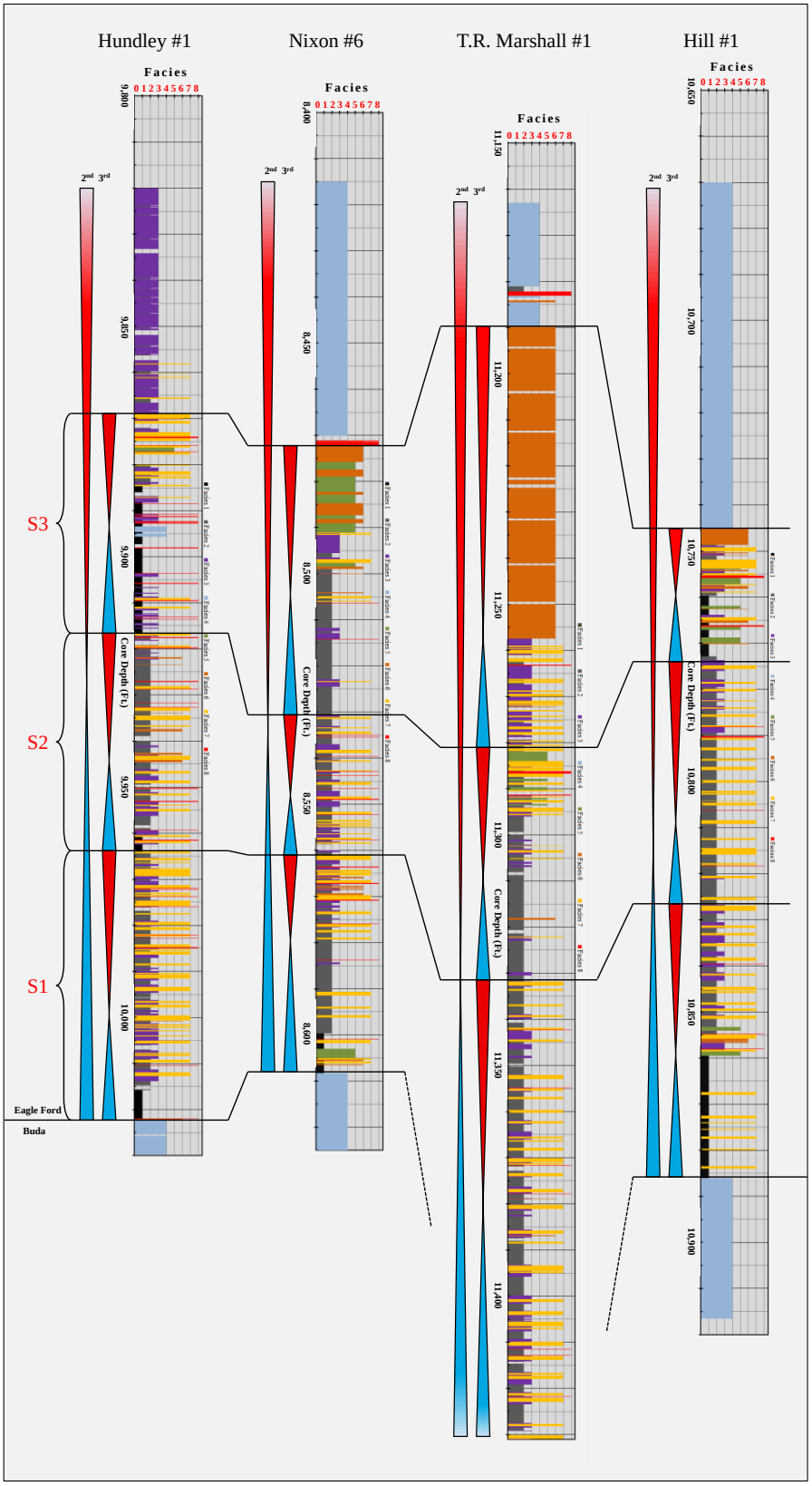
Hundley #1
Nixon #6
T.R. Marshall #1
Hill #1
Facies
0 1 2 3 4 5 6 7 8
2nd 3rd
9,800
9,850
9,900
9,950
10,000
8,400
8,450
8,500
8,550
8,600
11,150
11,200
11,250
11,300
11,350
11,400
10,650
10,700
10,750
10,800
10,850
10,900
Core Depth (Ft.)
S3
S2
S1
Eagle Ford
Buda

Figure 24: Cross section of depositional facies and 2nd and 3rd order sequences identified in core. Refer to figure 15 for facies/color associations. This cross section illustrates the regional continuity and relative symmetry of 3rd order sequences (S1, S2 and S3). The thickness of S1 increases in the T.R. Marshall #1 which is located in the Karnes Trough (Refer to discussion in section 2.2, and figures 4, 5 and 7). This likely reflects the influence of autocyclic processes and syndepositional faulting of the trough that increased accommodation and helped focus Eagle Ford sedimentation within the topographic low.

Small Scale High Frequency Sequences-/Cycles (HFS's/HFC's)

Third order sequences are composed of higher-frequency (20 k.y. to 400 k.y), orbitally-forced glacioeustatic sequences that are governed by periodic perturbations in Earth's orbit known as Milankovitch cycles (Mathews and Frohlich, 2002, Read *et al.*, 1995). Three orbital rhythms (eccentricity, obliquity, and precession) induce subtle irregularities in the amount of solar radiation received by earth that modulate climate and drive high-frequency sea level fluctuations (Schlager, 2005).

Fourth Order Sequences (HFS's)

Fourth order cyclicity, with deposits often referred to as high-frequency sequences (HFS's), correspond to changes in the elongation of Earth's elliptical orbit that occur at intervals of approximately 100 k.y. and 400 k.y. (short- and long-term eccentricity), with weaker modulations around 1.2 Ma and 2 Ma (Schlager, 2005). The thickness of HFS's generally range from 1.5 m to 20 m (5 ft. to 65 ft.), respectively, and are generally thickest during the transgressive phase of the associated 3rd order sequence (Figure 25). A total of 39 HFS's were identified in cores (Figure 25). Each represent shallowing upward sequences that follow the idealized facies stacking pattern illustrated in Figure 15. The HFS's are bound by flooding surfaces where deeper water facies (base of sequence) transition upward into a greater proportion of shallower water facies (top of sequence).

The numbers of HFS's within 3rd order sequences (S1, S2 and S3) are regionally consistent (Figure 26). Sequence 1 consists of 4-5 HFS's whereas S2 consists of 3-4 HFS's and S3 is composed of 2 HFS's. Thicknesses of HFS's, like 3rd order sequences, correspond to the associated structural setting of each core. HFS thicknesses are relatively consistent between the Hill #1, Nixon #6 and Hundley #1 cores but are thicker in the T.R. Marshall #1 core (Figure 25). This reflects the location of the T.R. Marshall #1 within the Karnes Trough (Figures 4, 5 and 7) and the influence of allocyclic and autocyclic processes acting during the time of sedimentation (i.e., syndepositional faulting, accommodation

development, sedimentation patterns and relative sea level fluctuations). Consistent numbers of HFS's and the distribution of HFS's between both the individual studied wells, and the identified 3rd order sequences, enable HFS's to be used for regional correlation and evaluation of the lateral-/vertical variability and continuity of facies belts (potential reservoir units and seals).

Fifth Order Cycles (HFC's)

Fifth order cyclicity, with deposits referred to as high-frequency cycles (HFC's), correspond to changes in the obliquity, or tilt of Earth's rotational axis between 21.1° and 24.5° relative to its orbital plane (40 k.y. and 50 k.y. intervals), and changes in precession, or wobble (19 k.y. to 23 k.y. intervals) as the direction in which the Earth's axis points gradually shifts (Schlager, 2005; Mathews and Frolich, 2002). HFC's are generally meter-scaled (approximately 3 ft.), and are described as 'parasequences' or 'genetic units' consisting of individual shallowing upward facies packages constrained by surfaces indicative of abrupt deepening (Myers and Milton, 1996; Read *et al.,* 1995). Identification of these units is important as they often represent the fundamental reservoir (flow) units in carbonates (Grammer *et al.*, 2004).

HFC's were identified following the ideal vertical succession of facies and commonly consist of alternating mudstone (Facies 1 and 2), and thoroughly lithified foraminiferal packstone to grainstone facies (Facies 7). Figure 25

illustrates this cyclicity where mudstones are depicted as black (Facies 1) and dark grey (Facies 2) colored intervals, and foraminiferal packstone to grainstone deposits (Facies 7) are portrayed as yellow intervals. Results from ODP Leg 166 document similar cyclicity off the western margin of the Great Bahama Bank (refer to discussion in sections 5.2 and 5.4).

The distribution and thicknesses of HFC's lack the regional consistency and correlativity associated with the identified 3rd and 4th order sequences (Figure 25). In general, the thickness of HFC's decrease and the numbers increase toward the top (regressive portion) of the associated 3rd order sequences. Furthermore, the numbers of HFC's vary considerably, both within, and between each 3rd order sequence. Regional inconsistencies of these depositional cycles are likely related to high-frequency sea level fluctuations and variations in accommodation that is created during each cycle of relative sea level change and sedimentation (Eberli and Grammer, 2004). The lateral continuity and thickness variations of these units are a function of sediment supply (carbonate production) and the rate of sea level rise (Eberli and Grammer, 2004).

The absence of any regional consistency prevents the use of HFC's for correlation purposes. However, identification of these cycles is important as the vertical stacking of these provides insight and an enhanced predictability of sedimentary packages, probable reservoir-/source potential, geometry, and the lateral-/vertical continuity of sedimentary packages in the subsurface.

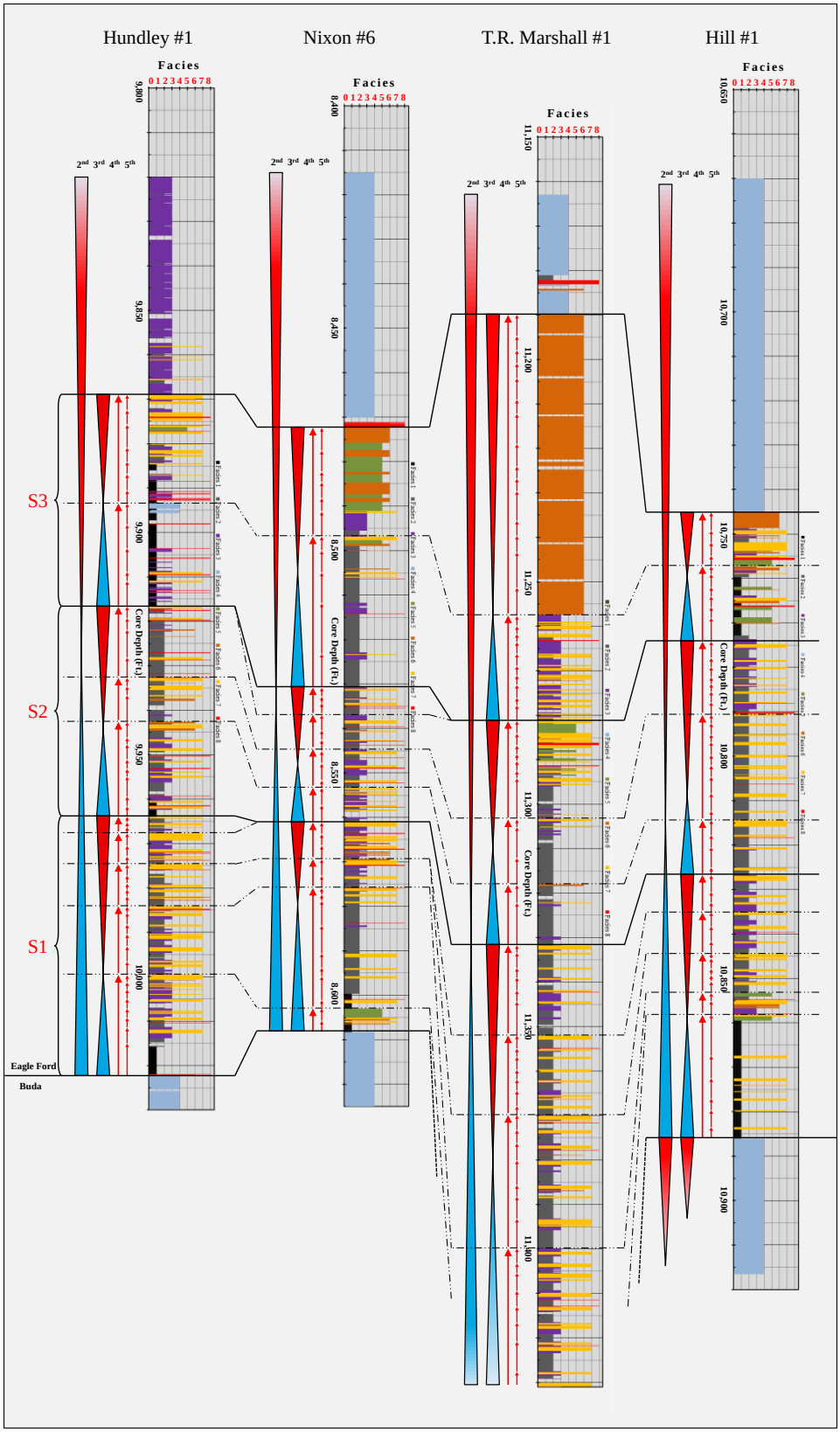
Hundley #1
Nixon #6
T.R. Marshall #1
Hill #1
Facies
0 1 2 3 4 5 6 7 8
2nd 3rd 4th 5th
Core Depth (Ft.)
S3
S2
S1
Eagle Ford
Buda
9,800
9,850
9,900
9,950
10,000
8,400
8,450
8,500
8,550
8,600
11,150
11,200
11,250
11,300
11,350
11,400
10,650
10,700
10,750
10,800
10,850
10,900

Figure 25: Cross section of depositional facies and 2nd, 3rd, and high-frequency sequences-/cycles (HFS's-/HFC's) identified in core. Refer to figure 15 for facies/color associations. Regionally consistent and relatively symmetrical sequences include 2nd, 3rd (S1, S2 and S3) and 4th order sequences. Regional variations in thickness and number of sequences suggest an influence of both eustatic sea level changes and autocyclic processes. High-frequency cycles (5th order) lack regional continuity, and are primarily controlled by high-frequency sea level fluctuations and the resultant effect on accommodation development and sediment supply.

Wire-line Logs and Sequence Stratigraphic Framework

Core data and interpretations were used to ground-truth conventional wire-line log data in order to provide a means of identifying and correlating sequences based on petrophysical character. This is important as core data is not often readily available and as a result, subsurface correlations are primarily made using wire-line logs.

To facilitate the comparison of facies and sequences identified in core with conventional wire-line log data (gamma ray, resistivity, bulk density, neutron porosity and density porosity), they were input into Petra® and depth-shifted using core gamma ray data. Comparison showed that 3rd order packages and HFS's (4th

order) are resolvable and regionally correlative using petrophysical log signatures. Sequences are best denoted by gamma ray, bulk density and density porosity wire-line log curves (Figure 26). In contrast, HFC's (5^{th} order) are problematic for correlation purposes as they not only show inconsistent distributions in core but lack a one-to-one correlation and are not always discernable using wire-line log signatures.

Overall, gamma ray values are consistently high through the Eagle Ford section. Large order sequences (2^{nd} and 3^{rd}) and HFS's (4^{th} order) are identifiable using gamma ray logs as cyclic packages characterized by elevated values at sequence bases (transgressive phase) and show an overall decreasing upward trend toward the top of sequences (regressive phase) (Figure 26). This 'cleaning upward' trend reflects the change in lithology where the proportion of clay-to-carbonate minerals decreases upward in depositional sequences.

Bulk density curves depict sequences as intervals marked by an initial drop in density (transgressive phase) before transitioning upward into a second leg of increasing density (regressive phase). This overall trend is composed of highly-cyclic alternations between elevated and decreased density which align with high- and low-gamma ray expressions (Figure 26). This also reflects the vertical stacking and change in lithology where carbonate content increases upward in sequences.

Depositional sequences are also recognized in density porosity curves and are characterized by a decreasing-upward trend in porosity values (Figure 26).

Highly-cyclic packages are also evident within the overall package where elevated porosities correspond with gamma ray ‘spikes’, drops in bulk density and deeper-water facies. On the contrary, intervals characterized by low porosity values correspond to low gamma ray signatures, high density values, and shallower-water facies. The most prominent highly-cyclic packages are HFC’s (5^{th} order) which consist of alternating organic-rich muds (transgressive phase) and well-lithified foraminiferal packstone-/grainstone deposits (late-highstand/early lowstand phase) (Figure 26).

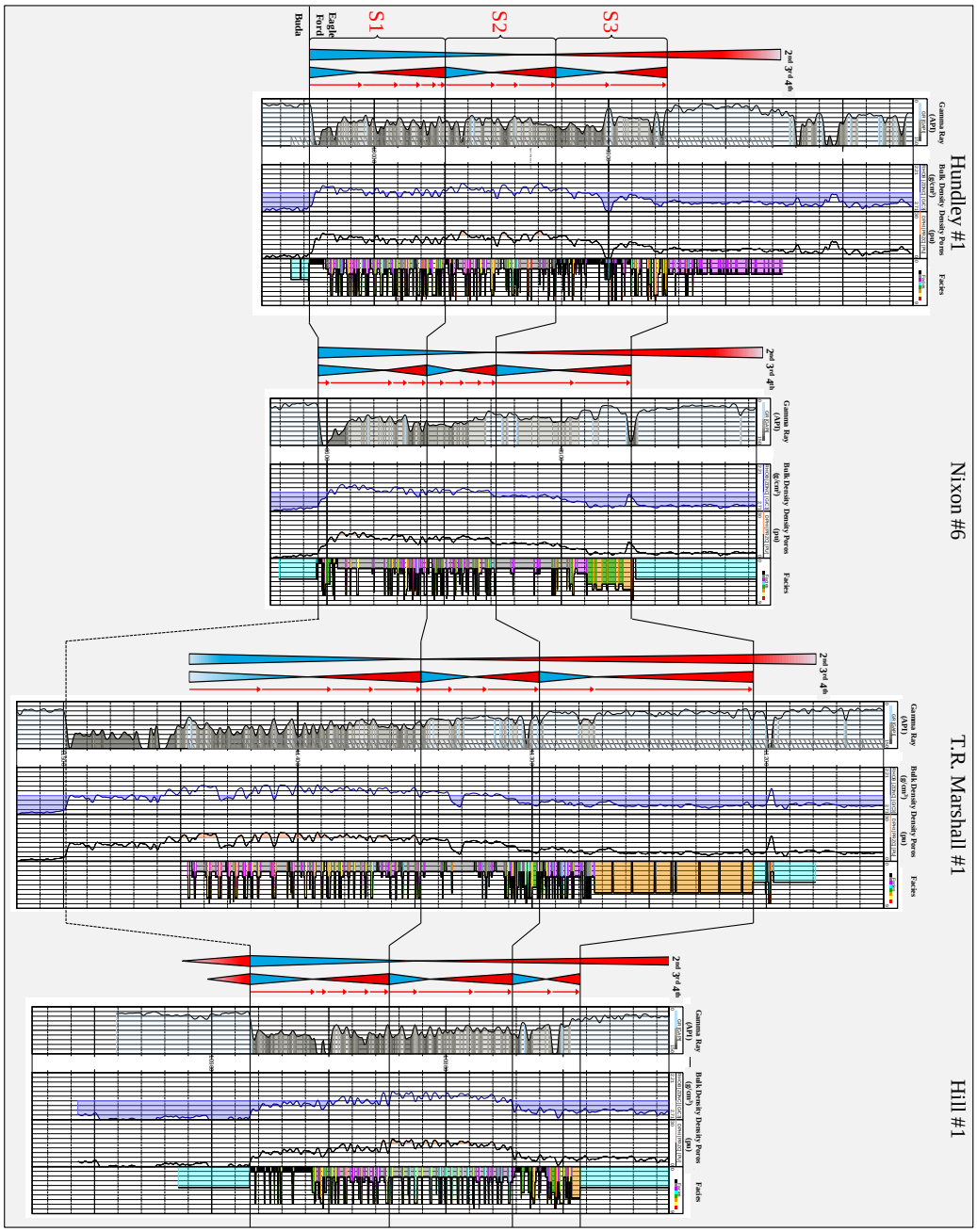

Figure 26: Cross section of all cores with 3rd order sequences (S1, S2, and S3) labeled and 2nd order and high-frequency (4th order) sequences on conventional wire-line logs (gamma-ray, bulk density and density porosity). Sequences show a progressive decrease in gamma ray and density porosity toward the top of

sequences; whereas bulk density increases upward. From left to right, track: 1) gamma ray (0-150 API); 2) bulk density (2.21-2.71 g/cm^3); 3) density porosity (30-0 pu); and 4) facies (0-8; refer to figure 15 for facies/color associations).

Summary of Sequences

The Eagle Ford—Austin Chalk interval records a 2nd order sequence (Phelps, 2011; Dawson, 2000). The Eagle Ford section is composed of three 3rd order sequences that are relatively symmetrical and regionally correlative (Figures 24, 25 and 26). These sequences are both identifiable, and correlative, in core and in wire-line log suites. Sequences are characterized by decreasing upward trends in gamma ray and density porosity; whereas, bulk density shows an initial drop before increasing toward the top of the sequence (Figure 26).

Third order sequences (S1, S2 and S3) are composed of high-frequency shallowing-upward sequences (4th order) that follow the ideal facies stacking pattern represented in Figure 15. In general, the distribution of HFS's is regionally consistent; where, S1 consists of 4-5 HFS's; S2 includes 3-4 HFS's; and, S3 is characterized by 2 HFS's (Figures 25 and 26). HFS's are also identifiable and correlative in wire-line log suites where they are characterized by similar trends in gamma ray, density porosity, and bulk density as the 3rd order sequences (Figure 26).

High-frequency cycles (5th order) were also identified in each core. However, the distribution and number of HFC's is highly variable making any

regional correlation problematic (Figures 25 and 26). Furthermore, the high cyclicity observed in wire-line logs lacks a one-to-one correlation with the identified HFC's which prevents any regional correlation of these. Variations observed primarily in the HFS's-/HFC's suggest these packages may not be a function solely of eustatic sea level changes but may also be influenced by autocyclic processes.

CHAPTER VI: DEPOSITIONAL ANALOGS

To accurately characterize and model potential reservoirs it is important that a thorough geologic understanding be developed of the local and regional spatial distributions of potential reservoir facies as well as any associated heterogeneities (Harris, 2010). Outcrop and subsurface datasets (i.e. core and wire-line logs) have traditionally been utilized to facilitate a more robust understanding and enhance predictability of changes in key reservoir components (Grammer *et al.,* 2004). These include changes in facies types, pore systems, facies specific diagenetic susceptibility and facies vertical stacking patterns. Though important, outcrops are inherently constrained by the limits of exposure (Grammer *et al.,* 2004). This makes information gained from the study of modern analogs and depositional systems invaluable in modeling and characterizing potential reservoirs (Grammer *et al.,* 2004, Harris, 2010).

The Bahama Banks have been widely accepted as a standard for interpreting many ancient carbonate deposits. Extensive work in the Bahamas has focused on platform evolution and sediment distribution trends (Schlager and Ginsburg, 1981). The western leeward margin of the Great Bahama Bank provides useful insight into Eagle Ford sediments where similar highly-cyclic periplatform slope deposits were observed in ODP Leg 166.

Belize, Central America, is another significant carbonate platform that has remained active since the Cretaceous and has drawn recent attention as a modern

analog for many ancient carbonate units (Mazzullo, 2006). The system in Belize is useful in providing a means to better understand Cretaceous carbonate deposition on the Comanche Shelf because it enables the interrelationship between variable facies distributions and differential subsidence along underlying tectonic structures to be better understood.

Great Bahama Bank

The Great Bahama Bank (GBB) is a shallow (generally ≤10 m, 33 ft.), aerially extensive, flat-topped carbonate platform (96,000 km^2, 37,000 mi^2), located between 20°-28°N latitude in a humid-subtropical climate and is bound by steepened flanks (Bergman *et al.*, 2010; Melim *et al.*, 2002; Tucker and Wright, 1990). Platform growth occurred in pulses during sea level highstands, with each depositional pulse generating an unconformity-bounded sequence during sea level lowstands (Betzler *et al.*, 2000). Progradation of the leeward margin is largely controlled by density driven currents and the southeasterly prevailing wind regime that conjunctively result in the off-bank transport of carbonate sediments (Rendle-Buhring and Reijmer, 2005).

Ocean Drilling Project (ODP) Leg 166 collected 5 cores along a platform-to-basin transect adjacent to the leeward margin of the GBB (Figure 27). The primary objective was to determine the influence of high-frequency sea level fluctuations on the production of carbonate sediments and platform, slope, and

basin sedimentation over the last 25 Ma. Cores from drill sites 1006 (most distal), 1007 (toe of slope) and 1003 (middle slope) record highly cyclic alternations of: 1) thick, dark grey finer-grained intervals of uncemented, strongly compacted, organic-rich and locally bioturbated pelagic sediments; and, 2) light grey intervals of pelagic material that are well cemented (microsparite or micrite matrix), nearly uncompacted, rarely bioturbated and consist of planktonic foraminifera and shallow-water bioclasts (Betzler *et al.*, 2000; Reuning *et al.*, 2002; Betzler *et al.*, 1999; Frank and Bernet, 2000; Kroon *et al.*, 2000; Karpoff *et al.*, 2002; Isern and Anselmetti, 2001). Dark grey intervals represent transgressive deposits whereas light grey zones correspond to late highstand to lowstand deposits during sea level cycles at the obliquity and precessional frequency (Betzel *et al.*, 2000; Kroon *et al.*, 2000). Syndepositional lithification of light grey intervals inhibits fluid flow with subsequent fluid migration pathways restricted to dark grey zones (Reuning *et al.*, 2002).

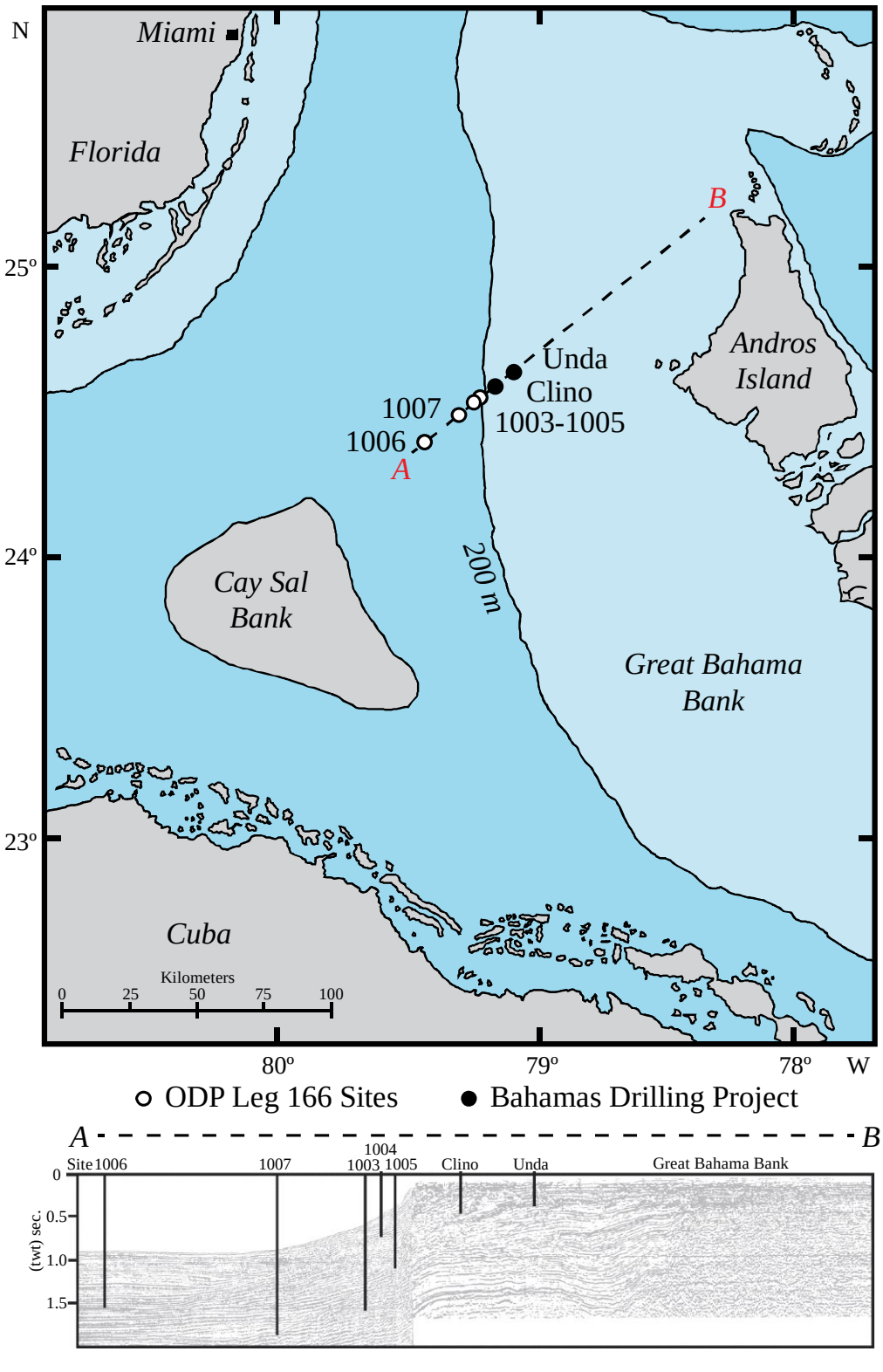
N
Miami
Florida
25°
24°
23°
B
Unda
Clino
1003-1005
1007
1006
A
Andros
Island
Cay Sal
Bank
200 m
Great Bahama
Bank
Cuba
Kilometers
0 25 50 75 100
80°
79°
78° W
ODP Leg 166 Sites
Bahamas Drilling Project
A
B
Site 1006
1007
1004
1003 1005
Clino
Unda
Great Bahama Bank
0
0.5
1.0
1.5
(twt) sec.

Figure 27: Map of the leeward margin of the Great Bahama Bank depicting the location of ODP Leg 166. A dip-oriented seismic section (bottom) shows the location of the seven drill sites (Sites 1003-1007, Clino and Unda), where core and log data were collected. Images modified from Karpoff *et al.* (2002) and Betzler *et al.* (1999).

The fundamental difference between the South Texas Eagle Ford and the leeward margin of the GBB is that this modern setting exists on the margin of an isolated carbonate platform (Figure 27), whereas the Eagle Ford of this study area was deposited in a restricted intraplatform basin environment. However, observations of ODP Leg 166 are similar to the Eagle Ford section in that sediments are highly cyclic between transgressive, dark, organic-rich calcareous mudstones and late highstand to early lowstand, light, thoroughly lithified foraminiferal packstone/grainstones. The thorough lithification of packstone/grainstone deposits in the Eagle Ford also serve as barriers to fluid flow and compartmentalize flow units.

Belize Barrier Reef

The Belize-Yucatan platform contains the longest continuous fringing and barrier reef complex in the Atlantic Ocean. It extends for 600 km (373 mi) along

the eastern coast of Central America (Figure 28; Gischler and Lomando, 1999; Reid *et al.,* 1992). Belize and southeastern Mexico have a subtropical climate and are located in the trade wind belt. The average air temperature ranges from 27° C (81° F) (summer) to 24° C (75° F) (winter) with wind directions predominantly from the east-northeast, but shift seasonally to the north-northwest during the winter (Gischler and Lomando, 1999). Accordingly, waves typically approach from the east-northeast and currents are predominantly southwest flowing (Yang *et al.,* 2004). Water temperatures vary seasonally from 29° C (84° F) (summer) to 27° C (81° F) (winter) and the average tidal range is 30 cm (12 in.) (Gischler, 2003).

The Belize-Yucatan reef complex is situated along a passive continental margin and the northern region has remained tectonically stable since the last interglacial highstand of sea level (125 k.y.a) (Gischler *et al.,* 2000). However, the southern region is situated 50 km (31 mi) north of the active North American and Caribbean plate boundary (Figure 28). Here, ongoing spreading at the Cayman Trough has resulted in continued subsidence (Gischler *et al.,* 2000). Differences in bathymetry and facies distributions on the platform interior are observed from north to south (Figure 29). These are primarily controlled by a series of underlying north-to-northeast trending tilted fault blocks, differential subsidence, and sea level rise (Gischler and Hudson, 2004; Gischler *et al.,* 2000; Gischler and Lomando, 1999). Wrench faulting and differential subsidence resulted in the development of topographic highs and three major structural features, the: 1)

Ambergris Caye-shoreline trend, 2) Turneffe-Chinchorro trend, and 3) the Glovers-Lighthouse trend (Figure 29; Gischler *et al.,* 2000).

The reef complex is divided into two sections. The Belize barrier reef extends for 250 km (155 mi) northward to Belize City before it transitions into the adjoining 350 km (217.5 mi) long Yucatan fringing reef (Figure 28; Gischler and Hudson, 2004). The reef impedes water movement from the open ocean and creates restricted intraplatform and lagoonal environments (James *et al.,* 1976; Scholle and Kling, 1972). Similarly, in the northern Gulf Coast, the Cretaceous Comanche reef margin also created restricted intraplatform environments during Eagle Ford deposition. North of Belize City, the platform is narrow and lagoons have an average depth of 6 m (20 ft.) (Figure 30: Reid *et al.,* 1992). South of Belize City, the platform progressively widens with water depths in the lagoon exceeding 50 m (164 ft.) (Figure 30; Purdy and Gischler, 2003).

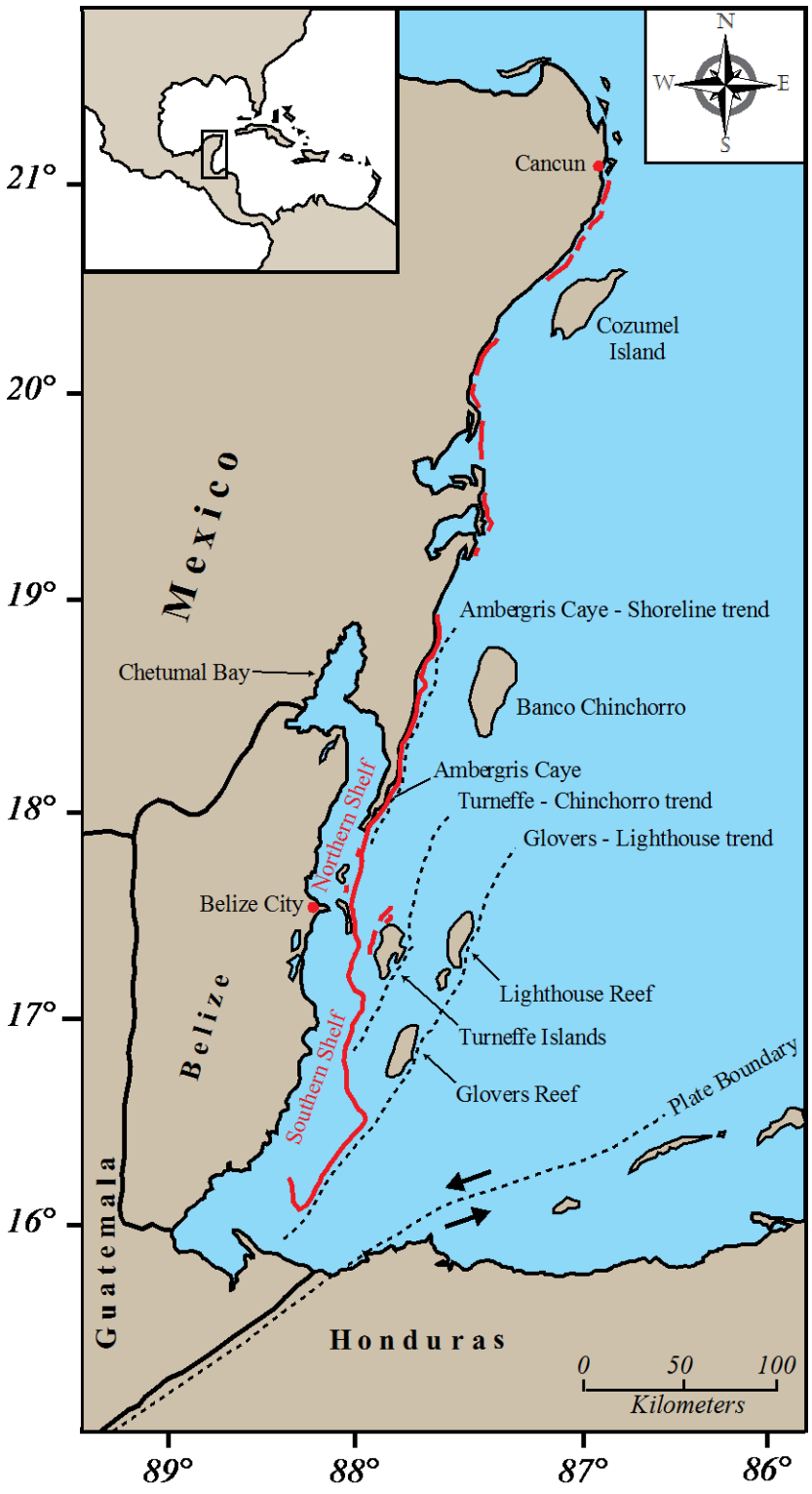
N
W
E
S
Cancun
Cozumel
Island
Mexico
Ambergris Caye - Shoreline trend
Chetumal Bay
Banco Chinchorro
Ambergris Caye
Turneffe - Chinchorro trend
Glovers - Lighthouse trend
Northern Shelf
Belize City
Belize
Lighthouse Reef
Turneffe Islands
Southern Shelf
Glovers Reef
Plate Boundary
Guatemala
Honduras
0 50 100
Kilometers
21°
20°
19°
18°
17°
16°
89°
88°
87°
86°
Barrier reef and platform margin.

Figure 28: Map of the Belize – Yucatan reef complex. Barrier reef architecture transitions into fringing reef and platform architectures north of Belize City. Three predominant trends in wrench faulting created topographic highs and isolated carbonate platforms. Modified from Gischler and Hudson (2004), Gischler *et al.* (2000), Gischler and Lomando (1999).

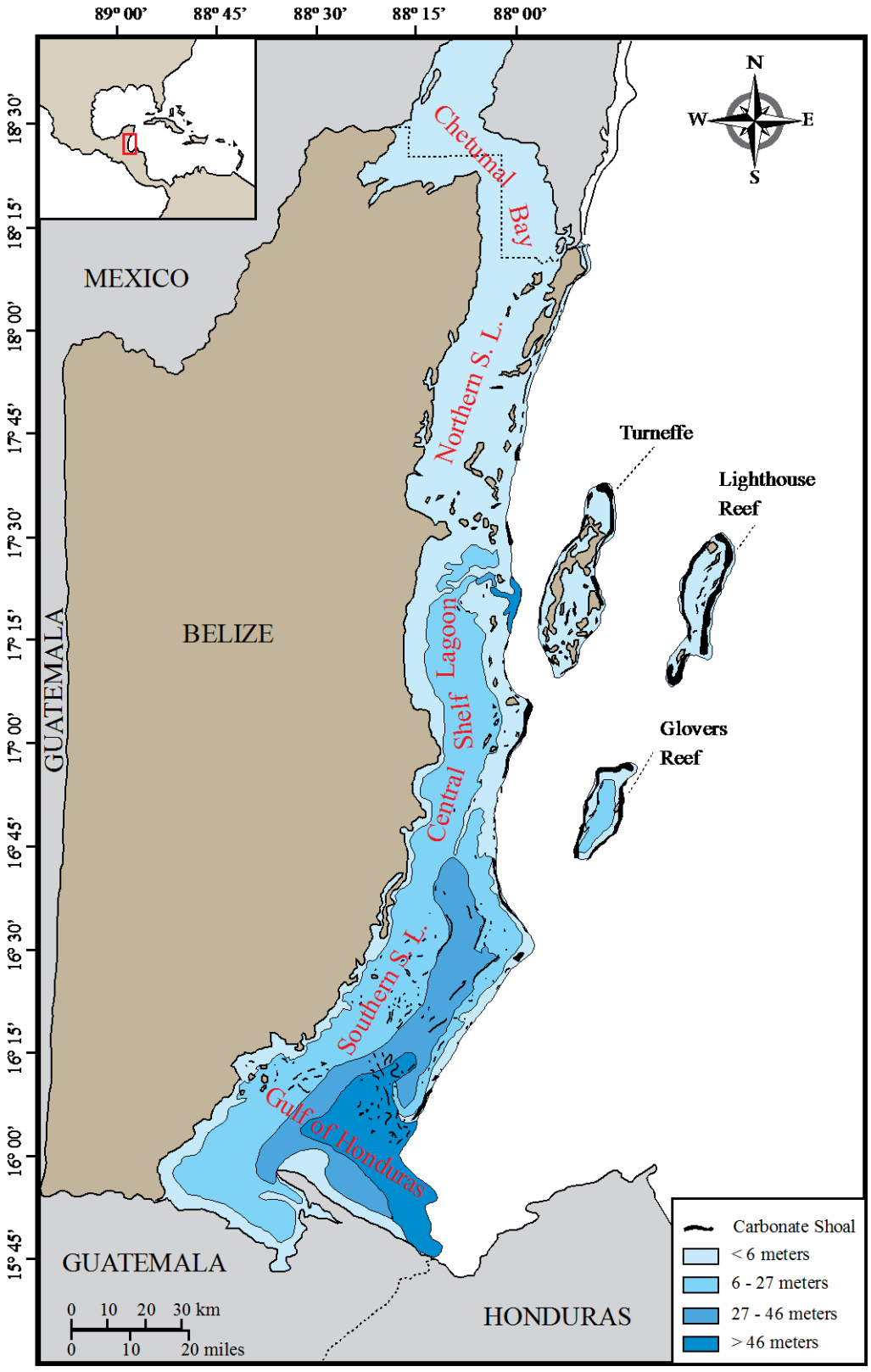
89° 00'
88° 45'
88° 30'
88° 15'
88° 00'
18° 30'
18° 15'
18° 00'
17° 45'
17° 30'
17° 15'
17° 00'
16° 45'
16° 30'
16° 15'
16° 00'
15° 45'
N
W
E
S
Chetumal Bay
MEXICO
Northern S. L.
Turneffe
Lighthouse Reef
BELIZE
GUATEMALA
Central Shelf Lagoon
Glovers Reef
Southern S. L.
Gulf of Honduras
GUATEMALA
HONDURAS
0 10 20 30 km
0 10 20 miles
Carbonate Shoal
< 6 meters
6 - 27 meters
27 - 46 meters
> 46 meters

Figure 29: Map depicting average water depths and width of the Belize Shelf. Depths average less than 6 m (20 ft.) north of Belize City in Chetumal Bay and progressively deepen southward where depths on the shelf exceed 46 m (151 ft.). The width of the shelf also shows a progressive widening trend southward. Modified after Purdy and Gischler (2003).

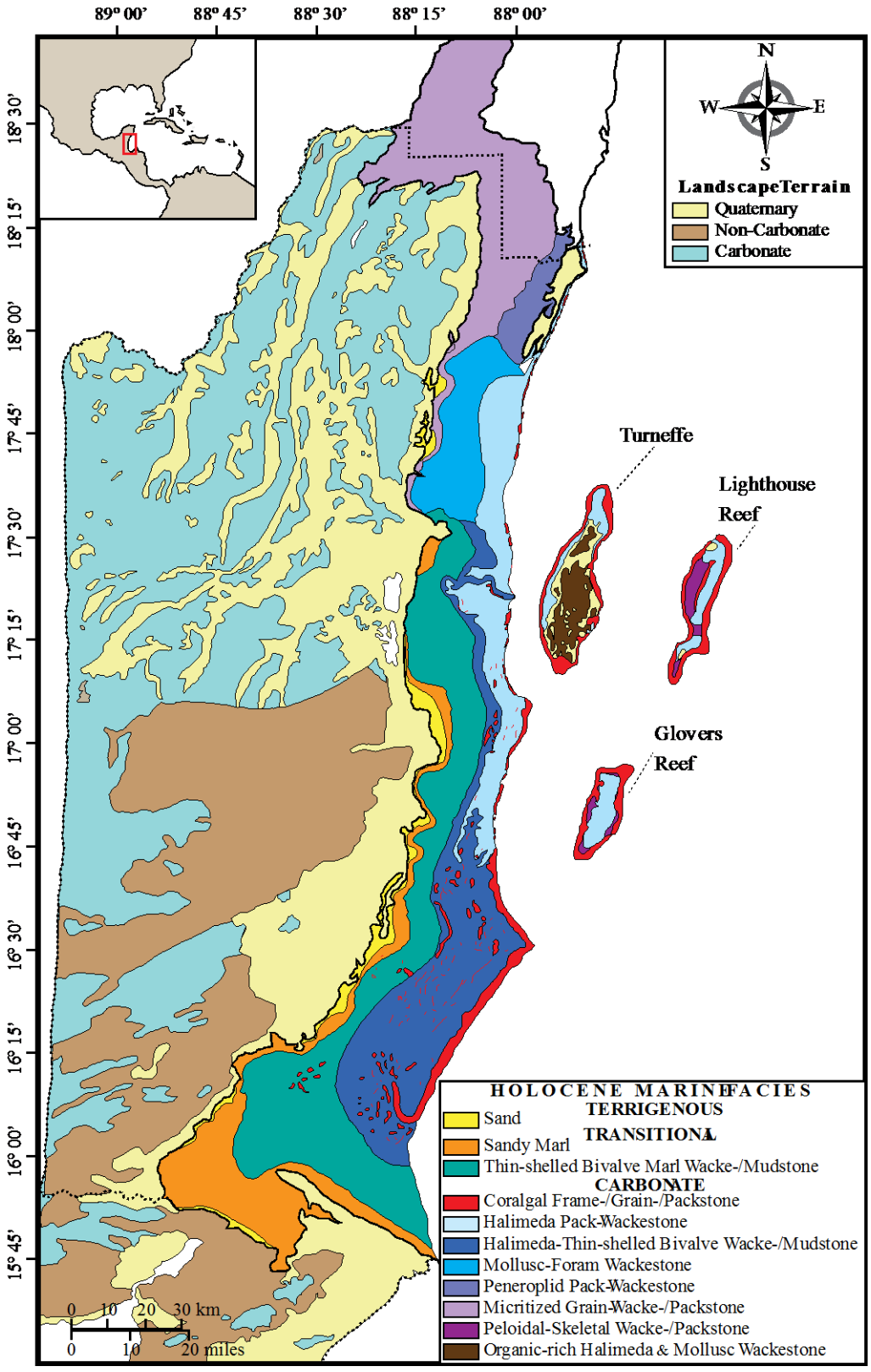
89° 00'
88° 45'
88° 30'
88° 15'
88° 00'
18° 30'
18° 15'
18° 00'
17° 45'
17° 30'
17° 15'
17° 00'
16° 45'
16° 30'
16° 15'
16° 00'
15° 45'
N
W
E
S
Landscape Terrain
Quaternary
Non-Carbonate
Carbonate
Turneffe
Lighthouse Reef
Glovers Reef
0 10 20 30 km
0 10 20 miles
HOLOCENE MARINE FACIES
TERRIGENOUS
Sand
TRANSITIONAL
Sandy Marl
Thin-shelled Bivalve Marl Wacke-/Mudstone
CARBONATE
Coralgal Frame-/Grain-/Packstone
Halimeda Pack-Wackestone
Halimeda-Thin-shelled Bivalve Wacke-/Mudstone
Mollusc-Foram Wackestone
Peneroplid Pack-Wackestone
Micritized Grain-Wacke-/Packstone
Peloidal-Skeletal Wacke-/Packstone
Organic-rich Halimeda & Mollusc Wackestone

Figure 30: Map of the Belize Shelf showing the distribution of primary depositional facies. The figure portrays the near-shore influence of siliciclastics and progressive dilution by carbonate sediments toward the shelf interior and margin. Modified after Purdy and Gischler (2003).

Northern Shelf Lagoon

Chetumal Bay is a wide, shallow bay located north of Belize City and bound by Ambergris Caye to the east and the Belize mainland to the west (Figures 28 and 29). Yang (2004) concentrated his work on carbonate muds deposited in tectonically derived intraplatform depocenters. Here, water salinity and temperature fluctuate. The lithologies of these consist predominantly of organic-rich carbonate muds and foraminiferal-/ peloidal wackestone/packstones (Figure 31; Dunn and Mazzullo, 1993). Sedimentation rates within these depocenters were calculated by Yang (2004) and ranged from 20 cm/k.y. to 460 cm/k.y. (8 in./k.y. to 181 in./k.y.). Yang (2004) showed, that: 1) sedimentation of organic-rich carbonate mud is not only focused into depocenters but depositional rates are also much greater than in non-depocenters, and 2) that the distribution and spatial variability of sediment is controlled by differential subsidence and bedrock topography, sediment production, direction and strength of storm-related wind, longshore and tidal currents, and the variable rates of sea-level rise.

Central and Southern Shelf Lagoon

South of Belize City the shelf lagoon is a mixed carbonate-siliciclastic depositional system where the distribution and character of depositional facies is strongly controlled by underlying structure (Figures 28, 29 and 30; Purdy and Gischler, 2003). River drainage of siliciclastic sediments eroded from the Maya Mountains are primarily deposited in near-shore shallow-water areas and seasonally carried further offshore during the wet season (June-October) (McNeill *et al.*, 2010). The clay mineral assemblage is a mix of kaolinite-/illite that reflect the proximity to the Maya Mountains and more thoroughly leached soils of southern Belize, and montmorillonite which is preferentially transported to the deeper shelf lagoon and offshore basin (McNeill *et al.*, 2010). Carbonate mud progressively increases and dilutes terrigenous material toward the barrier platform and is believed to originate from the breakdown of carbonate skeletons and nannoplankton (Purdy and Gischler, 2003). The primary marine sediments deposited on the Belize Shelf are depicted in Figure 30. Facies distributions reflect the influx of siliciclastics in the near-shore environment and the progressive carbonate dilution of siliciclastics southwestward toward the shelf interior and deeper water environments (Figures 29 and 30).

Isolated Carbonate Platforms

The Belize-Yucatan complex was also the focus of work by Gischler and Lomando (1999) that concentrated on variable sedimentary facies distribution among three isolated carbonate platforms (Figures 28, 29 and 30): 1) Glovers Reef, 2) Lighthouse Reef, and 3) the Turneffe Islands. Intraplatform depocenters and lagoons were identified around Glovers Reef and Turneffe Island where sediment from the marginal-reef and fore-reef environments is transported over the drop-offs into deeper waters. Gischler and Lomando (1999) noted temperatures and salinities as high as 31° C (88° F) and over 70‰, respectively, in the Turneffe restricted lagoons and depocenters. The lithology of these consist predominantly of organic-rich skeletal (mollusk, foraminifera, *Halimeda*) wackestone-packstone facies (Gischler and Lomando, 1999). Gischler and Lomando (1999) suggest that organic films around carbonate grains inhibit cementation. Their work showed that restricted intraplatform depocenters exhibit variable distributions of organic-rich carbonate mud as a consequence of differential subsidence along underlying tectonic structures. Like the work of Yang (2004), work by Gischler and Lomando (1999) enables a better understanding of carbonate facies distributions in modern, restricted intraplatform depocenters.

Similarities between the Belize Shelf and Comanche Shelf

The fundamental similarity between the modern Belize-Yucatan complex and Cretaceous Comanche Shelf is that both are mixed carbonate-siliciclastic systems. However, other aspects of the Belize Shelf also relate to the Comanche Shelf including primary depositional facies, and processes controlling sediment distribution and carbonate facies architecture. Bathymetric characteristics and facies distributions of both the Comanche Shelf and Belize Shelf are primarily controlled by differential subsidence, sediment production, and sea level fluctuations. Areas on the Comanche Shelf near the San Marcos Arch are generally shallower water environments-/facies and transition into deeper water environments-/facies toward the southwest. This is similar to the Belize Lagoon which progressively widens and deepens southwestward.

Cretaceous and modern sediments are dominated by organic-rich carbonate muds and foraminiferal-/peloidal wackestone/packstones with focused sedimentation into tectonically derived intraplatform depocenters. On the Comanche Shelf this resulted in expanded Eagle Ford sections in particular. Facies distributions in both the modern-/ancient settings reflect the influx of siliciclastics in the near-shore environment (proximal to the source) and the progressive dilution by organic-rich carbonate muds toward the shelf interior and deeper water environments. Work by Gischler and Lomando (1999) showed that organic films around carbonate grains inhibit cementation. This provides insight into the organic-rich, calcareous sediments observed in this study, and assists in

understanding the influence and preservation of organic material in the Eagle Ford.

CHAPTER VII: RESERVOIR CONSIDERATIONS

The evaluation of reservoir potential and attributes within depositional and stratigraphic trends provide insight in how reservoir quality and distribution is related to those aspects in the Eagle Ford. Observations and interpretations from core and wire-line log analyses indicate a depositional control on facies distributions in the Eagle Ford. As a result, if relationships can be determined between depositional and reservoir aspects, then depositional facies and the established vertical stacking pattern of facies can be used in conjunction to provide a more robust understanding of the spatial distribution of reservoir quality in the subsurface. Furthermore, a positive correlation of reservoir properties with depositional aspects can be combined with the wire-line logs to extrapolate predictions away from core observations.

The reservoir aspect of this study was limited to the core data acquired from three cores (Table 1; Figure 4). Comparison of gas shale core analyses data show identifiable trends in porosity and permeability that correspond to depositional facies (Table 5; Figure 31) and vertical stacking patterns (Figure 32). These data indicate nano-scaled heterogeneities dictate reservoir quality in the Eagle Ford. Relationships between reservoir properties and depositional facies are outlined below.

Primary Reservoir and Seal

Mudrocks are conventionally regarded as poor reservoirs because of the nano-scale porosity-permeability values; however, the high carbonate content and resultant ability to artificially propagate fractures makes these rocks excellent reservoirs. Lithologic trends (Table 5) and porosity-permeability cross plots show that organic-rich transgressive facies of the overall 2rd order sequence and particularly 4th order sequences (HFS's) and 5th order cycles (HFC's), Facies 2 (weakly laminated calcareous foraminiferal mudstone) and Facies 3 (laminated foraminiferal wackestone) have the highest reservoir potential (Table 5; Figures 31 and 32). Facies 2 has an average permeability of 2.35 nD and porosity of 3.28% whereas Facies 3 has a slightly lower permeability of 1.70 nD and porosity of 2.67%. The dominant pore type remains uncertain as porosity was not visible in thin section.

In contrast, latest highstand to early lowstand deposits, Facies 6 (skeletal packstone-/wackestone) and Facies 7 (foraminiferal packstone-/grainstone) positioned near 4th order high-frequency sequence and 5th order high-frequency cycle boundaries are thoroughly lithified and determine the vertical variability of, and compartmentalize reservoir units. Facies 6 has an average permeability of 0.24 nD and porosity of 2.19% (Table 5; Figures 31 and 32). Facies 7 has a slightly higher permeability of 1.18 nD and a comparable porosity of 2.10 % (Table 5; Figures 31 and 32).

Facies	Bulk Density	Matrix Permeability	Gas-filled Porosity	Gas Saturation		TOC	
#	(g/cc)	(nD)	(%)	(%)	No.	(%)	No.
1	2.51	1.94	2.61	26.11	10	3.29	8
2	2.43	2.35	3.28	32.02	25	3.71	38
3	2.55	1.70	2.67	49.49	15	2.46	12
4	2.52	5.85	4.46	54.11	2	0.82	16
5	2.57	1.11	2.77	47.73	2	1.89	1
6	2.61	0.24	2.19	46.74	4	0.98	13
7	2.56	1.18	2.10	32.68	7	0.57	2

Table 5: Table outlining the average bulk density, permeability, porosity and total organic carbon (TOC) values collected during gas shale core analyses. Table depicts facies with the highest TOC and reservoir potential (Facies 2 and 3) and facies with the least reservoir potential which serve to inhibit fluid flow and vertically compartmentalize reservoir units within the Eagle Ford due to characteristically low permeability values (Facies 6 and 7).

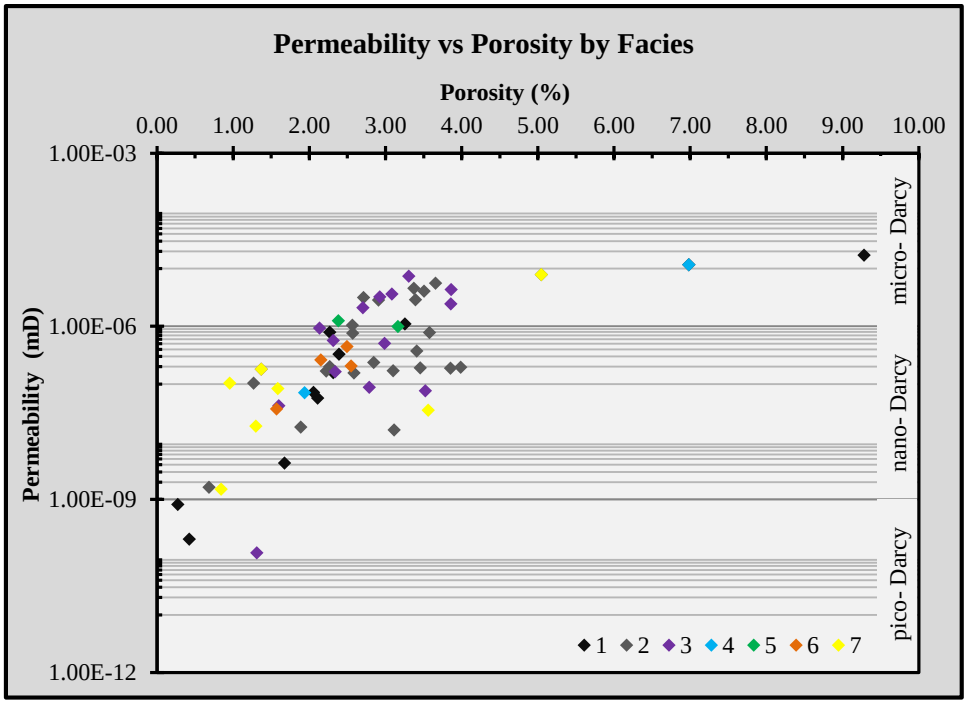

Figure 31: Porosity and permeability cross-plot of depositional facies. Note the elevated porosity and permeability values associated with Facies 2 and 3. In contrast, Facies 7 shows decreased values likely a result of early lithification that occluded primary porosity and permeability.

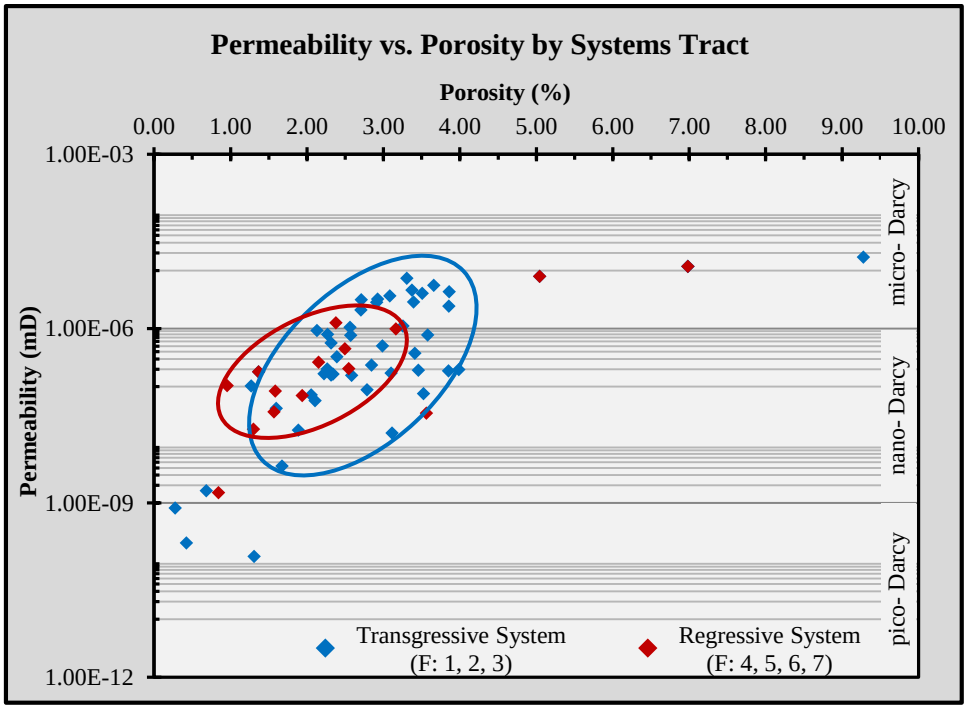

Figure 32: Porosity and permeability cross-plot of depositional facies associated with transgressive and regressive phases. Note the higher values associated with the organic-rich mudstones of the transgressive systems tract (blue) in respect to the more grain-rich and lithified sediments of the regressive tract (red).

CHAPTER VIII: CONCLUSIONS

This study increases understanding of the Eagle Ford in south Texas through detailed analysis of depositional facies and vertical facies stacking patterns in four cores. Additional insight was gained into the character and distribution of reservoir units in the Eagle Ford through the analysis of reservoir data constrained in a sequence stratigraphic framework.

1. Seven depositional facies and one lithofacies unrelated to a specific depositional setting were identified in the Eagle Ford interval: 1) Laminated Argillaceous Mudstone; 2) Weakly Laminated Calcareous Foraminiferal Mudstone; 3) Laminated Foraminiferal Wackestone; 4) Bioturbated Skeletal Lime Wackestone; 5) Laminated Inoceramid and Foraminiferal Wackestone to Packstone; 6) Skeletal Packstone to Wackestone; 7) Foraminiferal Packstone to Grainstone; and 8) Massive to Bioturbated Claystone (Volcanic Ash).
2. Eagle Ford sediments show an overall 2^{nd} order regressive, shallowing-upward sequence with a hierarchical distribution of higher-frequency sequences (3^{rd} and 4^{th} order) and cycles (5^{th} order) within. The overall regressive package is indicated by an upward: 1) change in lithology, 2) transition from pelagic- to traction-modes of deposition, 3) increase in coarser grains and

skeletal debris, 4) increase in bioturbation, and 5) an upward decrease in TOC.

3. The Eagle Ford interval consists of three relatively symmetrical and regionally consistent 3rd order sequences (S1, S2, and S3). Sequence 1 contains 4-5 HFS's (4th order), Sequence 2 shows 3-4 HFS's, and Sequence 3 includes 2 HFS's in the analyzed core interval. These 3rd and 4th order sequences can be identified confidently in the Eagle Ford interval. However, 5th order cycles (HFC's) lack regional continuity and cannot be correlated between wells.
4. Variations observed primarily in HFS's-/HFC's suggest these packages may not be a function solely of eustatic sea level changes but may also be influenced by autocyclic processes.
5. Depositional facies and sequences correlate directly to wire-line log signatures and are best identified using gamma ray, bulk density and density porosity curves. Sequences show an upward decrease in gamma ray and density porosity values and an upward increase in bulk density.
6. Primary reservoir quality porosity and permeability values correlate to position within the stratigraphic framework, where highest reservoir potential correlates to large-scale (2nd order) and higher-frequency sequences-/cycle transgressive trends identified

through facies stacking patterns. Stacking patterns of 4th order high-frequency sequences and 5th order cycles dictate the vertical variability of reservoir units in the Eagle Ford. These HFS's-/HFC's consist predominantly of transgressive- to early-highstand calcareous mudstones (highest reservoir potential) and well lithified, late highstand to early lowstand foraminiferal packstone-/grainstones (compartmentalize reservoir units).

7. Observations and results of this investigation demonstrate how techniques of identifying, and linking depositional facies to reservoir quality, and tying these to wire-line log signatures assist in the characterization of unconventional reservoirs and enhance the predictability of reservoir potential away from core observations.

BIBLIOGRAPHY

Abbott, P.L., 1974, Calcitization of Edwards Group dolomites in the Balcones Fault Zone aquifer, South-Central Texas, Geology, v. 2, No. 7 , p. 359-362.

Adams, A.E., and MacKenzie, W.S., 1998, A colour atlas of carbonate sediments and rocks under the microscope, London, Manson Publishing, 180 p.

Almon, W.D., and Cohen, P.A., 2008, Palaeoecological significance of turritelline gastropod-dominated assemblages from the mid-Cretaceous(Albian-Cenomanian) of Texas and Oklahoma, USA, Cretaceous Research, v. 29, p. 65-77.

Ambrose, W.A., Hentz, T.F., Bonnaffe, F., Loucks, R.G., Brown, L.F. Jr., Wang, F.P., and Potter, E.C., 2009, Sequence-stratigraphic controls on complex reservoir architecture of highstand fluvial-dominated deltaic and lowstand valley-fill deposits in the Upper Cretaceous (Cenomanian) Wooodbine Group, East Texas Field: Regional and local perspectives, American Association of Petroleum Geologists Bulletin, v. 93, No. 2, p. 231-269.

Aplin, A.C., Fleet, A.J., and Macquaker, J.H.S, 1999, Muds and mudstones: physical and fluid-flow properties, Geological Society, London, Special Publications, v. 158, p. 1-8.

Arthur, M.A., Jenkyns, H.C., Brumsack, H.J., and S.O. Schlanger, 1990, Stratigraphy, geochemistry, and paleoceanography of organic carbon-rich Cretaceous sequences, *in* Ginsburg, R.N., and Beaudoin, B., eds., Cretaceous resources, events and rhythms, Dordrecht, Kluwer Academic Publishers, p. 75-121.

Asmus, J.J., 2012, Characterization of deep-water carbonate turbidites and mass-transport deposits (MTDs) utilizing high-resolution electrical borehole image logs: Late Leonardian (E. Permian) Upper Bone Spring Limestone,

Delaware Basin, Southeast New Mexico and West Texas: M.S. Thesis, Western Michigan University.

Bartberger, C.E., Dyman, T.S., and Condon, S.M., 2002, Is there a basin-centered gas accumulation in Cotton Valley Group sandstones, Gulf Coast Basin, U.S.A.?, U.S. Geological Survey Bulletin 2184-D, http://geology.cr.usgs.gov/pub/bulletins/b2184-d/, Accessed January 12, 2012, 43 p.

Beebe, B.W., 1968, Deep Edwards trend of South Texas, *in* Beebe, B.W., and Curtis, B.F., eds., Natural gasses of North America, AAPG Memoir 9, v. 1, p. 961-975.

Bergman, K.L., Westphal, H., Janson, X., Poiriez, A., and Eberli, G.P., 2010, Controlling parameters on facies geometries of the Bahamas, and isolated carbonate platform environment, *in* Westphal, H., Riegl, B., and Eberli, G.P., eds., Carbonate depositional systems: Assessing dimensions and controlling parameters, Springer Science+Business Media B.V., p. 5-81.

Betzler, C., Pfeiffer, M., and Saxena, S., 2000, Carbonate shedding and sedimentary cyclicities of a distally steepened carbonate ramp (Miocene, Great Bahama Bank), International Journal of Earth Science, v. 89, p. 140-153.

_____, C., Reijmer, J.J.G., Bernet, K., Eberli, G.P., and Anselmetti, F.S., 1999, Sedimentary patterns and geometries of the Bahamian outer carbonate ramp (Miocene—Lower Pliocene, Great Bahama Bank), Sedimentology, v. 46, p. 1127-1143.

Bice, K.L., Bralower, T.J., Duncan, R.A., Huber, B.T., Leckie, R.M., and Sageman, B.B., 2002, Cretaceous climate-ocean dynamics: Future directions for IODP, JOI/USSSP and NSF Workshop, 44 p.

Blakey, R., 1994, North American paleogeography, Northern Arizona University. <http://www2.nau.edu/rcb7/nam.html>, Accessed December 13, 2011.

Bratovich, M., and Sommer, D.A., 2009, Applications of an integrated petrophysical evaluation approach to North American shale gas reservoirs, the Society of Petrophysicists and Well Log Analysts (SPWLA)-India Symposium, 14 p.

Brown, C.W. and Pierce, R.L., 1962, Palynologic correlations in Cretaceous Eagle Ford Group, Northeast Texas, American Association of Petroleum Geologists Bulletin, v. 46, No. 12, p. 2133-2147.

Carter, R.M., 1998, Two models: Global sea-level change and sequence stratigraphic architecture, Sedimentary Geology, v. 122, p. 23-36.

Cherry, M., 2011, A case history of the Eagle Ford oil shale play, South Texas: AAPG Search and Discovery Article #90122, <http://www.searchanddiscovery.com/abstracts/pdf/2011/hedberg-texas/abstracts/ndx_cherry.pdf>, Accessed October 15, 2011.

Christopher, R.A., 1982, The occurrence of the *Complexiopollis-Atlantopollis* Zone (Palynomorphs) in the Eagle Ford Group (Upper Cretaceous) of Texas, Journal of Paleontology, v.56., No. 2, p. 525-541.

Christie-Blick, N., 1990, Sequence stratigraphy and sea-level changes in Cretaceous time, *in* Ginsburg, R.N., and Beaudoin, B., eds., Cretaceous resources, events and rhythms, Dordrecht, Kluwer Academic Publishers, p. 1-21.

Cook, H.E., and Mullins, H.T., 1983, Basin margin environment, *in* Scholle, P.A., Bebout, D.G., and Moore, C.H., eds., Carbonate depositional environments, AAPG Memoir 33, p. 449-617.

Cooper, D.A., Cooper, R.W., Lehman, T., Lock, B., Stevens, J.B., Stevens, M.S., Alex, T., Alex, B., Traylor, R., and Urbanczyk, K., 2010, Cretaceous geology of the Big Bend Region, Texas, Field Trip Guidebook, 143 p.

Corbett, K., 2010, Eagleford Shale exploration models: Depositional controls on reservoir properties: AAPG Search and Discovery Article #10242,

<http://www.searchanddiscovery.com/documents/2010/10242corbett/ndx_corbett.pdf>, Accessed February 15, 2011.

Cronin, T.M., 2010, Paleoclimates: Understanding climate change past and present, New York, Chichester, West Sussex, Columbia University Press, 441 p.

Cusack, C., Beeson, J., Stoneburner, D., and Robertson, G., 2010, The discovery, reservoir attributes, and significance of the Hawkville Field and Eagle Ford Shale trend, Texas: Gulf Coast Association of Geological Societies Transactions, v. 60, p. 165-179.

Dawson, W.C., 1997, Limestone microfacies and sequence stratigraphy: Eagle Ford Group (Cenomanian-Turonian) North-Central Texas outcrops: Gulf Coast Association of Geological Societies Transactions, v. 47, p. 99-105.

_____, W.C., 2000, Shale Microfacies: Eagle Ford Group (Cenomanian-Turonian) North-Central Texas outcrops and subsurface equivalents: Gulf Coast Association of Geological Societies Transactions, v. 50, p. 607-621.

_____, W.C., and Almon, W.R., 2010, Eagle Ford Shale variability: Sedimentologic influences on source and reservoir character in an unconventional resource unit: Gulf Coast Association of Geological Societies Transactions, v. 60, p. 181-190.

Dean, W.E., and Arthur, M.A., 1998, Cretaceous Western Interior Seaway drilling project: An overview, *in* Dea, W.E. and Arthur, M.A., eds., Stratigraphy and paleoenvironments of the Cretaceous Western Interior Seaway. SEPM Concepts in Sedimentology and Paleontology, No. 6, p. 1-10.

Donovan, A.D., and Staerker, T.S., 2010, Sequence stratigraphy of the Eagle Ford (Boquillas) Formation in the subsurface of South Texas and outcrops of West Texas: Gulf Coast Association of Geological Societies Transactions, v. 60, p. 861-899.

Dravis, J.J., 1980, Sedimentology and diagenesis of the Upper Cretaceous Austin Chalk Formation, South Texas and Northern Mexico: PhD Dissertation, Rice University, Houston, Texas, 52 p.

Driskill, B., Suurmeyer, N., Rilling-Hall, S., Govert, A., and Garbowicz, A., 2010, Reservoir description of the subsurface Eagle Ford Formation, Maverick Basin area, south Texas, USA., Society of Petroleum Engineers Article #154528, 23 p.

Dunham, R.J., 1962, Classification of carbonate rocks according to depositional texture, *in* Ham, W.E., ed., Classification of Carbonate Rocks: AAPG Memoir, v. 1, p. 108-121.

Dunn, R.K., and Mazzullo, S.J., 1993, Holocene paleocoastal reconstruction and its relationship to Marco Gonzalez, Ambergris Caye, Belize, Journal of Field Archaeology, v. 20, No. 2, p. 121-131.

Durham, L.S., 2010, Eagle Ford joins shale elite: AAPG Explorer, <http://www.aapg.org/explorer/2010/01jan/eagleford0110.cfm>, Accessed January 15, 2011.

Dyer, M.J., and Bartolini, C., 2004, Sabinas basin Lower Cretaceous to Jurassic production—comparison to South Texas equivalents, Gulf Coast Association of Geological Societies Transactions, v. 54, p. 169-184.

Eberli, G.P., and Grammer, G.M., 2004, Carbonate sequence stratigraphy, AAPG Field Guide, p. 1-15.

EOG Resources, 2011, November 1, 2011 investor presentation, <http://www.eogresources.com/investors/investor_pres.html>, Accessed November 2, 2011.

_____, 2011, EOG Resources reports first quarter 2011 results, <http://investor.shareholder.com/eogresources/releasedetail.cfm?sh_print=yes&ReleaseID=575030>, Accessed October 29, 2011.

Eseme, E., Urai, J.L., Krooss, B.M., and Littke, R., 2007, Review of mechanical properties of oil shales: Implications for exploitation and basin modeling, Oil Shale, v. 24, No. 2, p. 159-174.

Ewing, T.E., 2010, Pre-Pearsall geology and exploration plays in South Texas, Gulf Coast Association of Geological Societies Transactions, v. 60, p. 241-260.

_____, T.E., 2009, The ups and downs of the Sabine Uplift and the Northern Gulf of Mexico Basin: Jurassic basement blocks, Cretaceous thermal uplifts, and Cenozoic flexure, Gulf Coast Association of Geological Societies Transactions, v. 59, p. 253-269.

_____, T.E., Geology in outcrop in the San Antonio area (an occasional series): South Texas Geological Society, <http://www.stgs.org/Feature%20Article.pdf>, Accessed November 29, 2011.

Fischer, A.G., De Boer, P.L., and Premoli Silva, I., 1990, Cyclostratigraphy, *in* Ginsburg, R.N., and Beaudoin, B., eds., Cretaceous resources, events and rhythms, p. 139-172.

Flügel, E., 2010, Microfacies of carbonate rocks, 2nd Edition, New York, Springer-Verlag, 983 p.

Frank, T.D., and Bernet, K., 2000, Isotopic signature of burial diagenesis and primary lithological contrasts in periplatform carbonates (Miocene, Great Bahama Bank), Sedimentology, v. 47, p. 1119-1134.

Freeman, V.L., 1961, Contact of Boquillas Flags and Austin Chalk in Val Verde and Terrell Counties, Texas, American Association of Petroleum Geologists Bulletin, v. 45, p. 105-107.

Friedman, G.M., Amiel, A.J., and Schneidermann, N., 1974, Submarine cementation in reefs: Example from the Red Sea, Journal of Sedimentary Petrology, v. 44, p. 816-825.

Fritz, A.D., Belsher, T.W., Medlin, J.M., Stubbs, J.L., Wright, R.P., and Harris, P.M., 2000, New exploration concepts for the Edwards and Sligo Margins, Cretaceous of onshore Texas, American Association of Petroleum Geologists Bulletin, v. 84, No. 7, p. 905-922.

Fullmer, S., and Lucia, F.J., 2005, Burial history of Central Texas Cretaceous carbonates, The Gulf Coast Association of Geological Societies Transactions, v. 55, p. 225-232.

Galloway, W.E., 1989, Genetic stratigraphic sequences in basin analysis I: Architecture and genesis of flooding-surface bounded depositional units, American Association of Petroleum Geologists, v. 73, No. 2, p. 125-142.

_____, W.E., 2000, Cenozoic depositional history of the Gulf of Mexico basin, American Association of Petroleum Geologists Bulletin, v. 84, No. 11, p. 1743-1774.

Ginsburg, R.N., Marszalek, D.S., and Schneidermann, N., 1971, Ultrastructure of carbonate cements in a Holocene algal reef of Bermuda, Journal of Sedimentary Petrology, v. 41, p. 472-482.

Gischler, E., 2003, Holocene lagoonal development in the isolated carbonate platforms off Belize, Sedimentary Geology, v. 159, p. 113-132.

_____, E., and Lomando, A.J., 1999, Recent sedimentary facies of isolated carbonate platforms, Belize-Yucatan system, Central America, Journal of Sedimentary Research, v. 69, No. 3, p. 747-763.

_____, E., Lomando, A.J., Hudson, J.H., and Holmes, C.W., 2000, Last interglacial reef growth beneath Belize barrier and isolated platform reefs, Geology, v. 28, No. 5, p. 387-390.

_____, E., and Hudson, J.H., 2004, Holocene development of the Belize Barrier Reef, Sedimentary Geology, v. 164, p. 223-236.

Goldhammer, R.K., and Johnson, C.A., 2001, Middle Jurassic-Upper Cretaceous paleogeographic evolution and sequence-stratigraphic framework of the northwest Gulf of Mexico rim, *in* Bartolini, C., Buffler, R.T., and Cantu-

Chapa, A., eds., The western Gulf of Mexico Basin: Tectonics, sedimentary basins, and petroleum systems: AAPG Memoir 75, p. 45-81.

_____, R.K., Dunn, P.A., and Hardie, L.A., 1990, Depositional cycles, composite sea-level changes, cycle stacking patterns, and the hierarchy of stratigraphic forcing: Examples from Alpine Triassic platform carbonates, Geological Society of America Bulletin, v. 102, No. 5, p. 535-562.

_____, R.K., Oswald, E.J., and Dunn, P.A., 1989, Hierarchy of stratigraphic forcing: Example from Middle Pennsylvanian shelf carbonates of the Paradox basin, Kansas Geological Survey, Bulletin 233, p. 361-413.

Grammer, G.M., Harris, P.M. and Eberli, G.P., 2004, Integration of outcrop and modern analogs in reservoir modeling: Overview with examples from the Bahamas, *in* Grammer, G.M., Harris, P.M., and Eberli, G.P., eds., Integration of outcrop and modern analogs in reservoir modeling: AAPG Memoir 80, p. 1-22.

_____, G.M., Crescini, C.M., McNeill, D.F., and Taylor, L.H., 1999, Quantifying rates of syndepositional marine cementation in deeper platform environments—New insight into a fundamental process, Journal of Sedimentary Research, v. 69, No. 1, p. 202-207.

_____, G.M., Ginsburg, R.N., and Harris, P.M., 1993, Timing of deposition, diagenesis, and failture of steep carbonate slopes in response to a high-amplitude/high-frequency fluctuation in sea level, Tongue of the Ocean, Bahamas, *in* Loucks, R.G., and Sarg, J.F., eds., Carbonate sequence stratigraphy, recent developments and applications, AAPG Memoir 57, p. 107-131.

Grosskopf, J.F., 2010, Using inoceramid bivalve taphonomy as a paleoenvironmental indicator across the Cenomanian/Turonian horizon at the Pueblo, Colorado GSSP: M.S. Thesis, Louisiana State University.

Handford, C.R., and Loucks, R.G., 1993, Carbonate depositional sequences and systems tracts—Response of carbonate platforms to relative sea-level

changes, *in* Loucks, R.G., and Sarg J.F., eds., Carbonate sequence stratigraphy: AAPG Memoir 57, p. 3-43.

Harbor, R.L., 2011, Facies characterization and stratigraphic architecture of organic-rich mudrocks, Upper Cretaceous Eagle Ford Formation, South Texas: M.S. Thesis, The University of Texas at Austin.

Hardy, R. and Tucker, M., 1988, Ch. 7, X-Ray Powder Diffraction of sediments, *in* Tucker, M., Techniques in Sedimentology, Blackwell, p. 191-227.

Harris, P.M., 2010, Delineating and quantifying depositional facies patterns in carbonate reservoirs: Insight from modern analogs, American Association of Petroleum Geologists Bulletin, v.94, No. 1, p. 61-86.

Haq, B.U., and Boersma, A., 1978, Introduction to marine micropaleontology, New York, Elsevier, p. 376.

Hentz, T.F., and Ruppel, S.C., 2010, Regional lithostratigraphy of the Eagle Ford Shale: Maverick Basin to East Texas Basin: Gulf Coast Association of Geological Societies Transactions, v. 60, p. 325-337.

_____, T.F., and Ruppel, S.C., 2011, Regional stratigraphic and rock characteristics of Eagle Ford Shale in its play area: Maverick Basin to East Texas Basin, Search and Discovery Article #10325, 20 p.

Hildred, G., Ratcliffe, K. and Schmidt, K., 2011, Application of inorganic whole-rock geochemistry to shale resource plays: An example from the Eagle Ford Shale, Texas. Houston Geological Society Bulletin, p. 31-38.

Hill, R.T., 1887a, The topography and geology of the Cross Timbers and surrounding regions in Northern Texas: American Journal of Science, 3rd series, v. 33, p. 291-303.

_____, R.T., 1887b, The Texas Section of the American Cretaceous: American Journal of Science, 3rd series, v. 34, p. 287-307.

_____, R.T., 1901, Geography and geology of the Black and Grand Prairies, Texas, United States Geological Society 21st Annual Report, pt. 7, 666 p.

Hull, D.C., 2011, Stratigraphic architecture, depositional systems, and reservoir characteristics of the Pearsall shale-gas system, Lower Cretaceous, South Texas: M.S. Thesis, The University of Texas at Austin.

Honarpour, M.M., Djabbarah, N.F. and Sampath, K., 2003, Whole core analysis—Experience and challenges: Society of Petroleum Engineers Article #81575, 16 p.

Howard Weil Incorporated, 2011, Eagle Ford Shale—Not all areas are created equal.

Isern, A.R., and Anselmetti, F., 2001, The influence of carbonate platform morphology and sea level on fifth-order petrophysical cyclicity in slope and basin sediments adjacent to the Great Bahama Bank, Marine Geology, v. 177, p. 381-394.

James, N.P., and Choquette, P.W., 1983, Limestones—The sea floor diagenetic environment, Geoscience Canada, v. 10, No. 4, p. 162-179.

James, N.P., Ginsburg, R.N., Marszalek, D.S., and Choquette, P.W., 1976, Facies and fabric specificity of early subsea cements in shallow Belize (British Honduras) Reefs, Journal of Sedimentary Petrology, v. 46, No. 3, p. 523-544.

Jiang, M., 1989, Biostratigraphy and geochronology of the Eagle Ford Shale, Austin Chalk, and Lower Taylor Marl in Texas based on calcareous nannofossils: PhD Dissertation, Texas A&M University, College Station, Texas, 524 p.

Karpoff, A.M., Destrigneville, C., Bartier, D., and Dejardin, P., 2002, Phyllosilicates and zeolite assemblages in the carbonate periplatform of the Great Bahama Bank: origin and relation to diagenetic processes (ODP Leg 166, Sites 1006 and 1007), Marine Geology, v. 185, p. 55-74.

Kauffman, E.G., 1984, Paleobiogeography and evolutionary response dynamic in the Cretaceous Western Interior Seaway of North America, *in* Westermann, G.E.G., ed., Jurassic-Cretaceous biochronology and

paleogeography of North America, Geological Association of Canada, Special Paper 27, p. 273-306.

_____, E.G., and Sageman, B.B., 1990, Biological sensing of benthic environments in dark shales and related oxygen-restricted facies, *in* Ginsburg, R.N., and Beaudoin, B., eds., Cretaceous resources, events and rhythms, Dordrecht, Kluwer Academic Publishers, p. 121-139.

Keahey, R.A., 1962, Fashing Field, Atascosa-Karnes counties, Texas, Gulf Coast Association of Geological Societies Transactions, v. 12, p. 205-211.

Kerans, C., 2002, Styles of rudist buildup development along the northern margin of the Maverick Basin, Pecos River Canyon, southwest Texas, Gulf Coast Association of Geological Societies Transactions, v. 52, p. 501-516.

_____, C., and Tinker, S.W., 1997, Sequence stratigraphy and characterization of carbonate reservoirs, SEPM Short Course Notes #40, 137 p.

Kroon, D., Williams, T., Pirmez, C., Spezzaferri, S., Sato, T., and Wright, J.D., 2000, Coupled Early Pliocene-Middle Miocene bio-cyclostratigraphy of site 1006 reveals orbitally induced cyclicity patterns of Great Bahama Bank carbonate production, *in* Swart, P.K., Eberli, G.P., Malone, M.J., and Sarg. J.F., eds., Proceedings of the Ocean Drilling Program, Scientific Results, v. 166, p. 155-166.

Laubach, S.E., and Jackson, M.L.W., 1990, Origin of arches in the northwestern Gulf of Mexico basin, Geology, v. 18, p. 595-598.

Lee, Y.N., 1997, The Archosauria from the Woodbine Formation (Cenomanian) in Texas, Journal of Paleontology, v. 71, No. 6, p. 1147-1156.

Lehmann, C., Osleger, D.A., Montanez, I.P., Sliter, W., Arnaud-Vanneau, A., and Branner, J., 1999, Evolution of Cupido and Coahuila carbonate platforms, Early Cretaceous, northeastern Mexico, Geological Society of America Bulletin, v. 111, No. 7, p. 1010-1029.

_____, C., Osleger, D.A., and Montanez, I., 2000, Sequence stratigraphy of Lower Cretaceous (Barremian-Albian) carbonate platforms of northeastern

Mexico: Regional and global correlations, Journal of Sedimentary Research, v. 70, No. 2, p. 373-391.

Linnert, C., Mutterlose, J., and Mortimore, R., 2011, Calcareous nannofossils from Eastbourne (Southeastern England) and the paleoceanography of the Cenomanian-Turonian boundary interval, Palaios, v. 26, p. 298-212.

Lock, B.E., Choh, S.J., and Willis, J.J., 2001, Tepees and other surficial deformation features of Cretaceous rocks in Central and West Texas, resulting from Late Cenozoic caliche formation: Gulf Coast Association of Geological Societies Transactions, v. 51, p. 173-186.

_____, B.E., and Peschier, L., 2006, Boquillas (Eagle Ford) Upper slope sediments, West Texas: Outcrop analogs for potential shale reservoirs: Gulf Coast Association of Geological Societies Transactions, v. 56, p. 491-508.

_____, B.E., Peschier, L., and Whitcomb, N., 2010, The Eagle Ford (Boquillas Formation) of Val Verde County, Texas—A window on the South Texas play: Gulf Coast Association of Geological Societies Transactions, v. 60, p. 419-434.

Loeblich, A.R. Jr., 1946, Foraminifera from the type Pepper Shale of Texas, Journal of Paleontology, v. 20, No. 2, p. 130-139.

_____, A.R. Jr., and Tappan, H., 1961, Cretaceous planktonic foraminifera: Part I. Cenomanian, Micropaleontology, v. 7, No. 3, p. 257-304.

Longman, M.W., Luneau, B.A., and Landon, S.M., 1998, Nature and distribution of Niobrara lithologies in the Cretaceous Western Interior Seaway of the Rocky Mountain Region, The Mountain Geologist, v. 35, No. 4, p.137-170.

Loucks, R.G., Reed, R.M., Ruppel, S.C., and Hammes, U., 2010, Preliminary classification of matrix pores in mudrocks, Gulf Coast Association of Geological Societies Transactions, v. 60, p. 435-441.

Lucia, F.J., Kerans, C., and Jennings, J.W. Jr., 2003, Carbonate reservoir characterization, Society of Petroleum Engineers Article #82071, p.1-3.

Lyell, C., 1875, Principles of Geology, Vol. 2, 12th Edition, London, John Murray, 652 p.

Mancini, E.A., Li, P., Goddard, D.A., Ramirex, V., and Talukdar, S.C, 2008, Mesozoic (Upper Jurassic-Lower Cretaceous) deep gas reservoir play, central and eastern Gulf Coastal Plain, American Association of Petroleum Geologists Bulletin, v. 92, No. 3, p. 283-308.

Marcou, J., 1862, Notes on the Cretaceous and Carboniferous Rocks of Texas: Boston Society of Natural History, Proc. 8, p. 86-97.

Mathews, R.K., and Frohlich, C., 2002, Maximum flooding surfaces and sequence boundaries: comparisons between observations and orbital forcing in the Cretaceous and Jurassic (65-190 Ma), GeoArabia, v. 7, No. 3, p. 503-539.

Mazzullo, S.J., 2006, Late Pliocene to Holocene platform evolution in northern Belize, and comparison with coeval deposits in southern Belize and Bahamas, Sedimentology, v. 53, p. 1015-1047.

_____, S.J., 2004, Overview of porosity evolution in carbonate reservoirs, Search and Discovery Article #40134, 19 p.

McCloskey, S.M., 2012, 3-D reservoir characterization of the South Buckeye Field Dundee Formation (Devonian), Michigan Basin, USA: M.S. Thesis, Western Michigan University.

McNeill, D.F., Janson, X., Bergman, K.L., Eberli, G.P., 2010, Belize: A modern example of a mixed carbonate-siliciclastic shelf, *in* Westphal, H., Riegl, B., and Eberli, G.P., eds., Carbonate depositional systems: Assessing dimensions and controlling parameters, Ch. 3, Springer Science+Business Media B.V., p. 81-143.

Melim, L.A., Westphal, H., Swart, P.K., Eberli, G.P., and Munnecke, A., 2002, Questioning carbonate diagenetic paradigms: Evidence from the Neogene of the Bahamas, Marine Geology, v. 185, p. 27-53.

Miall, A.D., 2010, The geology of stratigraphic sequences, 2nd Edition, New York, Springer, 522 p.

Montgomery, S.L., Petty, A.J., and Post, P.J., 2002, James Limestone, northeastern Gulf of Mexico: Refound opportunity in a Lower Cretaceous trend, American Association of Petroleum Geologists Bulletin, v. 86, No. 3, p. 381-397.

Mulder, T., and Alexander, J., 2001, The physical character of subaqueous sedimentary density flows and their deposits, Journal of Sedimentology, v. 48, p. 269-299.

Myers, K.J., and Milton, N.J., 1996, Concepts and principles of sequence stratigraphy, *in* Emery, D., and Myers, K.J., eds., Sequence Stratigraphy, Oxford, Blackwell Science Ltd., 297 p.

Perez C, E.R., Zapata A, J.F., Gonzalez, M., Herrera, M.N. and Ecopetrol, 2010, Abstract: Improvements in routine core analysis on whole core: Society of Petroleum Engineers Article # 139165, 17 p.

Pearson, K., 2010, Geologic controls on Austin Chalk oil and gas production: understanding a dual conventional-continuous accumulation, Gulf Coast Association of Geological Societies Transactions, v. 60, p. 557-570.

Peschier, L., 2011, The Boquillas (Eagle Ford) Formation of South Texas: Potential outcrop analogs for nonconventional Eagle Ford Shale reservoirs in the subsurface, <http://www.hgs.org/en/cev/1133/>, Accessed August 29, 2011.

Pessagno, E.A., 1969, Upper Cretaceous stratigraphy of the western Gulf Coast area of Mexico, Texas, and Arkansas: Geological Society of America Memoir 111, Boulder, Colorado, 129 p.

Phelps, R.M., Kerans, C., and Loucks, R.G., 2010, High-resolution regional sequence stratigraphic framework of Aptian through Coniacian strata in the Comanche shelf, Central and South Texas: Gulf Coast Association of Geological Societies Transactions, v. 60, p. 755-758.

_____, R.M., 2011, Middle-Hauterivian to Lower-Campanian sequence stratigraphy and stable isotope geochemistry of the Comanche Platform, South Texas: PhD Dissertation, The University of Texas, Austin, Texas, 240 p.

Powell, J.D., 1965, Late Cretaceous platform—Basin facies, Northern Mexico and adjacent Texas, American Association of Petroleum Geologists Bulletin, v. 49, No. 5, p. 511-525.

Prince, C.M., Stelle, D.D., Zelaya, R., and Devier, C.A., 2011, Shale diagenesis and permeability: Examples from the Barnett Shale and the Marcellus Formation, Search and Discovery Article #50372, 22 p.

Purdy, E.G., and Gischler, E., 2003, The Belize margin revisted: 1. Holocene marine facies, International Journal of Earth Science, v. 92, p. 532-552.

Railroad Commission of Texas, 2011, Eagle Ford information, <http://www.rrc.state.tx.us/eagleford/index#general>, Accessed August 15, 2012.

Read, J.F., Kerans, C., Weber, L.J., Sarg, J.F., and Wright, F.M., 1995, Milankovitch sea-level changes, cycles, and reservoirs on carbonate platforms in greenhouse and ice-house worlds, SEPM Short Course 35, 183 p.

Reid, R.P., Macintyre, I.G., and Post, J.E., 1992, Micritized skeletal grains in northern Belize Lagoon: A major source of Mg-calcite mud, Journal of Sedimentary Petrology, v. 62, No. 1, p. 145-156.

Reuning, L., Reijmer, J.J.G., and Betzler, C., 2002, Sedimentation cycles and their diagenesis on the slope of a Miocene carbonate ramp (Bahamas, ODP Leg 166), Marine Geology, v. 185, p. 121-142.

Ritter, A.L., 2008, Evaluating the controls on reservoir heterogeneity of Silurian pinnacle reefs, Michigan Basin: M.S. Thesis, Western Michigan University.

Robinson, M.R., 2012, Integrating depositional facies and stratigraphy in characterizing hydrothermal dolomite reservoirs: Trenton Group of the Albion-Scipio Trend, Michigan Basin: M.S. Thesis, Western Michigan University.

Roelofsen, J., 2011, A review of problems in reporting unconventional energy resources and potential applications of UNFC-2009, IHS Inc., 20 p.

Roundtree, R., Wright, J., and Miskimins, J., 2010, Unconventional resource recovery improvement using conventional reservoir engineering strategies, Search and Discovery Article #80088, 15 p.

Sarg, J.F., 1988, Carbonate sequence stratigraphy, *in* Wilgus, C.K., Hastings, B.S., Kendall, C., Posamentier, H.W., Ross, C.A., and Van Wagoner, J.C., eds., Sea-level changes: An integrated approach: SEPM Special Publication 42, p. 155-183.

_____, J.F., Markello, J.R., and Weber, L.J., 1999, The second-order cycle, carbonate-platform growth, and reservoir, source, and trap prediction, *in* Harris, P.M., Saller, A.H., and Simo, J.A., eds., Advances in carbonate sequence stratigraphy: Application to reservoirs, outcrops and models, SEPM Special Publication, No. 63, p. 11-34.

Saller, A., Armin, R., Ichram, L.W., and Glenn-Sullivan, C., 1993, Sequence stratigraphy of aggrading and backstepping carbonate shelves, Oligocene, Central Kalimantan, Indonesia, *in* Loucks, R.G., and Sarg, J.F., eds., Carbonate sequence stratigraphy: AAPG Memoir 57, p. 267-290.

Schlager, W., 2005, Carbonate sedimentology and sequence stratigraphy, SEPM Concepts in Sedimentology and Paleontology, No. 8, 200 p.

_____, W., and Ginsburg, R.N., 1981, Bahama carbonate platforms—The deep and the past, Marine Geology, v. 44, p. 1-24.

Schlanger, S.O., and Jenkyns, H.C., 1976, Cretaceous oceanic anoxic events: Causes and consequences, Geologie en Mijnbouw, v. 55, p. 179-184.

Schlumberger, Oilfield glossary, http://www.glossary.oilfield.slb.com/, Accessed January 13, 2011.

Scholle, P.A., and Kling, S.A., 1972, Southern British Honduras: Lagoonal Coccolith Ooze, Journal of Sedimentary Petrology, v. 42, No. 1, p. 195-204.

_____, P.A., and Ulmer-Scholle, D.S., 2003, A color guide to the petrography of carbonate rocks: grains, textures, porosity, diagenesis, AAPG Memoir 77, Tulsa, The American Association of Petroleum Geologists, 474 p.

Scott, R.W., 1993, Cretaceous carbonate platform, U.S. Gulf coast, *in* Simo, J.A., Scott, R.W., and Masse, J.P., eds., Cretaceous Carbonate Platforms: AAPG Memoir 56, p. 97-109.

_____, R.W., 1995, Global environmental controls on Cretaceous reefal ecosystems, Palaeogeography, Palaeoclimatology, Palaeoecology, v. 119, p. 187-199.

_____, R.W., 2004, The Maverick Basin: New technology—new success, Gulf Coast Association of Geological Societies Transactions, v. 54, p. 603-620.

_____, R.W., and Weaver, M., 2010, Ontogeny and functional morphology of a Lower Cretaceous caprinid rudist (Bivalvia, Hippuritoida), Turkish Journal of Earth Sciences, v. 19, p. 527-542.

Sellards, E.H., Adkins, W.S., and Plummer, F.B., 1932, The geology of Texas, Volume I, Stratigraphy: University of Texas Bulletin 3232, 1007 p.

Shanmugam, G., 1997, The bouma sequence and the turbidite mind set, Earth-Science Reviews, v. 42, p. 201-229.

Shinn, E.A., 1969, Submarine lithification of Holocene carbonate sediments in the Persian Gulf, *in* Tucker, M.E., and Bathurst, R.G.C., eds., Carbonate diagenesis, Reprint series 1, p. 11-46.

Shumard, B.F., 1860a, Observations upon the Cretaceous strata of Texas: Saint Louis Academy of Science Transactions, v. 1, p. 582-610.

_____, B.F., 1860b, Descriptions of new Cretaceous Fossils from Texas: Saint Louis Academy of Science Transactions, V.1, p. 590-610.

Slatt, R.M., and Abousleiman, Y., 2011, Margin sequence stratigraphy and geomechanics for unconventional gas shales, The Leading Edge, p. 274-282.

Slingerland, R., Kump, L.R., Arthur, M.A., Fawcett, P.J., Sageman, B.B., and Barrown, E.J., 1996, Estuarine circulation in the Turonian Western Interior seaway of North America, Geological Society of America Bulletin, v. 108, No. 7, p. 941-952.

Sohl, N.F., 1987, Cretaceous gastropods: Contrasts between Tethys and the Temperate Provinces, Journal of Paleontology, v. 61, No. 6, p. 1085-1111.

Strasser, A., Hillgartner, H., Hug, W., and Pittet, B., 2000, Third-order depositional sequences reflecting Milankovitch cyclicity, Terra Nova, v. 12, p. 303-311.

Stefani, M., and Burchell, M., 1990, Upper Triassic (Rhaetic) argillaceous sequences in northern Italy: Depositional dynamics and source potential, *in* Huc, A.Y., ed., Deposition of organic facies, AAPG Studies in Geology #30, p. 93-107.

Swanson, R.G., 1981. *Sample Examination Manual*, AAPG Methods in Exploration Series, 118 p.

Treadgold, G., Campbell, B., McLain, B., Sinclair, S., and Nicklin, D., 2011a, Eagle Ford Shale prospecting with 3D seismic data within a tectonic and depositional framework, The Leading Edge, v. 30, No. 1, p. 48-53.

_____, G., McLain, B., Sinclair, S., and Nicklin, D., 2011b, Eagle Ford Shale prospecting with 3D seismic data within a tectonic and deposition system framework: AAPG Search and Discovery Article #90122, <http://www.searchanddiscovery.com/abstracts/pdf/2011/hedberg-texas/abstracts/ndx_treadgold.pdf>, Accessed February 24, 2011.

Trevino, R.H. III, 1988, Facies and depositional environments of the Boquillas Formation, Upper Cretaceous of southwest Texas, M.S. Thesis, The University of Texas at Arlington, 120 p.

Tucker, D.R., 1968, Lower Cretaceous geology, northwestern Karnes County, Texas, American Association of Petroleum Geologists Bulletin, v. 52, No. 5, p. 820-851.

Tucker, M.E., and Wright, V.P., 1990, Carbonate sedimentology, Blackwell Scientific Publications, Oxford, 482 p.

_____, M.E., 2001, Sedimentary petrology: An introduction to the origin of sedimentary rocks, 3rd Edition, Blackwell Publishing, Oxford, 262 p.

Turgeon, S.C., and Creaser, R.A., 2008, Cretaceous oceanic anoxic event 2 triggered by a massive magmatic episode, Nature, v. 454, p. 323-327.

Weimer, R.J., 1990, Sequence stratigraphy and paleotectonics, Denver Basin area of lower Cretaceous foreland basin, U.S.A., *in* Ginsburg, R.N., and Beaudoin, B., eds., Cretaceous resources, events and rhythms, Dordrecht, Kluwer Academic Publishers, p. 23-33.

White, T., Gonzalez, L., Ludvigson, G., and Poulsen, C., 2001, Middle Cretaceous greenhouse hydrologic cycle of North America, Geological Society of America, v. 29, No. 4, p. 363-366.

Wilson, J.L., and Jordan, C., 1983, Middle Shelf Environment, *in* Scholle, P.A., Debout, D.G., and Moore, C.H., eds., Carbonate depositional environments, AAPG Memoir 33, p. 297-345.

Winker, C.D., and Buffler, R.T., 1988, Paleogeographic evolution of early deep-water Gulf of Mexico and margins, Jurassic to Middle Cretaceous (Comanchean), American Association of Petroleum Geologists Bulletin, v. 72, No. 3, p. 318-346.

Winter, J.A., 1961, Stratigraphy of the Lower Cretaceous (Subsurface) of South Texas: Gulf Coast Association of Geological Societies, v. 11, p. 15-24.

Yang, W., Mazzullo, S.J., and Teal, C.S., 2004, Sediments, facies tracts, and variations in sedimentation rates of Holocene platform carbonate sediments and associated deposits, Northern Belize-Implications for "representative" sedimentation rates, Journal of Sedimentary Research, v. 74, No. 4, p. 498-512.

Young, K., 1972, Cretaceous paleogeography: Implications of endemic ammonite faunas, The Bureau of Economic Geology, The University of Texas, Geological Circular, v. 72, No. 2, 13 p.

Yurewicz, D.A., Marler, T.B., Meyerholtz, K.A., and Siroky, F.X., 1993, Early Cretaceous carbonate platform, north rim of the Gulf of Mexico, Mississippi and Louisiana, *in* Simo, J.A., Scott, R.W., and Masse, J.P., eds., Cretaceous Carbonate Platforms: AAPG Memoir 56, p. 81-96.

APPENDIX A

Sequence Stratigraphy and Facies Stacking Patterns

Microsoft Powerpoints containing figures referenced in the discussion of ‘Sequence Stratigraphy and Facies Stacking Patterns’ may be obtained by contacting Seth Jordan Workman via e-mail (seth.workman@gmail.com).